THE ROLE OF PRE-EXISTING PRECAMBRIAN STRUCTURES AND THERMAL ANOMALY IN RIFT INITIATION AND EVOLUTION-THE ALBERTINE AND RHINO GRABENS IN UGANDA

By

ANDREW BUSHEKWIRE KATUMWEHE

Bachelor of Science (Honors) in Geology and Chemistry

Makerere University

Kampala, Uganda

1995

Master of Science in Applied Geophysics.
International Institute for Aerospace Survey and Earth Observation (ITC)
Delft, The Netherlands
2000

Submitted to the Faculty of the Arts and Science
Graduate College of the Arts and Science
Oklahoma State University
in partial fulfillment of
the requirements for
the Degree of Geology
DOCTOROF PHILOSOPHY
MAY, 2016

THE ROLE OF PRE-EXISTING PRECAMBRIAN STRUCTURES AND THERMAL ANOMALY IN RIFT INITIATION AND EVOLUTION-THE ALBERTINE AND RHINO GRABENS IN UGANDA.

Dissertation Approved:

Estella E Atekwana, Ph.D., Chair

Dissertation Adviser

Mohamed Gamal Abdelsalam, Ph.D.

Daniel Lao-Davila, Ph.D.

Amy Elizabeth Frazier, Ph.D.

ACKNOWLEDGEMENTS

This research has finally been accomplished and this has benefited from contributions from different people. I would like to express my deepest appreciation to my committee chair and Advisor, Dr. Estella Atekwana for her unique criticism, continuous support and in depth analysis, without her guidance this dissertation would not have been possible. I thank my co-advisor and committee member, Dr. Mohamed Abdelsalam whose motivation and encouragement was paramount in completing the research. In addition, special thanks to committee member Dr. Daniel Lao-Davila for his contributions towards refining my work. I genuinely thank my external Committee member Dr. Amy Frazer for allowing to be part of this exciting research. Farther more special thanks to Dr. Kevin Mickus of Missouri State University (MSU) for assisting me with some of the data, and insightful contributions towards the research. I wish to thank the National (NSF) Continental Dynamics grant # EAR 1255233, and Oklahoma State University Boone Pickens of Geology for the financial support towards this research. The Government of Uganda is applauded for its free airborne geophysical data policy for research. My sincere gratitude to the family of Jim Cox, Lynn Swartz Cox, Peterson Johnson Swartz, Stephen Mukembo for hosting me during our stay in USA. I deeply appreciate the intellectual contribution of the tectonics group as well as special thanks to the Boone Pickens School of Geology Staff and graduates. Finally, to my family Pheonah, Shawn, Rodney, Ryan, Brandon, Sisters Jova, Evas and brother Benon for all the encouragement and support during my research time.

Andrew Katumwehe, March 2016

Name: ANDREW BUSHEKWIRE KATUMWEHE

Date of Degree: May, 2016

Title of Study: THE ROLE OF PRE-EXISTING PRECAMBRIAN STRUCTURES AND THERMAL ANOMALY IN RIFT INITIATION AND EVOLUTION- THE ALBERTINE AND RHINO GRABENS IN UGANDA.

Major Field: GEOLOGY

Abstract: We integrated Shuttle Radar Topography Mission Digital Elevation Models, airborne magnetic, radiometric, three-dimensional Full Tensor Gravity Gradiometry and Satellite gravity data to investigate the role of Precambrian structures in the evolution of the amagmatic Albertine-Rhino Grabens. The northern part of the Albertine-Rhino Graben extends within Mesoproterozoic Madi-Igisi fold belt wedged between two cratonic blocks. The southwestern part of the Albertine-Rhino Graben and the Edward-George Rift (EGR) extends within the Rwenzori and Kibara-Karagwe-Ankole orogenic belts. These extensional structures are separated by the ~5 km high Rwenzori Mountains and represent the northern segment of the Western Branch of the East African Rift System. No expression of surface volcanic activities is observed within the Albertine-Rhino Graben except the Toro-Ankole (TAVF) volcanic fields that are found within the EGR. Our results suggest that: (1) Strain localization, strain transfer, rift segmentation as well as rift termination against the Aswa Shear Zone (ASZ) as due to the presence of different Precambrian structures. (2) The ASZ extent is ~550 km in Uganda and South Sudan with a wider (~50 km) deformation belt and its evolution was due to E–W to NE–SW oblique collision between East and West Gondwana with strain localized at the boundary between the Saharan Metacraton and the Northern Uganda Terrane. (3) Rift initiation in the Albertine–Rhino Graben is associated with a thermal structure that shows shallow CPD and high heat flow beneath the EGR and TAVF. We observed a localized thin crust beneath the Rwenzori Mountains, the western Albertine border fault, EGR and TAVF due to the removal of sub-continental lithospheric mantle as a result of delamination. The northward migration of the mantle fluids within lithospheric scale Madi-Igisi Fold and Thrust Belt facilitated strain localization during Albertine–Rhino Rift initiation.

PUBLICATION DISSERTATION OPTION

This dissertation has been structured in two sections. The first section gives a brief outline of the dissertation and introduces the scientific question that we investigated in this research. This section also presents two manuscripts that have been published and one in review for publication.

Paper 1: "Katumwehe, A.B., Abdelsalam, M.G., Atekwana, E.A., 2015. The role of pre-existing Precambrian structures in rift evolution: The Albertine and Rhino Grabens, Uganda. Tectonophysics 646, 117-129. doi:10.1016/j.tecto.2015.01.022.

Paper 2: "Katumwehe, A.B., Abdelsalam, M.G., Atekwana, E.A., Laó-Dávila, D.A., 2015. Extent, kinematics and tectonic origin of the Precambrian Aswa Shear Zone in eastern Africa. Gondwana Research. " Gondwana Research. doi:10.1016/j.gr.2015.03.007.

Paper 3: "Katumwehe, A.B., Atekwana, E.A., Abdelsalam, M.G., Kevin M., 2016. Evolution of the Magma-poor Albertine-Rhino Graben and Edward-George Rift, East African Rift System through Mantle Delamination, Melting and Precambrian Suture Zone Guided Fluid Migration. This work been submitted to Geophysics, Geochemistry, Geosystems (G^3) Journal and is under review.

TABLE OF CONTENTS

PAPER III

LIST OF TABLES

LIST OF FIGURES

Figure Page

PAPER I

Figure Page

PAPER II

PAPER III

SECTION I

GENERAL OVERVIEW

1.0 PROJECT MOTIVATION

Continental rifts play an important role in the creation of new crust and the evolution of continental lithosphere. An overarching objective of the Rift Initiation and Evolution (RIE), an initiative of the National Science Foundation (NSF) Geodynamic Processes at Rifting and Subducting Margins (GeoPRISM) program, is to identify the key processes that initiate and drive continental rifting. In particular, the major processes required for the initiation of rifting remain debatable. For example, studies by Buck (2004, 2006) have advocated for an important role of magmatism in the initiation of continental rifting suggesting that the forces that drive plate tectonics such as slab pull are insufficient to rupture normal continental lithosphere. Analogue models suggest that magma plays an important role in softening the lithosphere, enhancing lithospheric stretching, and strain localization (Buck, 2006). Indeed, magma is documented to have played an important role in initiating continental rifting in the more extended portions of the eastern branch of the East African rift system (EARS) especially in the Main Ethiopian rift and the Afar Depression (Morgan and Baker, 1983).

The timing of onset of flood basalt magmatism and rift development in this region is said to have initiated with the 45-30 Ma volcanic events that led to the separation of Arabia from Africa (Macdonald et al., 2001; Ebinger and Casey, 2001; Nyblade, 2002; Agostin et al., 2011; Rooney et al., 2012;). The recent Dabbahu diking event in Ethiopia provided yet another opportunity to examine the role played by magma in relation to strain localization

and segmentation in initiating lithospheric rupture (Ebinger et al., 2008; Grandin et al., 2009).

1.2 CURRENT STATE OF KNOWLEDGE

Seismic results from the highly extended portions of the EARS highlight lower P and S wave velocities, an indication of asthenosphere upwelling beneath the rift (Keranen et al., 2009). New data from studies below East Africa indicate the presence of a low wave speed anomaly that has been associated with infiltration of melt in the lower lithosphere that ultimately creates an increased geotherm (Nyblade et al, 2002; Mulibo and Nyblade, 2009, Adams et al., 2012; Wolbern et al., 2012; Jackolev et al., 2013). In contrast, the northern end of the Western Branch of the EARS occupied by the Albertine and Rhino Grabens shows no indication of flood basalts or any other surface expression of magmatism. Therefore fundamental questions about rift initiation in this part remain unanswered, specifically what controls rift initiation in amagmatic regions? The absence of magma to initiate rifting, or thermally erode the lithosphere (Buck, 2006; Wright et al., 2006) implies other factors are responsible for rift initiation. For example the Western branch of the EARS is highly segmented and is associated with deep (greater than 30 km) seismic events (Craig et al., 2011). What is peculiar is that the Western Branch of the EARS closely follows the western margin of the Tanzanian Craton localized within the Mesoproterozoic-Neoproterozoic Ubendian-Kibaran-Rwenzori Mobile Belt sandwiched between the Tanzanian and the Congo cratons. This suggests that rift extension initiated within pre-existing weaknesses in an otherwise strong and cold cratonic lithosphere. Numerical models suggest that the localization of faults along cratonic margins is related to strength contrast and presence of pre-existing fabrics (Corti et al, 2013). Moreover the presence of

pre-rift lithospheric heterogeneities and variations in lithospheric thickness promotes localization as well as the orientation and polarity of nascent rifting (Korme et al., 2004; Al-Damegh et al., 2005; Van Wijk, 2005). The Western Branch terminates against the Neoproterozoic Aswa Shear Zone (ASZ) a sinistral strike slip deformation belt that may represent an orogenic boundary between the Tanzania Craton to the south and Sahara Metacraton to the north (Abdelsalam et al., 2002, 2011). The ASZ is believed to represent a proto-intercontinental transform where the bifurcation of the rift system from a single discrete rift in southern Ethiopia to two rifts is represented by the Eastern and Western Branches. The ASZ depicts a major gradient in the thickness of the seismogenic zone (Craig et al., 2011). North of the rift bifurcation, the seismogenic zone is at 20 km or less depth whereas it is 20-35 km deep to the south. Therefore we need to answer pertinent question on what is the extent and kinematics of this intra-continental proto-transform ASZ. There are possibly few centers to study rift termination or locked regions that stifle rift propagation and at the same time show rift refraction. This study area provides us with an excellent opportunity to understand the role of mechanical heterogeneity of continental lithosphere on rift propagation. Our poor understanding of the above processes could partly be due to lack of high resolution geophysical data especially aeromagnetic data to characterize the sites or even lack of better sites.

1.3 PRESENT KNOWLEDGE GAP

Understanding the nature of the lithosphere beneath the rifts and surrounding cratons is important for determining what controls extensional localization in the absence of

magmatism to initiate rifting within cold strong continental lithosphere. Therefore this research will answer some of the pertinent questions related to continental rift initiation and evolution including: (1) how is strain accommodated and partitioned throughout the lithosphere and how is strain localized in amagmatic rifts?, 2) how do pre-existing fabrics within the continental lithosphere influence rift initiation and evolution?, 3) how does the presence or absence of an upper mantle plume influence extension? The lack of data has been an impediment in understanding continental rifting. This research uses the Albertine and Rhino Grabens to address this knowledge gap by investigating the role of pre-lithospheric structures in rift initiation and evolution. This has been achieved by testing the following hypothesis that;

1. Pre-existing structures affect the location and orientation of rift propagation through strain localization, transfer, segmentation and termination.

2. In the absence of surface volcanism, strain localization is facilitated by a lithopsheric thermal anomaly.

1.4 RESEARCH OBJECTIVES

In order to address our hypothesis, the fundamental objectives of this research are to: 1. Map in detail the location and orientation of basement structures to determine their role on rift initiation and evolution of the Rhino and Albertine Grabens.

2. Map the extent of the ASZ, determine its kinematics and elucidate its evolution role as a proto-continental transform fault.

3. Determine the thermal structure and crustal thickness beneath the Lakes Edward-George Rift and the Albertine-Rhino Grabens and the surrounding cratons by looking at the lateral variations of heat flow in the lithosphere and how this contributes to strain localization during rift initiation.

Our objectives are best addressed to the northern part of the Western Branch of the EARS occupied by the Albertine and Rhino Grabens (Figures 1B and 2). These sites are critical in that they represent arch type amagmatic rifts, and this provides an opportunity to assess the role of pre-existing structures in rift initiation and propagation. The Grabens show along-strike variation in terms of change in basin architecture and provide a classical example where different rifting processes can be examined such as the role of pre-existing structures on rift localization, strain transfer, rift segmentation and eventual termination. The Western Branch is localized within the Kibaran mobile belt, at the western margin of the Tanzanian Craton (Figure 1B), and this setting allows us the opportunity to understand the role of pre-existing heterogeneities. We used high-resolution airborne geophysical data (aeromagnetic, 3D-FTG and radiometrics) together with SRTM DEM and Satellite gravity data.

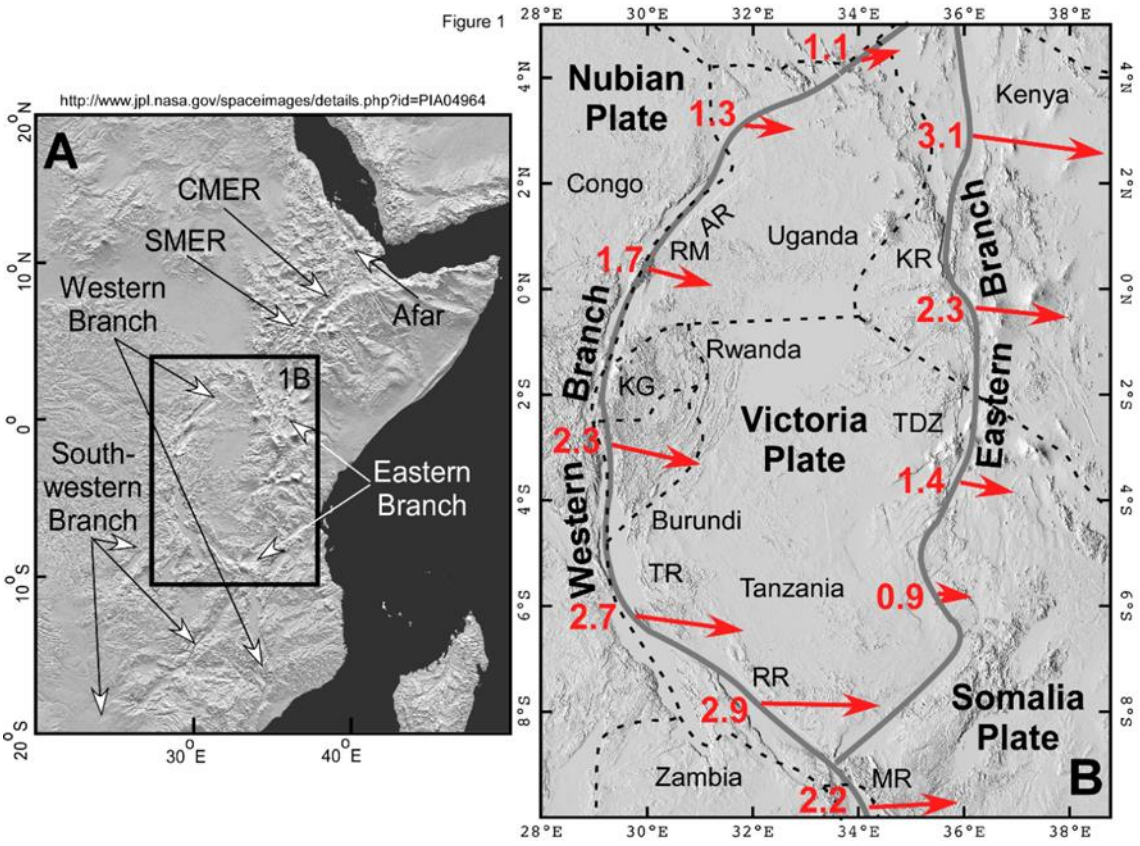

Figure 1: (A): Shuttle Radar Topography Mission (SRTM) Digital elevation Model (DEM) of the East African Rift System (EARS) from www.jpl.nasa.gov and the Eastern and the Western Branches of the EARS (B). CMER = Central Main Ethiopian Rift. SMER = Southern Main Ethiopian Rift. KR = Kenya Rift. TDZ = Tanzania Divergent Zone. AR = Albertine and Rhino Grabens. KG = Kivu Graben. TR = Tanganyika Rift. RR = Rukwa Rift. MR = Malawi Rift. ASZ = Aswa Shear Zone. RM = Rwenzori Mountains. MM = Mitumba Mountains. RV = Rungwe Volcanic Field. Red arrows with numbers represent the angular velocities in mm/year of the Victoria and Somalia plates relative to the Nubia plate as reported by Saria et al., (2014).

1.4 RESEARCH FINDINGS

1.4.1: ROLE OF PRE-EXISTING FABRIC IN THE EVOLUTION OF THE ALBERTINE –RHINO GRABEN.

The development of the Albertine basin as a full-Graben was facilitated by the presence of two NE-trending Grabens connected by a right-stepping transfer zone. The Grabens extend within the Archean–Paleoproterozoic Northeast Congo Block which represents the northeastern extension of the Congo Craton. Our results highlight the importance of pre-existing structures in the evolution of continental rift systems and show the following: (1) The NE-extent of the Albertine full-Graben is controlled by NE-trending Precambrian fabric and the Graben terminates at its northeastern end when it encounters a multiply folded Precambrian basement terrain with poorly-developed NW-trending structural grain. Additionally, the northeastern termination of the Albertine Graben coincides with the presence of NW-trending right-stepping high-density bodies within the Precambrian terrain. (2) The transfer zone between the Albertine and Rhino Grabens is controlled by NE-trending Precambrian structures which might have facilitated the development of relay ramp faults. (3) Strain localization within the better-developed southeastern border fault of the Rhino half-Graben is facilitated by the presence of Precambrian structures better aligned in a NE-direction in the southeastern part of the basin compared to its northwestern part. (4) Further to the northeast, the Rhino Graben is segmented and transitions into a narrower ENE-trending half-Graben with a better-developed border fault on its northwestern side. This segmentation coincides with the presence of N-trending Precambrian structures. (5) The Rhino Graben terminates farther northeast against the NW-trending Precambrian Aswa Shear Zone; a prominent structure with complex, but generally

NW-trending fabric partially due to differences in lithospheric structure and lack of preferably oriented Precambrian structure of the Saharan Metacraton prevented strain from being localized within a narrow rift.

1.4.2: EXTENT, KINEMATICS, AND TECTONIC ORIGIN OF THE PRECAMBRIAN ASWA SHEAR ZONE IN EAST AFRICA

The tectonic evolution of the NW-trending lithospheric scale ASZ based on the kinematics and extent suggest that (1) the ASZ extends in a NW-SE for ~550 km in Uganda and South Sudan. (2) The airborne magnetic and radiometric data revealed a much wider (~50 km) deformation belt than the 5-10 km of exposed surface expression of the ASZ. The deformation belt is defined by three NW-trending sinistral strike-slip shear zones bounding structural domains with magnetic fabrics showing splays of secondary shear zones and shear-related folds. These folds are tight close to the discrete shear zones with their axial traces becoming sub-parallel to the strike of the shear zones. A similar fold pattern is observed in South Sudan in the SRTM DEM. We interpret these folds as due to ENE-WSW contraction associated with the sinistral strike-slip movement. (3) To the northeast, the magnetic patterns suggest a series of W-verging nappes indicative of strong E-W oriented shortening. (4) We relate the evolution of the ASZ to Neoproterozoic E-W collision between East and West Gondwana. This collision produced E-W contraction resulting in W-verging thrusts to the east and a sinistral strike-slip movement along the NW-trending ASZ with strain localization at the boundary between the Saharan Metacraton and the Tanzania craton.

1.4.3: EVOLUTION OF THE MAGMA-POOR ALBERTINE-RHINO GRABEN AND EDWARD-GEORGE RIFT, EAST AFRICAN RIFT SYSTEM THROUGH MANTLE DELAMINATION, MELTING AND PRECAMBRIAN SUTURE ZONE GUIDED FLUID MIGRATION

We found shallower Curie Point Depth (CPD) (~19-22±1 km) and high heat flow (~62-79±0.2 mWm-2) beneath the Edward-George Rift, the southern part of the Albertine Graben and the region between the Albertine and Rhino Graben. In contrast, deeper CPD (~24-26±1 km) and lower heat flow (~57-63 ±0.2 mWm-2) occur beneath the Precambrian basement. We also found thin crust (~25-30 km) beneath the Edward-George Rift, the Rwenzori Mountains and part of the northwestern border fault of the Albertine Graben (Bunia Border Fault) which is characterized by ~3 km high escarpment as well as the region between the Albertine and Rhino Graben. Based on this observation and those of previous studies we propose that strain localization during the initiation of rifting in the northern segments of the Western Branch was facilitated by sub-continental lithospheric mantle delamination beneath the Edward-George Rift, the Rwenzori Mountains, and the Bunia Escarpment of the Albertine Graben. This delamination was accompanied by mantle melting that produced the Toro-Ankole Volcanic Field and resulted in rapid uplift of the Rwenzori Mountains and the Bunia escarpment. Hot fluids generated from the mantle melting were channelized northward and guided by Madi-Igisi Fold and Thrust Belt which marks the remnants of the suture zone. Hence, this migration favored the northern part of the Albertine-Rhino Graben to localize between the two cratonic blocks represented by the North Uganda Terrane and West Nile Terrane.

1.5 RESEARCH SIGNIFICANCE

Different research groups especially Project for Rift Initiation and Development (PRIDE), Geological Process at Rifting and Subducting Margins (GeoPRISMS) and its precursor Margins funded by the National Science foundation (NSF) initiatives selected the EARS aimed at understanding the plate boundary deformation and geodynamic processes controlling rift initiation and propagation and crustal and upper mantle structures. Their broader research aims at answering specific questions such as: (1) how is strain accommodated and partitioned throughout the lithosphere and what are the controls on strain localization and migration. 2) how does mechanical heterogeneity of continental lithosphere influence rift initiation evolution? 3) what factors control the distribution of ponding of volatiles and how are they related to extensional fault systems bounding the rift? 4) how does the presence or absence of an upper mantle plume influence extension?

Our research is timely as it will contribute towards understanding the role of pre-existing structures in rift initiation, what do we know and what has been lacking? This has been due to lack of enough data to characterize these sites and the role of pre-existing entities in rift initiation and evolution. To achieve our objectives we need to study the best sites that have a number of elements involved in rifting processes. The Kenyan Main Rift and the Albertine-Rhino Grabens represent magmatic and amagmatic rifts respectively, and provide excellent locations to answer questions such as what causes continental rifts to initiate, what are the fundamental rifting processes such as tectonic and magmatism and what controls rift architecture at continental rift margins. For example, why is the northern end of the Western Branch is segmented and why does it finally terminate against NW-trending ASZ? This study will improve on the scientific input on the variations between

crustal and upper mantle thermal structures beneath rift basins and surrounding cratons in tectonic rifts. Exploration for hydrocarbons in extensional settings requires an understanding of lithospheric processes that control rift geometry, sediment accumulation and thermal maturity. This research will complement the mineral, oil industry and potential geothermal energy resources, especially in Uganda. The recent discovery of about 3.5 billion barrels of hydrocarbon in the Albertine Graben has renewed interest in the EARS as a potential frontier for hydrocarbons. Other recent discoveries of oil and gas reserves have been reported in the Kenyan Main Rift of the Eastern branch and sizeable gas reserves in the Kivu Sector. The along-rift variation between the well-explored Albertine full Graben and the unexplored Rhino half Graben allows us the opportunity to understand the two different basin architectures in terms of basin evolution and hydrocarbon systems.

1.6. REFERENCES

Abdelsalam, M.G., Liégeois, J.-P., Stern, R.J., 2002. The Saharan Metacraton. Journal of African Earth Sciences 34, 119-136.

Abdelsalam, M.G., S.S. Gao, and J.P. Liegeois, 2011. Upper mantle structure of the Saharan Metacraton. Journal of African Earth Sciences 60, 328-336.

Adams, A., Nyblade, A., Weeraratne, D., 2012. Upper mantle shear wave velocity structure beneath the East African plateau: evidence for a deep, plateauwide low velocity anomaly. Geophysical Journal International 189, 123-142.

Agostini, A., Bonini, M., Corti, G., Sani, F., Mazzarini, F., 2011. Fault architecture in the Main Ethiopian Rift and comparison with experimental models: Implications for rift evolution and Nubia–Somalia kinematics. Earth and Planetary Science Letters 301, 479-492.

Al-Damegh, K., Sandvol, E., Barazangi, M., 2005. Crustal structure of the Arabian plate: new constraints from the analysis of teleseismic receiver functions. Earth and Planetary Science Letters 231, 177-196.

Buck, W.R., 2006. The role of magma in the development of the Afro-Arabian Rift System. Geological Society of London Special Publications 259, 43-54.

Buck, W.R., 2004. Consequences of asthenospheric variability on continental rifting. Rheology and deformation of the lithosphere at continental margins. Columbia University Press, New York 1-30.

Craig, T.J., Jackson, J.A., Priestley, K., McKenzie, D., 2011. Earthquake distribution patterns in Africa: their relationship to variations in lithospheric and geological structure, and their rheological implications. Geophysical Journal International 185, 403-434.

Corti, G., Iandelli, I., Cerca, M., 2013. Experimental modeling of rifting at craton margins. Geosphere 9, 138-154.

Ebinger, C., Casey, M., 2001. Continental breakup in magmatic provinces: An Ethiopian example. Geology 29, 527-530.

Ebinger, C.J., Keir, D., Ayele, A., Calais, E., Wright, T.J., Belachew, M., Hammond, J.O.S., Campbell, E., Buck, W.R., 2008. Capturing magma intrusion and faulting processes

during continental rupture: seismicity of the Dabbahu (Afar) rift. Geophysical Journal International 174, 1138-1152.

Grandin, R., Socquet, A., Binet, R., Klinger, Y., Jacques, E., de Chabalier, J.B., King, G.C.P., Lasserre, C., Tait, S., Tapponnier, P., Delorme, A., Pinzuti, P., 2009. The September 2005 Manda Hararo-Dabbahu rifting event, Afar (Ethiopia): Constraints provided by geodetic data. Journal of Geophysical Research: Solid Earth 114, B08404.

Jakovlev, A., Rümpker, G., Schmeling, H., Koulakov, I., Lindenfeld, M., Wallner, H., 2013. Seismic images of magmatic rifting beneath the Western branch of the East African rift. Geochemistry, Geophysics, Geosystems 14, 4906-4920.

Keranen, K.M., Klemperer, S.L., Julia, J., Lawrence, J.F., Nyblade, A.A., 2009. Low lower crustal velocity across Ethiopia: Is the Main Ethiopian Rift a narrow rift in a hot craton? Geochemistry Geophysics Geosystems 10, 1525-2027.

Korme, T., Acocella, V., Abebe, B., 2004. The Role of Pre-existing Structures in the Origin, Propagation and Architecture of Faults in the Main Ethiopian Rift. Gondwana Research 7, 467-479.

MacDonald, R., Rogers, N., Fitton, J., Black, S., Smith, M., 2001. Plume–lithosphere interactions in the generation of the basalts of the Kenya Rift, East Africa. Journal of Petrology 42, 877-900.

Meert, J. G. and B. S. Lieberman 2008. The Neoproterozoic assembly of Gondwana and its relationship to the Ediacaran–Cambrian radiation. Gondwana Research 14, 5-21.

Morgan, P., Baker, B.H., 1983. Introduction—processes of continental rifting. Tectonophysics 94, 1-10.

Mulibo, G., Nyblade, A., 2009. The 1994–1995 Manyara and Kwamtoro earthquake swarms: variation in the depth extent of seismicity in northern Tanzania. South African Journal of Geology 112, 387-404.

Nyblade, A. A., 2002. Crust and upper mantle structure in East Africa: Implications for the origin of Cenozoic rifting and volcanism and the formation of magmatic rifted margins. Volcanic rifted margins 362: 15.

Van Wijk, J., 2005. Role of weak zone orientation in continental lithosphere extension. Geophysical research letters 32, L02303.

Wölbern, I., Rümpker, G., Link, K., Sodoudi, F., 2012. Melt infiltration of the lower lithosphere beneath the Tanzania craton and the Albertine rift inferred from S receiver functions. Geochemistry, Geophysics, Geosystems 13 1525-2027.

Wright, T.J., Ebinger, C., Biggs, J., Ayele, A., Yirgu, G., Keir, D., Stork, A., 2006. Magma-maintained rift segmentation at continental rupture in the 2005 Afar dyking episode. Nature 442, 291-294.

PAPER I

THE ROLE OF PRE-EXISTING PRECAMBRIAN STRUCTURES IN RIFT EVOLUTION: THE ALBERTINE AND RHINO GRABENS, UGANDA

2.0 ABSTRACT

We integrated Shuttle Radar Topography Mission (SRTM) Digital Elevation Models (DEM), airborne magnetic, radiometric and three-dimensional Full Tensor Gravity Gradiometry (3D-FTG) data to investigate the role of Precambrian structures in the evolution of the largely amagmatic Miocene–Recent aged Albertine and Rhino Grabens in Uganda. These Grabens represent the northern segment of the Western Branch of the East African Rift System (EARS). The two NE-trending Grabens are connected by a right-stepping transfer zone and they extend within the Archean–Paleoproterozoic Northeast Congo Block which represents the northeastern extension of the Congo craton. Our results show the following and highlight the importance of pre-existing structures in the evolution of continental rift systems: (1) The NE-extent of the Albertine full Graben is controlled by NE-trending Precambrian fabric and the Graben terminates at its northeastern end when it encounters multiple folded Precambrian basement terrain with poorly developed NW-trending structural grain. Additionally, the northeastern termination of the Albertine Graben coincides with the presence of NW-trending right stepping high density bodies within the Precambrian terrain. (2) The transfer zone between the Albertine and Rhino Grabens is controlled by NE-trending Precambrian structures which might have facilitated the development of relay ramp faults. (3) Strain localization within the better-developed southern border faults of the Rhino Graben is facilitated by the presence of Precambrian structures better aligned in a NE-direction in the southeastern part of the basin compared to its northwestern part.

(4) Further to the northeast, the Rhino Graben is segmented and transitions into a narrower ENE-trending half-Graben with a better-developed border fault on its northwestern side. This segmentation coincides with the presence of N-trending Precambrian structures. (5) The Rhino Graben terminates farther northeast against the NW-trending Precambrian Aswa Shear Zone; a prominent structure with complex, but generally NW-trending fabric.

2.1 INTRODUCTION

Continental rifts are widespread extensional structures on Earth and have occurred from the Archean to the Present. The study of these extensional structures remains of great interest because: (1) They represent the initial stages of continental breakup transitioning into seafloor spreading and continental passive margins; (2) They are sites of thick sediments accumulation, with the potential to form and trap hydrocarbon resources. Rift systems and passive continental margins have provided the oil and gas industry with ~61% of global hydrocarbon discoveries, while rift systems alone account for ~30% of these discoveries (Fraser et al., 2007); and (3) They are sites of geologic hazards such as earthquakes, volcanism and associated poisonous gas emissions and landslides (Abdelsalam et al., 2004). Progress has been made in understanding the evolution of continental rifting. However, major process-oriented questions such as how strain is localized and partitioned, what controls rift segmentation and how it affects basins' architecture remain unanswered, especially for largely amagmatic rift systems. Relevant to this study are a number of questions that need to be addressed: (1) What is the role of pre-existing Precambrian structures in strain localization during the early stages of extension in dominantly amagmatic rifts? (2) What are the relative roles of the thickness and rheology of the Precambrian lithosphere and shallow regional fabric representing the inherited anisotropy in shaping rift architecture? (3) How do pre-existing structures influence strain transfer and rift segmentation? and (4)What controls continental rift termination? Geological and geophysical observations from the East African Rift System (EARS; Fig. 1A) suggest that pre-existing structures can influence the evolution of continental rift systems

at different scales. For example, at the regional scale, the Western Branch of the EARS developed within Precambrian entities in the northwestern, western and southwestern margin of the Tanzania craton (Fig. 2). The northern segment of the

Western Branch (represented by the Albertine and Rhino Grabens (Figs. 1B and 3), the focus of this study) extends in a NE–SW direction within the Northeast Congo Block (representing the northeastern edge of the Congo craton) in the north and the Ruwenzori fold belt to the south (Fig. 2; Tack et al., 2010; Fernandez-Alonso et al., 2012; Nyakecho and Hagemann, 2014). Begg et al. (2009) and Westerhof et al. (2014) suggested that the trace of this part of the Western Branch follows a fundamental tectonic boundary separating different bocks of Archean cratons represented by the Ugandan craton or Northern Uganda Terrane in the east and the Bomu–Kibalian shield or the West Nile Block to the west (Fig. 4). The central part of the Western Branch, approximately from Lake Edward to the northern half of Lake Tanganyika, extends in a N–S direction within the Kibara and Karagwe–Ankole orogenic belt (Fig. 2; Tack et al., 2010; Aanyu and Koehn, 2011; Fernandez-Alonso et al., 2012). From the southern half of Lake Tanganyika to the Rungwe volcanic field at the northern tip of Lake Malawi the Western Branch extends in a NW–SE direction within the Ubende orogenic belt (Daly, 1986; Delvaux et al., 2012; Lenoir et al., 1994).This work examines the role of pre-existing Precambrian structures in strain localization and transfer, and rift segmentation and termination in largely amagmatic rifts. It focuses on the NE-trending Albertine and Rhino Grabens in Uganda which represent the northeastern part of the Western Branch of the EARS (Fig. 1B). The major processes required for the initiation of rifting remain controversial. For example, studies by Hayward and Ebinger (1996) and Buck (2006) have advocated for the important role of magmatism in the initiation of continental rifting suggesting that the forces driving the tectonic plates such as slab pull are insufficient to rupture normal continental lithosphere. Analog models suggest that magma plays an important role in softening the lithosphere, enhancing lithospheric stretching and strain localization (Buck, 2006). Indeed, magma

is documented to have played an important role in initiating continental rifting in the Eastern Branch of the EARS especially the Main Ethiopian Rift and the Afar Depression (Fig. 1A; Ebinger and Casey, 2001; Kendall et al., 2005; Wright et al., 2006). This work benefited from the availability of high-resolution airborne magnetic, radiometric and gravity data for mapping regional Precambrian structures which are barely exposed at the surface. Additionally, Digital Elevation Models (DEMs) extracted from the Shuttle Radar Topography Mission (SRTM) data were used to map the Miocene–Recent structures associated with the Albertine and Rhino Grabens. The aim of the work is to examine in detail the complex interplay between the Precambrian and Miocene–Recent structures, not only parallelism, but also the complex interaction between the two structural sets when their trends depart from parallelism.

2.2 TECTONIC SETTING

2.2.1. THE EAST AFRICAN RIFT SYSTEM (EARS)

The Albertine and Rhino Grabens occupy an important location within the EARS. They represent part of the extensional structures showing the bifurcation of the rift system from a single discrete rift in central Ethiopia (the Central Main Ethiopia Rift) to two rifts represented by the Eastern and Western Branches (Fig. 1A). Buck (2006) and Corti et al. (2013) suggested that the bifurcation of the EARS around the Tanzania craton (Fig. 2) demonstrates the inability of continental rifts to propagate through thick cratonic lithospheres. In addition, the bifurcation of the EARS is associated with a number of important tectonic elements: (1) It coincides with the trace of the NW-trending Neoproterozoic Aswa Shear Zone, which represents a fundamental lithospheric-scale boundary between the Northeast Congo Block in the southwest and the Saharan Metacraton to the northeast (Fig. 2; Abdelsalam et al., 2002, 2011). Seismic tomography imaging has shown that the lithospheric thickness of the Saharan Metacraton is ~100 km compared to the ~250 km of the

lithospheric thickness of the Northeast Congo Block (Abdelsalam et al., 2011). (2) It also coincides with a change in the depth of the seismogenic zone (Craig et al., 2011). North of the rift bifurcation, the depth of the seismogenic zone is 20 km or less whereas it is between 20 and 35 km deep to the south. Northeast of the bifurcation, the EARS is represented by the Southern Main Ethiopian Rift where extensional strain is broadly distributed (Fig. 1A) leading some researchers to refer to this segment of the Main Ethiopian Rift as the 'Ethiopian Basin and Range' (Bonini et al., 2005; Chorowicz, 2005; Corti et al., 2011). The EARS to the south of the Southern Main Ethiopian Rift narrows into the Kenyan rift in the north and the Tanzanian divergent zone to the south which represent the Eastern Branch (Fig. 1B)

2.2.2. THE WESTERN BRANCH

The Western Branch starts from the NE-trending Albertine and Rhino Grabens through the N-trending Kivu Graben into the NW-trending Tanganyika rift (Fig. 1B). It continues further southeast into the NW- trending Rukwa rift before entering the N-trending Malawi rift (Fig. 1B; Kampunzu et al., 1998). Rift initiation in the Western Branch is suggested to have started ~12Ma ago, later than the ~20Ma rift initiation of the Eastern Branch (Cohen et al., 1993; Ebinger, 1989). However, a recent study from the Rukwa rift using 40Ar/39Ar and U–Pb age dating of volcanic tuffs, detrital zircon for sediments provenance, change in sedimentological depositional environment and flow direction of ancient rivers found that by 26–25 Ma the Rukwa rift was a well-developed basin bounded by border faults and uplifted shoulders as well as witnessing volcanic activities (Roberts et al., 2012). The Western Branch is largely amagmatic with the exception of small outcrops of Pliocene–Pleistocene volcanic fields including Toro-Ankole, Virunga, Bukavu, Mwenga–Kamituga and Rungwe which appear to occupy the tips of various rift segments (Fig. 2; Kampunzu et al., 1998). From seismic studies melt infiltration to at least the base

of the crust is inferred beneath the southern part of the Albertine Graben around the Ruwenzori Mountains (Fig. 1B) with possible lower lithospheric melt accumulation to the east of the rift itself (Jakovlev et al., 2013). Additionally, seismic studies from the southern margin of the Albertine Graben show evidence of a thinned lithosphere beneath the rift reaching ~125 km compared to ~210 km to the east within the Tanzania craton (Wölbern et al., 2012). The seismic data also show a mid-lithospheric discontinuity interpreted to represent the boundary between pristine upper lithosphere and a heavily metasomatized lower lithosphere (Adams et al., 2012; Wolbern et al., 2012).

Building on previous studies (Calais et al., 2006; Stamps et al., 2008) Saria et al. (2014) presented a refined kinematic model for the EARS based on Global Position System (GPS) measurement, earthquakes slip vector and transform fault azimuth data. In this model, the kinematics of the Eastern and Western Branches are interpreted to be largely controlled by the motion of the Victoria plate (represented by the Tanzania craton) between the Nubian and Somalian plates (Fig. 1B). Saria et al. (2014) found that the best "t model of the data used in the study favors an eastward movement of the Victoria plate away from the Nubian plate (along the Western Branch from the Rhino Graben to Rukwa rift) with the plate's angular velocity increasing from 1.1 mm/year in the north to 2.9 mm/year to the south (Fig. 1B). Differently, this model prefers a decrease of the eastward motion of the Somalian plate relative to the Nubian plate (along the Eastern Branch) from 3.1 mm/year in the north to 0.9 mm/year to the south (Fig. 1B).

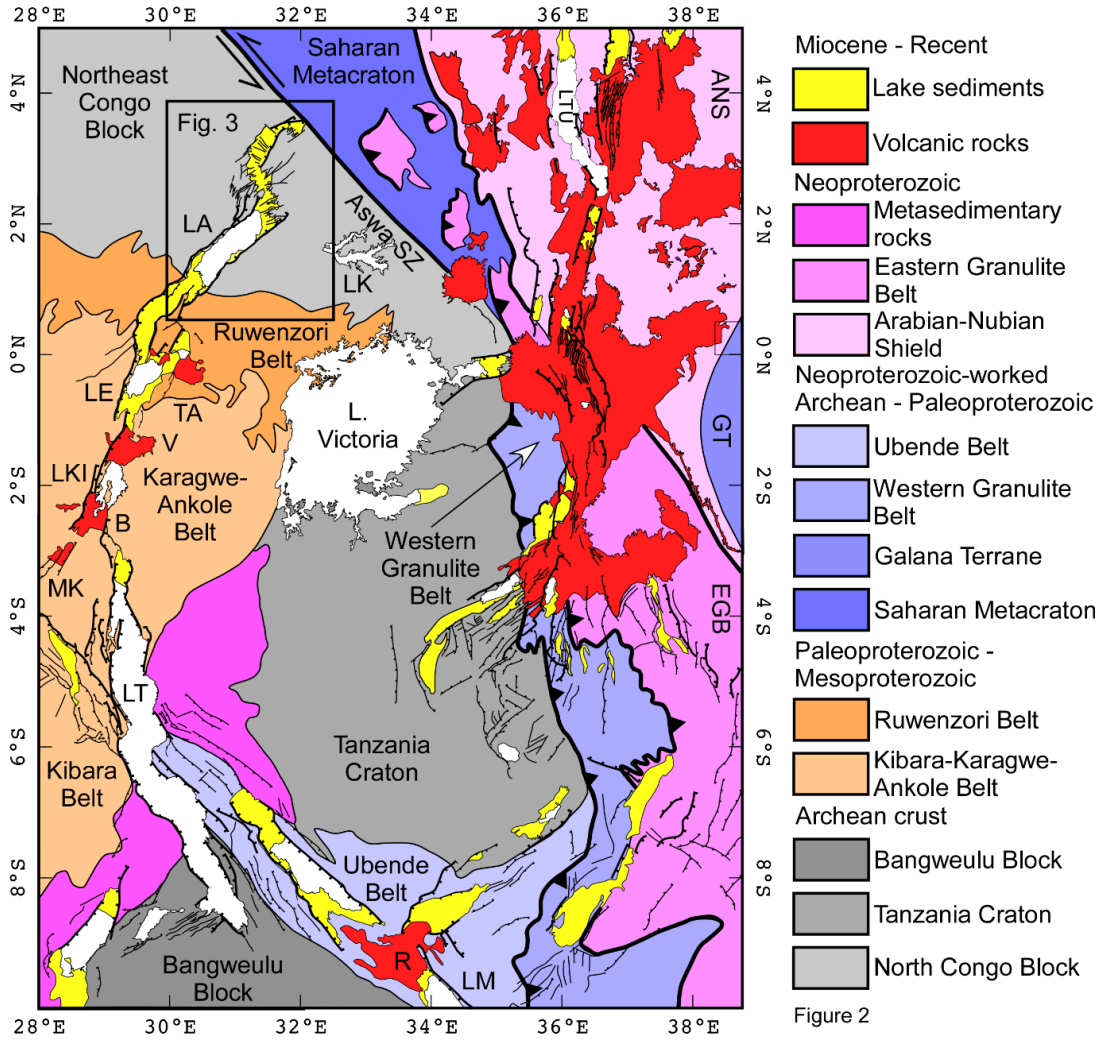

Figure 2: Tectonic map of the Eastern and Western Branches of the East African Rift System (EARS). The normal faults and lake sediments are interpreted from the Shuttle Radar Topography Mission (SRTM) Digital Elevation Model (DEM) in Fig. 1B. The spatial extent of the Miocene–Recent volcanic rocks are modified from Chorowicz (2005) for the Eastern Branch and Kampunzu et al. (1998) and Nyakecho and Hagemann (2014) for the Western Branch. Boundaries of different Precambrian entities are modified from Tack et al. (2010), Fernandez-Alonso et al. (2012) and Fritz et al. (2013). ANS=Arabian–Nubian Shield, EGB=Eastern Granulite Belt, GT=Galana Terrane. The volcanic fields in the Western Branch are Toro Ankole (TA), Virunga (V), Bukavu (B),

Mwenga–Kamituga (MK), and Rungwe (R). The lakes are Albert (LA), Kyoga (LK), Kivu (LKI), Tanganyika (LT), Turkana (LTU), and Malawi (LM).

2.2.3. THE ALBERTINE AND RHINO GRABENS

The Albertine Graben extends in a NE-direction from the Ruwenzori Mountains for ~200 km with a uniform width of 60 to 80 km and well-developed topographic escarpments defining the border faults (Fig. 3).It is described as an asymmetrical full Graben with well-developed border faults (Ebinger, 1989). The northwestern escarpment of the Graben represents the surface expression of the Bunia fault with escarpment significantly higher than the southeastern escarpment, reaching in places ~1300 m compared to the ~400 m height of the southeastern escarpment (Fig. 5A). The Albertine and Rhino Grabens extend, for the large part within the Archean Northeast Congo Block with the exception of the southernmost part of the Grabens where the Paleoproterozoic–Mesoproterozoic Ruwenzori fold belt is exposed (Figs. 2 and 4; Tack et al., 2010; Fernandez-Alonso et al., 2012; Nyakecho and Hagemann, 2014). The Northeast Congo Block represents the exposures of the Congo craton in northeastern Congo and northwestern Uganda. Based on synthesis of published geological data, Begg et al. (2009) divided the Northeast Congo Block into the Bomu–Kibalian shield in the west and the Ugandan craton to the east (Fig. 4). Also, based on geological and geochronological studies, Westerhof et al. (2014) proposed dividing the Northeast Congo Block into the North Uganda Terrane east of the Albertine and Rhino Grabens and the West Nile Block west of the Grabens (Fig. 4). Begg et al. (2009) stated that Archean granulites that experienced ultra-high pressure metamorphism at ~2.4 Ga are present within the Ugandan craton, hence this cratonic block must be fundamentally different from the Bomu–Kibalian shield west of the Albertine–Rhino Grabens. Both Begg et al. (2009) and Westerhof et al. (2014) suggested that the boundary between the Ugandan craton–North Uganda Terrane and the Bomu–Kibalian shield–

West Nile Block might be found under the Western Branch of the EARS (Fig. 4). Further, Westerhof et al. (2014) mapped a number of Precambrian SE and NW-verging thrust faults that coincides with the proposed boundary between the two cratonic blocks (Fig. 4).

Interpretation of airborne magnetic and radiometric data, together with previously published maps, enabled Nyakecho and Hagemann (2014), Ruotoistenmaki (2014) and Westerhof et al. (2014) to establish the spatial extent of major lithological units constituting the Northeast Congo Block and the Ruwenzori fold belt in northwestern Uganda (Fig. 4).Most of the Northeast Congo Block is dominated by Mesoarchean and Neoarchean granitoids, gneisses, granulites and charnockites (Fig. 4). However, within this block less abundant Mesoproterozoic and Neoproterozoic volcano-sedimentary rocks and granitoids are also exposed (Fig. 4). The Ruwenzori fold belt contains heterogeneous interfolded units of Paleoproterozoic granitic gneisses, metasedimentary and meta-volcanic rocks and granites (Fig. 4).

The Albertine Graben is filled with Miocene–Recent sedimentary rocks in the form of sandstones and shales derived from the surrounding Precambrian rocks. These sediments are thicker in the northwestern part of the Graben reaching ~5400 m compared to ~1250 m in the southeastern side of the Graben (Ring, 2008; Upcott et al., 1996). This together with the escarpment heights (Fig. 5A), suggests a maximum vertical throw of ~6700 m in the northwestern border fault of the Albertine Graben and 1650 m in its southeastern border fault.

Little information is available about the Rhino Graben and all studies have assumed that it represents the northeastern extension of the Albertine Graben (Corti et al., 2011; Ebinger, 1989). It constitutes a NE-trending segment in the southwest and an ENE-trending segment in the northeast (Fig. 3). Observations from the SRTM DEM show that the Graben narrows from a ~40 km width in the southwest to ~10 km width to the northeast (Figs. 3 and 5B and C). Additionally, the surface

topography suggests that the southwestern part of the Rhino is a SE-dipping half-Graben whereas it is a NW-dipping half-Graben in the northeast (Fig. 5B and C).

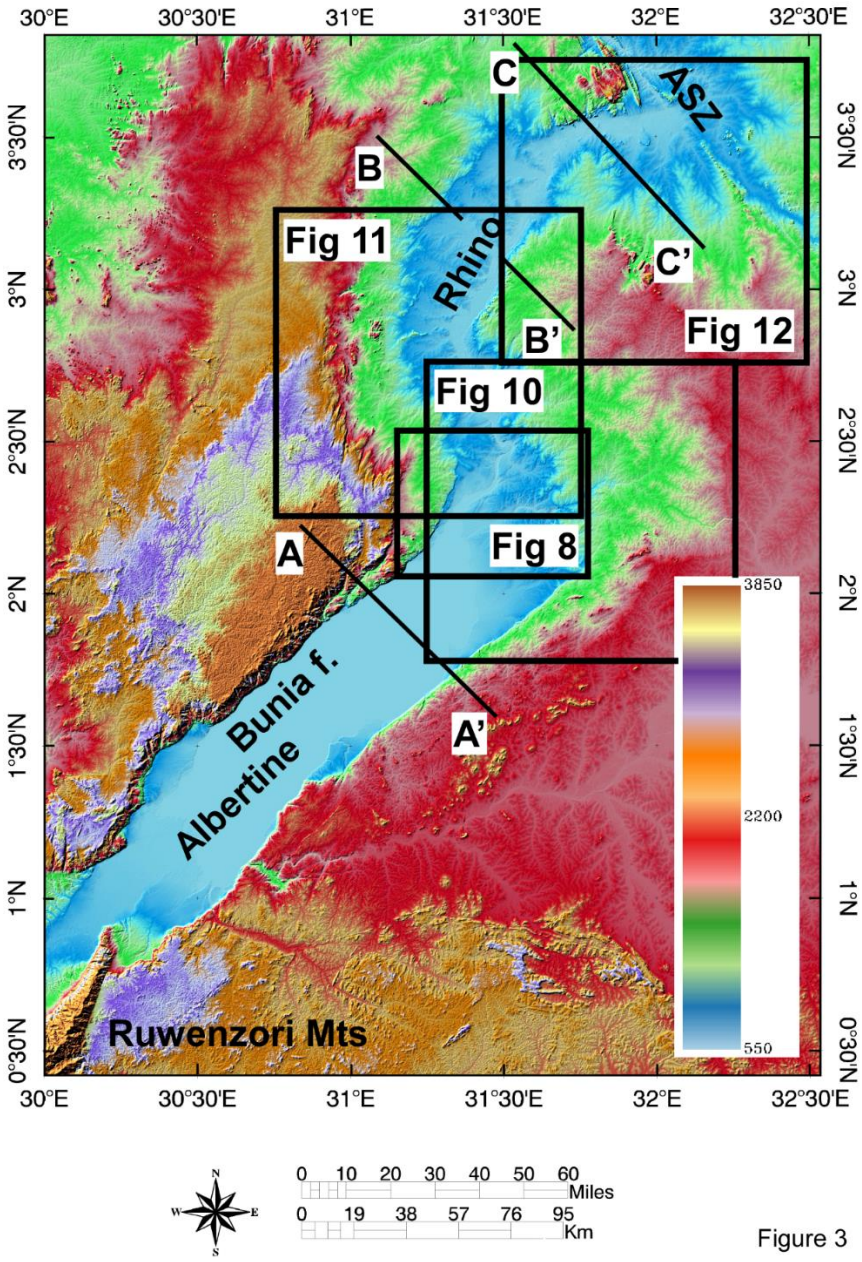

Figure 3: Shuttle Radar Topography Mission (SRTM) Digital Elevation Model (DEM) of the Albertine and Rhino Grabens.

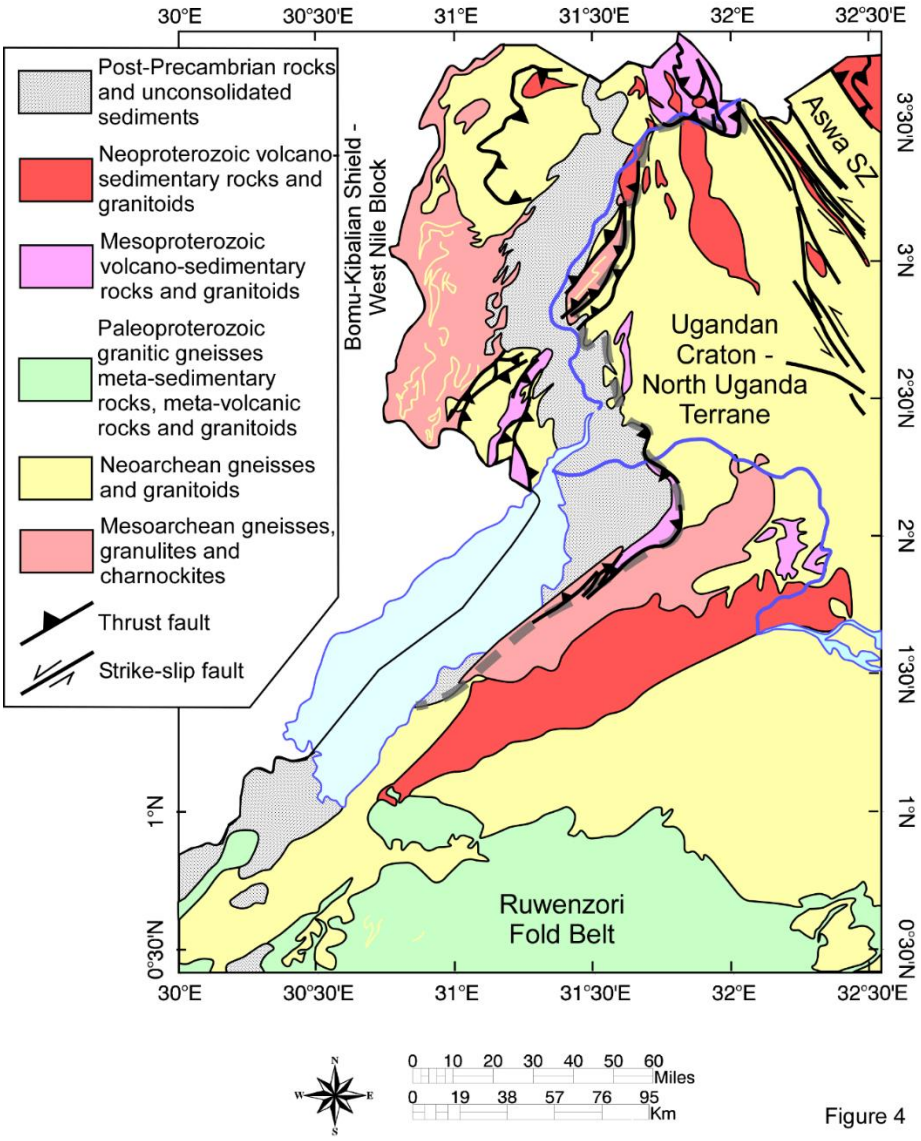

Figure 4

Figure 4: Generalized geological map of northwestern Uganda (modified after Nyakecho and Hagemann, 2014; Ruotoistenmaki, 2014; Westerhof et al., 2014). The dashed gray line is the suggested boundary between the Bomu–Kibalian shield–West Nile Block and the Ugandan craton–North Uganda Terrane.

Figure 5

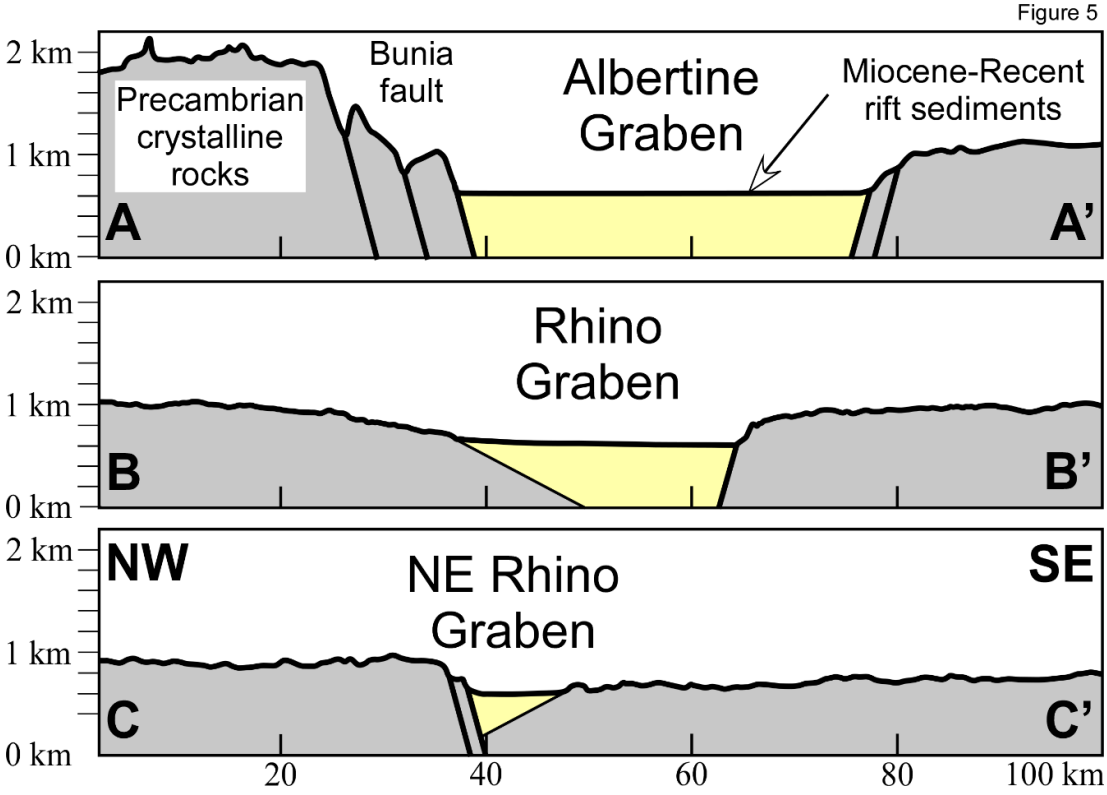

Figure 5: Geological sections across the central Albertine Graben (top), the central Rhino Graben (center), and the northeastern part of the Rhino Graben (bottom). See Fig. 3 for location of the geological cross-sections baselines. Vertical Exaggeration (VE) =10.

2.3. DATA AND METHODS

We used airborne magnetic, radiometric and high resolution Full Tensor Gravity Gradiometry (3D-FTG) data in addition to SRTM DEM to examine the role of pre-existing Precambrian structures in the evolution of the Albertine and Rhino Grabens.

2.3.1. AIRBORNE MAGNETIC DATA

The magnetic data (Fig. 6) were acquired between 2006 and 2009 by the Ugandan Government through the Geological Survey and Mineral Department to cover ~80% of the country. The data were collected with a flight altitude of ~80 m and line spacing of ~200 m oriented at 55°. A magnetic anomaly map was developed by subtracting the International Geomagnetic Reference Field (IGRF) of 2005 from the measured total magnetic field. The magnetic inclination in the study region varies between −14° and −22° and this low inclination of the magnetic field makes it difficult to identify the sources of the magnetic anomalies using conventional methods such as reduction to the pole (RTP). We applied the horizontal derivative filter to the total intensity magnetic anomaly for the data covering northwestern Uganda including the Albertine and Rhino Grabens (Fig. 6). The horizontal derivative method focuses on imaging the edges of the magnetized bodies along and in between fight lines. The advantage of this filter is that it is not affected by inclination, declination and remanence and hence is a good edge detection tool (Smith and Salem, 2005; Thurston and Smith, 1997). To enhance the magnetic linear features associated with the Precambrian structures, we applied a high-frequency spatial filtering on the total magnetic field to create a horizontal derivative image (Fig. 6). This method is most effective in imaging anomalies from shallow depths as a response to rock types with relatively large contrasts in magnetization and this amplifies the signature of the Precambrian structures.

In order to quantify the dips of the Precambrian structures, we developed a tilt angle image by obtaining the ratio of vertical derivative to horizontal derivative grids (Salem et al., 2007; Smith and Salem, 2005; Thurston and Smith, 1997). The calculated tilt angles ranges between +90° and −90°. The angle values with (+) sign represent the variation of the tilt within the magnetic source, the angle values with (−) sign quantify the tilt variation outside the magnetic source, and the zero degree values lies over the edges of the magnetic source (Salem et al., 2007). This tilt distribution

happens across the contacts between high and low susceptibility geological materials (Salem et al., 2007). The tilt angle image will be discussed later under the results section.

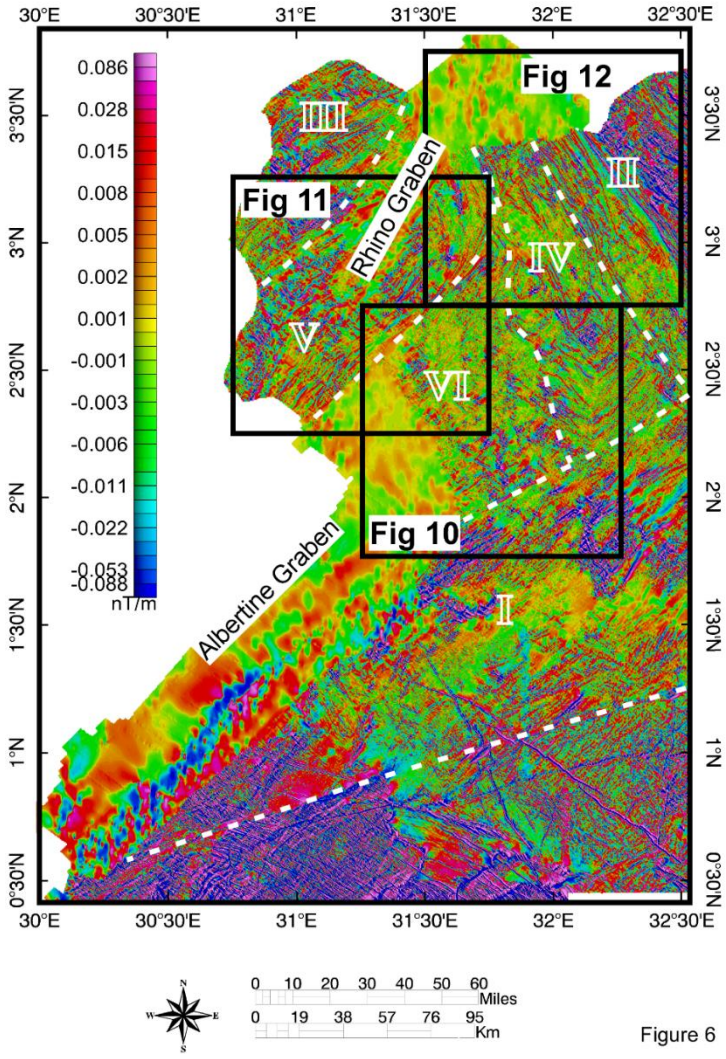

Figure 6. Horizontal derivative airborne magnetic map of northwestern Uganda including the southeastern part of the Albertine Graben and the entire Rhino Graben. The numbers I–VI are the structural domains bounded by the dashed white lines.

2.3.2. AIRBORNE RADIOMETRIC DATA

The radiometric data (Fig. 7) were simultaneously acquired with the airborne magnetic data using the same flight parameters. The radioactive decay of naturally occurring gamma rays has proven useful for mapping geological materials (Duval, 1983; Minty, 1997). Potassium (40K) decays to stable argon (40Ar) through the emission of gamma rays, hence this radioactive decay process can be used to directly estimate the amount of K in the rocks. Uranium (U) occurs in nature as radioisotopes 238U and 235Uwhich decay to stable lead isotopes 206Pb and 207Pb, respectively. Thorium (Th) occurs naturally as radioisotope 232Th whose decay series terminates into 208Pb. Neither isotope 238U nor 232Th emits gamma rays during their radioactive decay cycle. However, the concentration of these radioisotopes can be estimated from gamma ray emission of their radioactive daughter products.

Interpretation of radiometric data depends on the assumption that the radioactive daughter products are under equilibrium, therefore the concentration estimations are based on equivalents eU and eTh in parts per million (ppm). Gamma ray surveys are therefore a direct measurement of the geochemical distribution of radioelements from the upper 30 cm of the Earth surface (Erdi-Krausz et al., 2003). Numerous low-lying Precambrian outcrops are exposed in northwestern Uganda (Westerhof et al., 2014), hence we believe that the radiometric signatures we are using in this study dominantly reflect the composition of the Precambrian rocks rather than the unconsolidated sedimentary overburden.

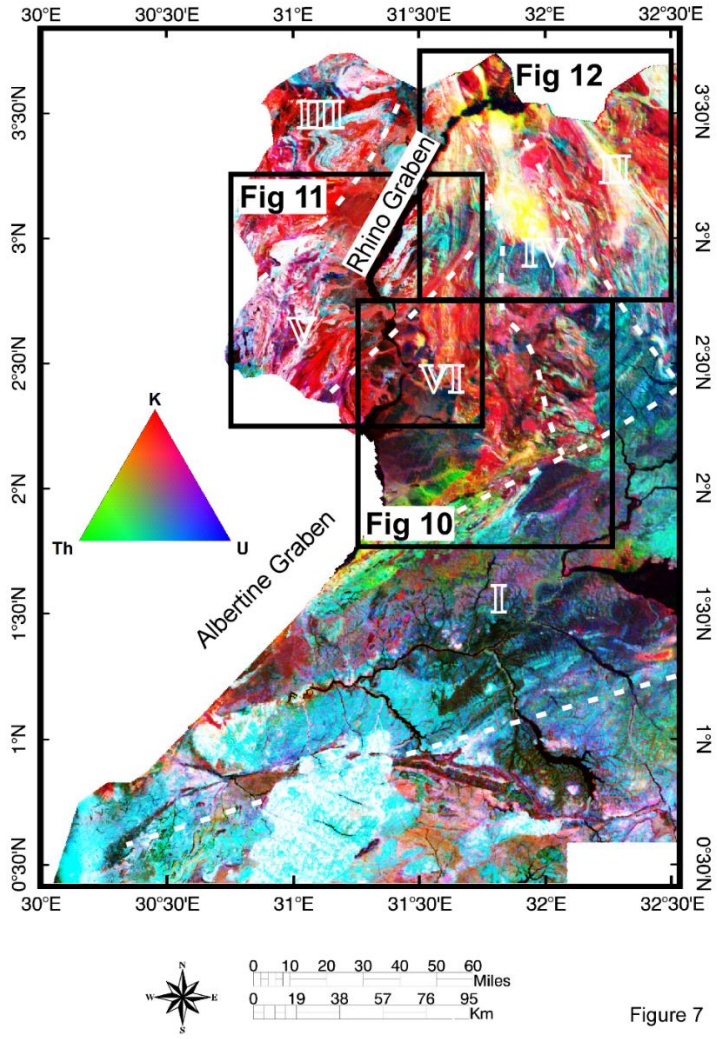

Figure 7: Ternary image of the airborne radiometric data of northwestern Uganda including the southeastern part of the Albertine Graben and the entire Rhino Graben. The numbers I–VI are the structural domains bounded by the dashed white lines.

We processed the airborne radiometric data by the minimum curvature gridding algorithm (Briggs, 1974; Grasty, 1997; Grasty et al., 1997; Minty and McFadden, 1998) to obtain K, eTh, eU and total count on a grid cell size of 50 m. The noise from the data was removed by the noise-adjusted singular value decomposition method. We used these data to create a ternary image where K is

represented as red, eTh as green and eU as blue (Fig. 7). Areas with high K and Th concentrations appear yellow, those with high K and U concentrations are highlighted in magenta, whereas those with high Th and U concentrations are depicted as cyan. White areas indicate regions with high concentrations of all K, Th and U, whereas areas shown in black color such as water bodies reflect the absence of all the radioelements (Fig. 7).

2.3.3. THREE-DIMENSIONAL FULL TENSOR GRAVITY GRADIOMETRY (3D-FTG) DATA

The high resolution airborne 3D-FTG data over the northeastern part of the Albertine Graben (Fig. 8) was acquired by Tullow Oil at a flight height of ~80 m and line spacing of ~150 m. These data are composed of three vectors (Gx, Gy and Gz) where each vector contains three gradients that represent the rate of change of the vector in three orthogonal directions producing nine cross-line tensor gradients. The 3D-FTG data we used were already line-leveled, corrected for the terrain elevation change, modeled for bathymetry response using the density of 1.0 g/cm3 and processed for Bouguer correction using the density of 2.67 g/cm3.

To delineate Precambrian structures we produced a 3D-FTG image from the Tzz tensor component (Fig. 8) based on the method of invariant computation equations (Dickinson et al., 2009). This image provides an independent measure of the 3D density distributions and resolves relatively small structures with a small density contrast. The vertical tensor component (Tzz) measures the plan view of density changes. The 3D-FTG image revealed the presence of prominent NW-trending structures at the northeastern end of the Albertine Graben and strong NE-trending pattern within the Graben (Fig. 8).

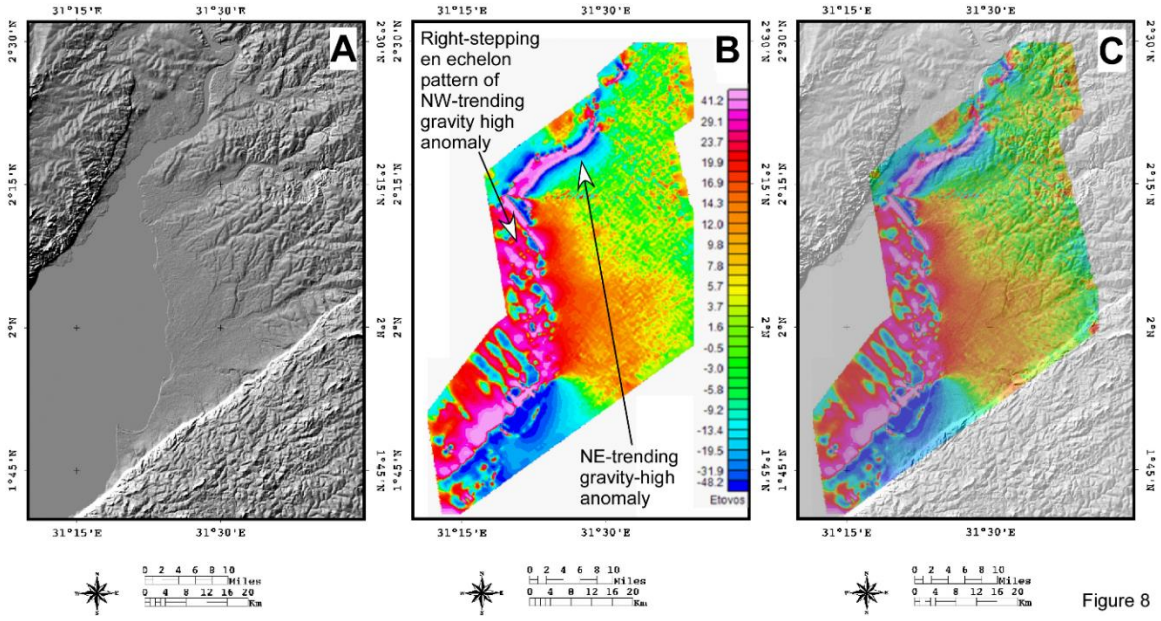

Figure 8: (A) Shuttle Radar Topography Mission (SRTM) Digital Elevation Model (DEM) of the northeastern part of the Albertine Graben. (B) Three-dimensional Full Tensor Gravity Gradiometry (3D-FTG) image covering the same area covered by the SRTM DEM. (C) Overlay of the 3D-FTG image onto the SRTM DEM.

2.4. RESULTS

2.4.1. PRECAMBRIAN STRUCTURAL DOMAINS

The horizontal derivative airborne magnetic (Fig. 6) and the ternary airborne radiometric images (Fig. 7) allowed us to establish a number of structural domains dominated by different orientations of the Precambrian regional fabric and different lithologies. We discuss the structural and lithological characteristics of these domains and compare these characteristics with the geological map in Fig. 4 which is compiled from Nyakecho and Hagemann (2014), Ruotoistenmaki (2014) and Westerhof et al. (2014): (1) The region in the southeastern part of the study area (labeled I in

Figs. 6 and 7) is dominated by NE-trending fabric (Fig. 6) and lithologies with high U concentration (Fig. 7). This domain corresponds to the NE-trending belt of Mesoarchean gneisses, granulites and charnockites and Neoproterozoic volcano-sedimentary rocks and granulites (Fig. 4). The northeastern boundary of this domain coincides with mapped SE-verging thrust faults (Fig. 4). (2) The domain in the northeastern part of the study area (labeled I in Figs. 6 and 7) shows strong NW-trending fabric (Fig. 6) and lithologies with high K, U and Th or K concentration (Fig. 7). This region constitutes part of the Neoarchean gneisses and granitoids Terrane where NW-trending strike-slip faults are mapped (Fig. 4). Both domains I and II are within the Ugandan craton–North Uganda Terrane (Fig. 4). (3) The northwestern part of the study area (labeled III in Figs. 6 and 7) shows complex fold patterns defined by the magnetic anomalies (Fig. 6) and alternation of lithologies with high K, U and K interleaved within lithologies with high K concentration (Fig. 7).

This region corresponds to the Bomu–Kibalian shield–West Nile Block where Mesoarchean gneisses, granulites and charnockites are interfolded with Neoarchean gneisses and granitoids (Fig. 4). (4) The north-central part of the study area is dominated by the Neoarchean gneisses and granitoids of the Ugandan craton, North Uganda Terrane and a NW-trending belt of Mesoproterozoic–Neoproterozoic volcano-sedimentary rocks and granitoids (Fig. 4). This region is divided into three domains. The eastern domain (labeled IV in Figs. 6 and 7) shows magnetic anomaly pattern defining N-trending folds (Fig. 6) with its northern part dominated by lithologies with high K, U and Th concentration (corresponding to the Mesoproterozoic–Neoproterozoic belt) and its southern part with various K,U, and Th concentrations (Fig. 7). Differently, the western domain (labeled V in Figs. 6 and 7) shows consistent NE-trending magnetic anomaly pattern in its southern part that swings to N-trending pattern to the north (Fig. 6).Southeast and NW-verging thrusts are mapped in the northern and southern parts of this domain, respectively (Fig. 4). The central domain (labeled VI in Figs. 6 and 7) shows crude NW-trending fabric (Fig. 6) and lithologies with either high K concentration or low concentrations in all radioelements (Fig. 7).

2.4.2. THE INTERPLAY BETWEEN THE PRECAMBRIAN STRUCTURES AND THE ALBERTINE GRABEN.

To examine the interplay between the Precambrian and rift structures associated with the Albertine and Rhino Grabens, we generated a combined structural map (Fig. 9) showing the Precambrian structural trend by applying edge detection filter to the airborne magnetic data (Fig. 6), interpretation of normal faults from the SRTM DEM (Fig. 3) and previously mapped Precambrian structures (Westerhof et al., 2014).We also developed a tilt image from the airborne magnetic data for portions of the Albertine and Rhino Grabens to evaluate the inclination of the Precambrian structures.

Both the northwestern and the southeastern border faults of the Albertine Graben coincide with NE-elongated magnetic fabric defined by alternating magnetic highs and lows (Fig. 10A). This magnetic pattern is interpreted as defining NE-trending structures which dip steeply to the northwest and southeast (Fig. 10B). Additionally, the southeastern margin of the Albertine Graben coincides with a NE-trending zone with varying K, Th, and U concentrations apparent in the airborne radiometric data (Figs. 7 and 10C). The region just southeast of the Albertine Graben was previously mapped as dominated by NE-elongated belt of Mesoarchean granulites and charnockites juxtaposed with a NE-elongated belt of Neoproterozoic meta-sedimentary rocks to the south- east (Fig. 4; Nyakecho and Hagemann, 2014; Ruotoistenmaki, 2014). Additionally, SE-verging thrust faults have been mapped in the southeastern margin of the Graben (Fig. 4; Westerhof et al., 2014).The presence of such strong Precambrian inherited structures might have resulted in localization of extensional strain in both border faults of the Albertine Graben allowing its development as a full Graben (Fig. 5A).

In contrast, the Albertine Graben terminates in the northeast against Precambrian rocks with different structural trends, but generally poorly-developed NW-trending fabric because of multi-

phase folding (Figs. 6 and 10A). The multi-phase folding is apparent from the magnetic pattern in the airborne magnetic image (Figs. 6 and 10A) indicative of steep pre-existing Precambrian fabric (Fig. 10B). This region also shows high K concentration in the airborne radiometric image (Figs. 7 and 10C). This region was previously mapped as part of the Neoarchean gneisses and granitoids (Fig. 4; Nyakecho and Hagemann, 2014; Ruotoistenmaki, 2014). However, its appearance in the airborne radiometric image is tempting to consider it a separate lithological/tectonic unit. Strikingly, the magnetic fabric just northeast of the Albertine Graben is NW-trending; orthogonal to the NE-trend of the Graben (Fig. 10A and B). The NW-trend is also evident in the 3D-FTG image through the presence of a right-stepping en-echelon pattern of high density bodies (Fig. 8).

Comparing the structural trends extracted from the airborne magnetic data with the trends of brittle structures mapped from the SRTMDEM indicates close parallelism between the northwestern and southeastern border faults of the Albertine Graben with the Precambrian structures (Fig. 10D). However, the northeastern termination of the Albertine Graben seems to be dominated by less-developed NE-trending brittle structure that disappears farther northeast outside the Graben and these structures cross-cut the Precambrian structures (Fig. 10D). It is worth mentioning here that Westerhof et al. (2014) mapped NE-verging thrust faults at the northeastern tip of the Albertine Graben indicating that the orientation of the Precambrian structure is orthogonal to the trend of the Graben (Fig. 9). Hence, it can be concluded that the presence of multiply-deformed Precambrian Terrane with fabric orientations departing from the NE-trend might have prevented the Albertine Graben from propagating further to the northeast.

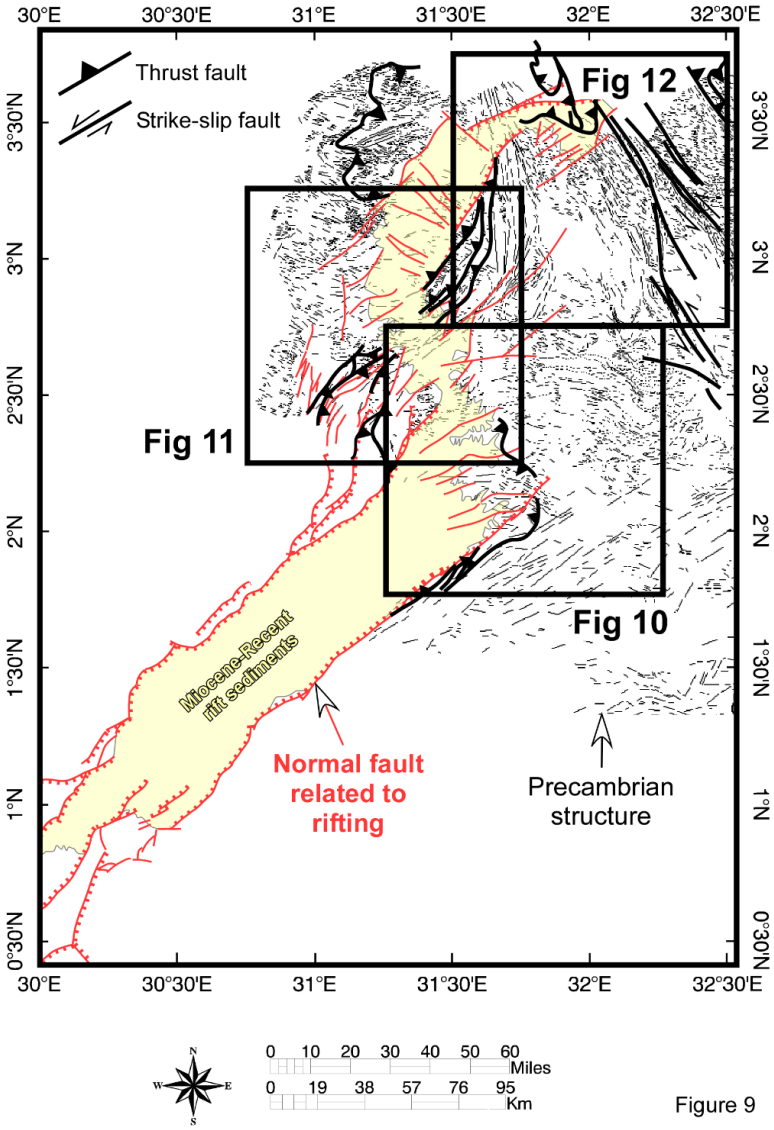

Figure 9. Structural map of the Albertine and Rhino Grabens generated through the extraction of the Precambrian structural trends by applying edge detection filter to the horizontal derivative airborne image of Fig. 6, the interpretation of rift-related structures from the Shuttle Radar Topography Mission (SRTM) Digital Elevation Model (DEM) in Fig. 3 and previously mapped Precambrian structures by Westerhof et al. (2014).

2.4.3. THE INTERPLAY BETWEEN PRECAMBRIAN STRUCTURE AND THE OVERLAP ZONE BETWEEN THE ALBERTINE AND RHINO GRABENS.

The overlap zone between the Albertine and Rhino Grabens, which shows NE-trending rift-related faults, might have exploited steep NE- trending Precambrian structures evidenced by the presence of strong magnetic fabric defined by NE–SW elongated magnetic highs and lows (Figs. 6, 11A and B). The NE-trending fabric is also evidenced in the airborne radiometric ternary image through white belts suggestive of the presence of Precambrian rocks with relatively high K, Th and U concentrations (Fig. 11C). These were previously mapped as NE-trending belts of Mesoarchean granulites and charnockites, Neoarchean gneisses and granitoids and Mesoproterozoic volcano-sedimentary rocks and granitoids (Fig. 4; Nyakecho and Hagemann, 2014; Ruotoistenmaki, 2014). The overlap zone between the two Grabens was also mapped by Westerhof et al. (2014) as being dominated by NW and SE-verging thrust faults (Fig. 9). The NE-trending Precambrian structure is also defined by the presence of a NE-elongated gravity high anomaly apparent in the 3D-FTG image between the Albertine and the Rhino Grabens (Fig. 8). This anomaly is interpreted as defining the trend of the Precambrian structure that has facilitated the development of the transfer zone dominated by relay ramp faults between the Albertine and the Rhino Grabens. This is evidenced from the apparent parallelism between the Precambrian structures extracted from the airborne magnetic data and the brittle structures mapped from the SRTM DEM (Fig. 11D).

2.4.4. THE INTERPLAY BETWEEN THE PRECAMBRIAN STRUCTURES AND THE RHINO GRABEN

The southwestern part of the Rhino Graben extends between Precambrian structural domains with different structural trends. To the southeast, the Precambrian structures are defined by the presence of NE-trending magnetic fabric apparent in the airborne magnetic data (Figs. 4 and 11A) suggestive

of the presence of steep NE-trending Precambrian fabric (Fig. 11B). This is also reflected in the airborne radiometric data where the southeastern side of the Graben is delineated by a NE-trending belt of high K, Th and U concentrations evident from its white color (Figs. 7 and 11C). This region was mapped by Nyakecho and Hagemann (2014) and Ruotoistenmaki (2014) as a NE-trending belt of Mesoarchean granulites and charnockites (Fig. 4). Also, Westerhof et al. (2014) mapped SE-verging thrust faults in the southeastern margin of the Rhino Graben (Fig. 9). To the northwest, the Precambrian structures display different orientations reflecting multi-phase folding. This is particularly evident in the airborne radiometric image showing the complex nature of folding with wavy zones of various K, Th, and U concentrations (Fig. 7). This is also reflected in the distribution of lithological units where previous geological maps show this region as a Terrane of inter-folded Mesoarchean granulites and charnockites and Neoarchean gneisses and granitoids (Fig. 4; Nyakecho and Hagemann, 2014; Ruotoistenmaki, 2014). The southeastern margin of the Rhino Graben also coincides with what has been proposed as the boundary between the Bomu–Kibalian shield–West Nile Block and the Ugandan craton– North Uganda Terrane (Begg et al., 2009; Westerhof et al., 2014). The surface expression of rift-related faults extracted from the SRTM DEM as well as topographic profiles from the same source indicates that this part of the Rhino Graben is a SE-dipping half-Graben with well-developed southeastern border fault (Figs. 5B and 12D). Hence, it can be suggested that the presence of pre-existing Precambrian fabric with preferred NE-orientation in the southeast and the lack of it to the northwest has influenced the development of this part of the Rhino Graben as a SE-dipping half-Graben.

The Rhino Graben is segmented into a NE-trending segment in the southwest and an ENE-trending segment to the northeast (Fig. 3). Additionally, the Graben changes its polarity from a SE-dipping half-Graben in the southwest to a NNW-dipping half-Graben to the northeast (Figs. 5B and C and 12D). This segmentation and change of half-Graben polarity coincides with the presence of N-trending magnetic fabric (Fig. 12A) related to the presence of steep N-trending pre-existing

Precambrian structure (Fig. 12B). This structure is also well-defined in the airborne radiometric image by the presence of NW-trending zones of high K, Th, and U concentrations (Figs. 7 and 2C). This magnetic fabric and radiometric anomaly coincides with the N-trending belt of Mesoproterozoic–Neoproterozoic belt of volcano-sedimentary rocks and granitoids (Fig. 4; Nyakecho and Hagemann, 2014; Ruotoistenmaki, 2014). To the east-northeast of this N-trending Precambrian structure, the Rhino Graben continues in an ENE-direction for ~50 km where it narrows to a width of ~10 km before it terminates against the NW-trending Precambrian Aswa Shear Zone. This zone is shown by impressively well-defined NW-trending steep magnetic fabric (Fig. 12A and B) as well as a radiometric anomaly of high K, Th, and U (Fig. 12C). It is likely that the Graben segmentation and termination was controlled by the N to NW-trending Precambrian structures. This is evidenced from the comparison between the trends of the Precambrian structures extracted from the airborne magnetic data and the brittle structures mapped from the SRTM DEM (Fig. 12D).

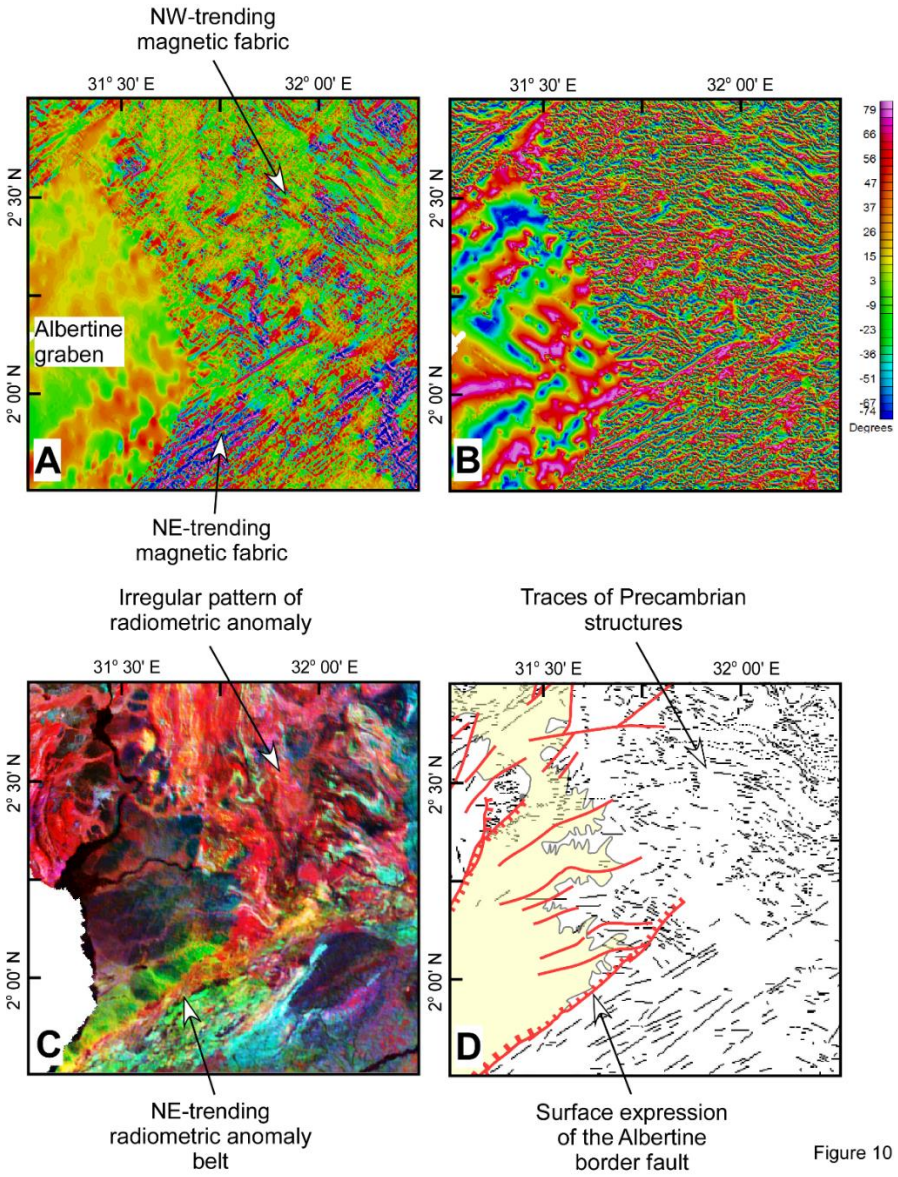

Figure 10: (A) Horizontal derivative airborne magnetic map of the southeastern boarder fault and the northeastern end of the Albertine Graben. (B) Tilt angle map of the airborne magnetic data of the same region covered in A. (C) Ternary airborne radiometric image of the same region covered in A. (D) Structural interpretation map of the same region covered in A showing Precambrian structural trends extracted from the airborne magnetic data and rift related structures extracted from the Shuttle Radar Topography Mission (SRTM) Digital Elevation Model (DEM). See Fig. 9 for location.

2.5. DISCUSSION

Fig. 13 summarizes the possible ways pre-existing structures have influenced the evolution of the Albertine and Rhino Grabens. Below we discuss our results in terms of strain localization and transfer, rift segmentation and rift termination.

2.5.1. STRAIN LOCALIZATION

The Albertine and Rhino Grabens show no indications of surface volcanic activities. Differently, volcanic provinces have been observed in other parts of the Western Branch south of the Albertine Graben where they are restricted to the tips of rift segments (Fig. 2; Ebinger, 1989). Seismic tomographic studies close to the Rwenzori Mountains (Fig. 2) suggest the presence of upper mantle melt inclusions only beneath the southern part of the rift (Jakovlev et al., 2013). Hence, mantle-derived magmatism does not seem to play the major role in strain localization during the evolution of the Albertine and Rhino Grabens, at least at the upper crustal level.

Numerical models highlighted the important role of magmatic activities in strain localization during extension (Buck, 2006). These models predict that magma is responsible for initial softening of the lithosphere enhancing lithospheric stretching, hence allowing for asthenospheric upwelling and decompression melting. Final injection of magmatic dikes at the upper level of the continental lithosphere focusses extensional strain within narrow zones leading to the onset of continental rifts. The numerical model predictions are amply supported by geological and geophysical observations in the more-developed portions of the EARS such as the Main Ethiopian Rift and the Afar Depression (Fig. 1A; Ebinger and Casey, 2001; Kendall et al., 2005; Wright et al., 2006).

In the absence of magmatism, there remain two other possibilities for strain localization. These are edge-driven convection and pre-existing inherited lithospheric structures. Small-scale mantle

convection is believed to occur at the boundary between thick stable lithosphere of Archean cratons and thinner lithosphere represented by orogenic belts (King and Anderson, 1998; King and Ritsema, 2000). Numerical models show that small-scale convection in the upper mantle can develop due to strong lateral temperature and viscosity gradients at the edges of cratons (King and Anderson, 1995, 1998; King and Ritsema, 2000). The induced flow produces down-welling convection cells that can extend as deep as the mantle transition zone beneath the margins of cratons, with up-welling at 500–1000 km distance from the margins of cratons (King and Anderson, 1995; King and Ritsema, 2000). The presence of the temperature gradient increases convection cells (advection and convection) at the margins and this changes the rheology of the lithosphere (Vauchez et al., 1998). The Albertine and Rhino Grabens follow the boundary between two different cratonic blocks represented by the Ugandan craton–North Uganda Terrane in the east and the Bomu–Kibalian shield–West Nile Block to the west (Fig. 4; Begg et al., 2009; Westerhof et al., 2014). However, there are no geophysical studies that suggest that there is difference in the lithospheric thickness between the two cratonic blocks. Hence, awaiting future geophysical investigations (such as shear wave splitting and magnetotelluric studies) aimed at imaging asthenospheric flow, strain localization during the initiation of the Albertine and Rhino Grabens through edge-driven convection remains a possibility.

Upper level Precambrian structures might be the major cause of strain localization during the initiation of the Albertine and Rhino Grabens. Geological and geophysical studies have shown that the shallow inherited pre-existing structures are important in localizing strain in the crust during rift initiation (Keranen and Klemperer, 2008; Korme et al., 2004). Different geological and geophysical observations have shown that both the Kenyan and the Main Ethiopian Rifts (Fig. 1A) developed as narrow rifts with strong strain localization regardless of the fundamentally different lithosphere underlying them. The Kenyan rift initiated in a cold strong lithosphere and the Main Ethiopian Rift initiated in hot lithosphere. However, both extensional structures developed as

narrow rifts suggesting that rift initiation was aided by the presence of the pre-existing crustal fabric of the East African orogeny (Keranen et al., 2009). The presence of the Precambrian structures might have also influenced the architecture of the Albertine and the Rhino Grabens. Corti et al. (2013) suggested that the development of deep symmetrical full Grabens such as the Albertine Graben with a uniform width of ~60 to 80 km and well-developed border faults (Figs. 3 and 5A) is influenced by its development within well-developed pre-existing structures.

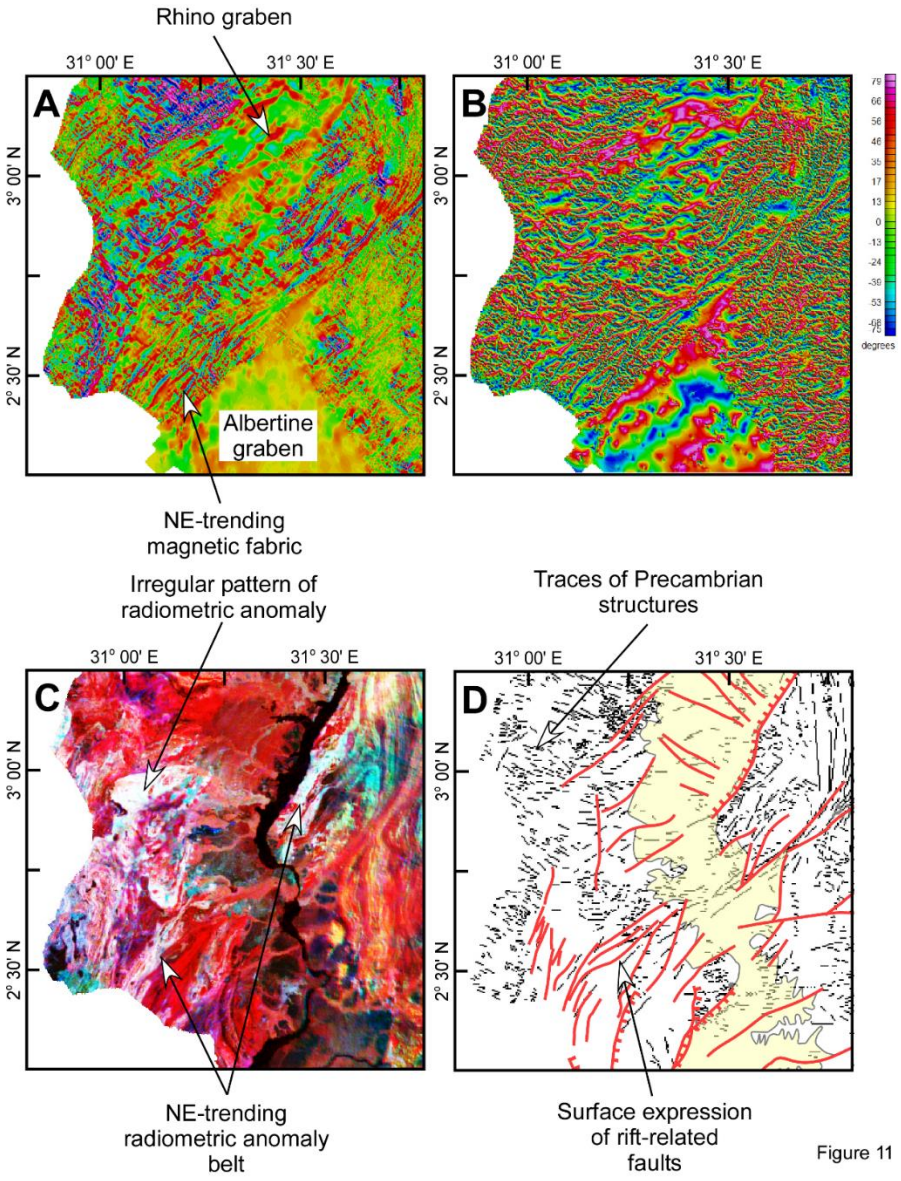

Figure 11

Figure 11: (A) Horizontal derivative airborne magnetic map of the transfer zone between the Albertine and Rhino Grabens. (B) Tilt angle map of the airborne magnetic data of the same region covered in A. (C) Ternary airborne radiometric image of the same region covered in A. (D) Structural interpretation map of the same region covered in A showing Precambrian structural trends extracted from the airborne magnetic data and rift related structures extracted from the Shuttle Radar Topography Mission (SRTM) Digital Elevation Model (DEM). See Fig. 9 for location.

2.5.2. STRAIN TRANSFER

The Albertine and the Rhino Grabens are connected through a transfer zone forming a ~90 km wide overlap zone between the two basins (Fig. 3). However, the length of this overlap zone is insignificant compared to its width (Fig. 3). Physical and centrifugal models have shown that the length of the overlap zone is directly related to the obliquity of rifting (Corti, 2008; McClay and White, 1995; McClay et al., 2002; Tentler, 2003). Longer overlap zones are usually associated with highly oblique extension. Extension within the Western Branch is explained through the ESE-movement of the Victoria plate relative to Nubian plate, with the extension increasing from north (1.3 mm/year) to south (2.9 mm/year) (Fig. 1B; Sariah et al., 2014). The NE- to ENE-trend of the Albertine and Rhino Grabens in relation to the ESE-movement of the Victoria plate favors orthogonal extension across the Albertine Graben and a slightly oblique extension across the Rhino Graben. Hence, the geometrical arrangement of the Albertine and Rhino Grabens cannot be attributed to the obliquity of extension. Rather, such geometrical arrangement (where the two Grabens are connected with an overlap zone with a considerable width, but insignificant length) was the result of the dominant orientation of the pre-existing structures. The two Grabens nucleated within dominantly NE-tending pre-existing fabric while the lack of this fabric prevented the Albertine Graben from propagating further in the northeast direction, hence transferred strain to the Rhino Graben.

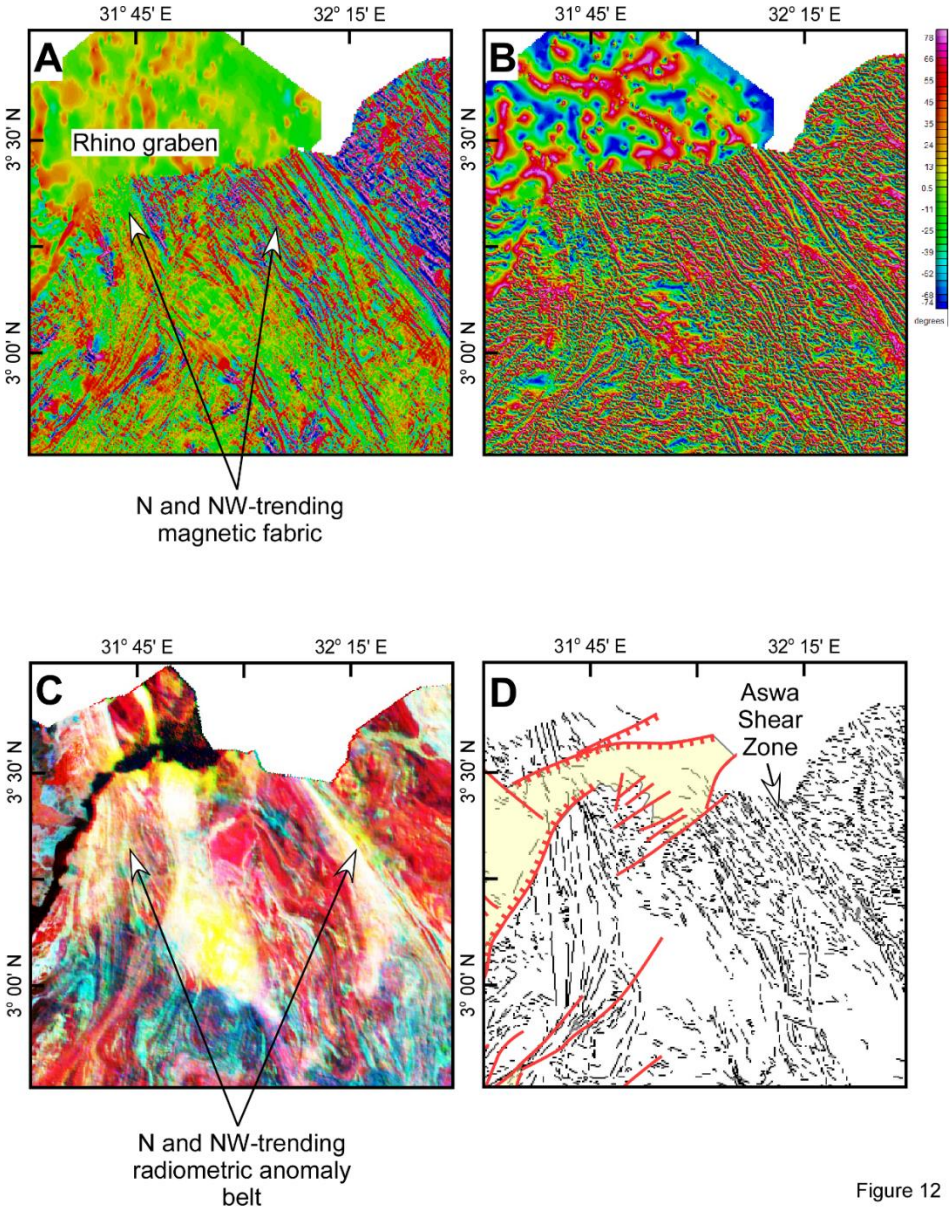

Figure 12

Figure 12: (A) Horizontal derivative airborne magnetic map of the segmented region and termination of the Rhino Graben against the NW-trending Aswa Shear Zone. (B) Tilt angle map of the airborne magnetic data of the same region covered in A. (C) Ternary airborne radiometric image of the same region covered in A. (D) Structural interpretation map of the same region covered in A showing Precambrian structural trends extracted from the airborne magnetic data and rift related

structures extracted from the Shuttle Radar Topography Mission (SRTM) Digital Elevation Model (DEM). See Fig. 9 for location.

2.5.3. RIFT SEGMENTATION

The architecture of the Western Branch seems to have been shaped by a first order and a second order rift segmentation. The first order segmentation resulted in the development of a series of individual basins. These are from north to south Albertine–Rhino, Kivu, Tanganyika, Rukwa and Malawi (Fig. 1B). This high-order segmentation seems to be controlled by volcanic activities. It has been noticed that volcanic rocks within the Western Branch are only found within zones between individual segments (Fig. 2; Ebinger, 1989). This is exemplified by the presence of volcanic rocks between the Albertine–Rhino and Kivu Grabens, between the Kivu Graben and Tanganyika rift, and between the Rukwa and Malawi rifts (Fig. 1B).

The second order segmentation occurs within individual basins through the development of overlapping border faults that controlled the alternation between full Grabens and half-Grabens with opposite polarities. This is best exemplified by the Malawi rift (Fig. 1B) which is segmented into at least eight 50–90 km long full Grabens and half Grabens (Ebinger et al., 1987). Ebinger et al. (1987) concluded that the development of the border faults within the Malawi rift was strongly influenced by the presence of Proterozoic–Mesozoic pre-existing structures.

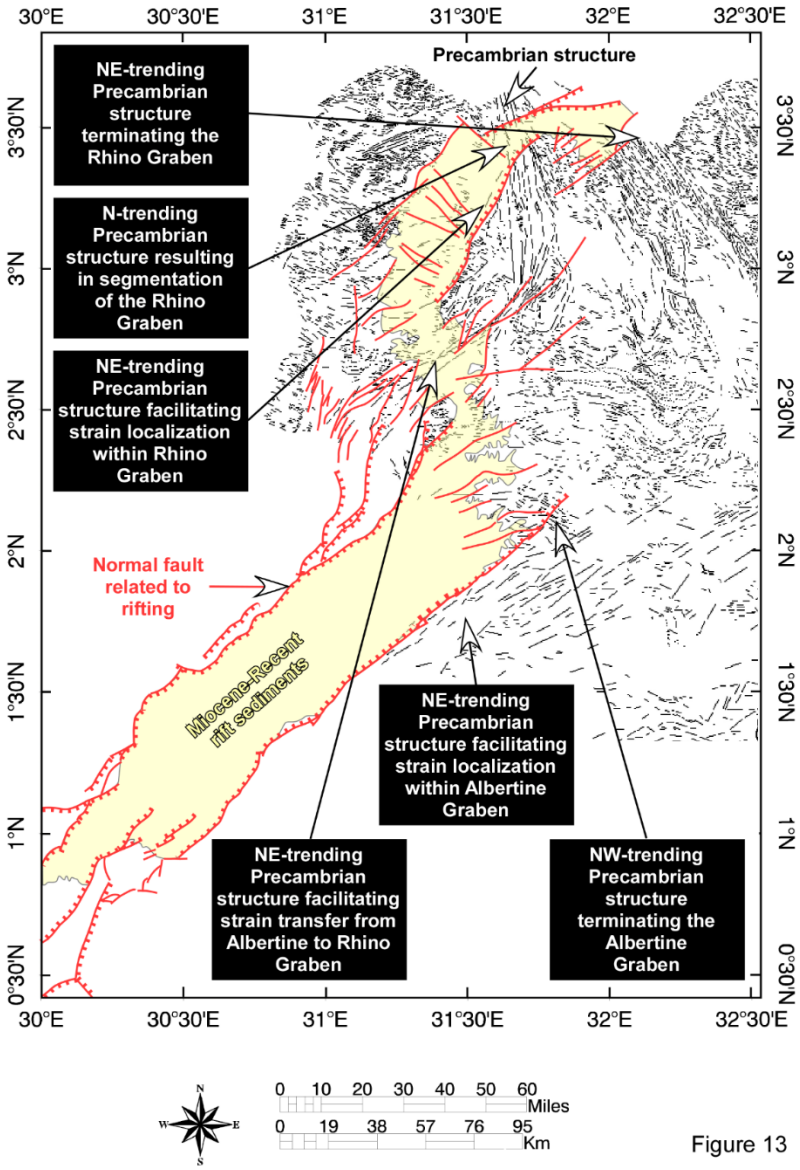

Figure 13: Possible controls of the Precambrian structures on the evolution of the Albertine and Rhino Grabens.

The segmentation of the Rhino Graben into a SE and NNW-dipping half-Grabens is similar to the geometry of segmentation observed in other rifts constituting the Western Branch. Additionally, the length of border fault segments of the Graben (~ 80 km in the southwest and ~50 km in the

northeast) is similar to those reported from other rifts of the Western Branch such as the Malawi rift (Ebinger et al., 1987). In the absence of extension obliquity, we argue that such segmentation has been strongly controlled by the pre-existing Precambrian structures notably the presence of N-trending fabric where the basin is segmented into SE and NW-dipping half Grabens (Fig. 13).

2.5.4. RIFT TERMINATION

The northeastward continuation of the Western Branch into South Sudan has been a subject of conflicting propositions. For example, the 1991 earthquake events of South Sudan have been interpreted as an indication of the continuation of the Western Branch further northeast beyond the Rhino Graben (Girdler and McConnell, 1994). At the Rhino Graben, the angular velocity of the Victoria plate relative to the Nubian plate decreases to only 1.3 mm/year (Fig. 1B; Sariah et al., 2014) predicting that velocity will diminish to zero further north as the pole of rotation between the Victoria and Nubian plates is approached resulting in rift termination. It is clear from the surface geology and the airborne magnetic data that the Rhino Graben continues for ~50 km in a NE-direction after it encounters the N-trending Precambrian structures before ultimately terminating against the NW-trending Aswa Shear Zone (Fig. 12). Results from limited passive seismic data suggest that the lithospheric structure is different across the shear zone. Abdelsalam et al. (2002, 2011) suggested that the Saharan Metacraton to the northeast of the Aswa Shear Zone has a heterogeneous crust and upper mantle and that the region might have undergone sub-continental lithospheric mantle delamination during the Neoproterozoic. Hence, it is tempting to suggest that such heterogeneous and thinned lithosphere that lacks zones of well-developed pre-existing lithospheric fabric, combined with diminishing plate's angular velocity, might have prevented strain localization during the onset of rifting, hence leading to the apparent termination of the Western Branch against the Aswa Shear Zone.

2.6. CONCLUSIONS

Analysis of airborne magnetic, radiometric, and gravity data together with SRTMDEM covering the Albertine and Rhino Grabens in northwestern Uganda highlighted the importance of pre-existing Precambrian structures in the evolution of largely amagmatic continental rift systems.

(1) The development of the Albertine basin as a full-Graben was facilitated by the presence of NE-trending Precambrian fabric and the continuation of the Graben to the northeast was hindered by the presence of NW- trending Precambrian structures oblique to the Graben propagation direction. (2) The transfer of extensional strain from the Albertine Graben to the Rhino Graben was not due to extensional obliquity. Rather, this was due to the regional orientation of the Precambrian fabric that facilitated transfer of extension from the northwestern and southeastern border faults of the Albertine to the southeastern border fault of the Rhino Graben. This produced an overlap zone with significant width (90 km) and insignificant length unlike those expected to be developed during rift obliquity. (3) The segmentation of the Rhino Graben into two half Grabens with opposite polarities is similar to that of other rifts of the Western Branch and was developed across N-trending Precambrian structure, oblique to the basin's trend. (4) The termination of the Rhino Graben at the Aswa Shear Zone might be partially due to difference in lithospheric structure where heterogeneous crust and lack of preferably oriented Precambrian structure of the Saharan Metacraton prevented strain from being localized within a narrow rift.

2.7 ACKNOWLEDGMENTS

The Government of Uganda allowed free access to the airborne magnetic, radiometric and gravity data. This project is supported by the National Science Foundation Continental Dynamics grant # EAR 1255233.We thank D. Delvaux and an anonymous reviewer for detailed comments. This is Oklahoma State University Boone Pickens School of Geology contribution number 2015-16.

2.8 REFERENCES

Aanyu, K., Koehn, D., 2011. Influence of pre-existing fabrics on fault kinematics and rift geometry of interacting segments: Analogue models based on the Albertine Rift (Uganda), Western Branch-East African Rift System. Journal of African Earth Sciences 59, 168-184.

Abdelsalam M.G., Liégeois, J.P., Stern, R.J., 2002. The Saharan Metacraton. Journal of African Earth Sciences 34, 119-136.

Abdelsalam, M.G., Atekwana E.A., Keller G.R., and Klemperer S.L., 2004. The life cycle of continental rifting as a focus for US-African scientific collaboration, EOS, 85-47.

Abdelsalam, M.G., Gao S.S., Liegeois J.P., 2011. Upper mantle structure of the Saharan Metacraton, Journal of African Earth Sciences 60, 328-336.

Adams, A., Nyblade, A., Weeraratne, D., 2012. Upper mantle shear wave velocity structure beneath the East African plateau: evidence for a deep, plateauwide low velocity anomaly. Geophysical Journal International 189, 123-142.

Begg, G.C., Griffin, W.L., Natapov, L.M., O'Reilly, S.Y., Grand, S.P., O'Neill, C.J., Hronsky, J.M.A., Poudjom Djomani, Y., Swain, C.J., Deen, T., Bowden, P., 2009. The lithospheric architecture of Africa: seismic tomography, mantle petrology, and tectonic evolution. Geosphere 5, 23–50.

Bonini, M., Corti, G., Innocenti, F., Manetti, P., Mazzarini, F., Abebe, T., Pecskay, Z., 2005. Evolution of the Main Ethiopian Rift in the frame of Afar and Kenya rifts propagation. Tectonics 24, TC1007. doi:10.1029/2004TC001680

Briggs, I.C., 1974. Machine contouring using minimum curvature. Geophysics 39, 39-48.

Buck, W.R., 2006. The role of magma in the development of the Afro-Arabian Rift System. Geological Society of London Special Publications 259, 43-54.

Mosley-Bufford, K.M., Atekwana, E.A., Abdelsalam, M.G., Shemang, E., Atekwana, E.A., Mickus, K., Moidaki, M., Modisi, M.P., Molwalefhe, L., 2012. Geometry and faults

tectonic activity of the Okavango Rift Zone, Botswana: Evidence from magnetotelluric and electrical resistivity tomography imaging. Journal of African Earth Sciences 65, 61-71.

Calais, E., Ebinger C., Hartnady C., Nocquet J.M., 2006. Kinematics of the East African Rift from GPS and earthquake slip vector data. Geological Society of London Special Publications 259, 9-22.

Chorowicz, J., 2005. The East African Rift System. Journal of African Earth Sciences 43, 379-410.

Cohen, A.S., Soreghan, M.J., Scholz C.A., 1993. Estimating the age of formation of lakes: An example from Lake Tanganyika, East African Rift System. Geology 21, 511-514.

Corti, G., 2008. Control of rift obliquity on the evolution and segmentation of the Main Ethiopian Rift. Nature Geoscience 1, 258-262.

Corti, G., van Wijk, J., Cloetingh, S., Morley, C.K., 2007. Tectonic inheritance and continental rift architecture: Numerical and analogue models of the East African Rift System, Tectonics, 26, TC6006, doi: 10.1029/2006TC002086.

Corti, G., Calignano, E., Petit, C., Sani, F., 2011. Controls of lithospheric structure and plate kinematics on rift architecture and evolution: An experimental modeling of the Baikal rift. Tectonics 30. TC3011, doi: 10.1029/2011TC002871.

Corti, G., Iandelli, I., Cerca, M., 2013. Experimental modeling of rifting at craton margins. Geosphere 9, 138-154.

Craig, T.J., Jackson, J.A., Priestley, K., McKenzie, D., 2011. Earthquake distribution patterns in Africa: their relationship to variations in lithospheric and geological structure, and their rheological implications. Geophysical Journal International 185, 403-434.

Daly, M.C., 1986. Crustal shear zones and thrust belts: their geometry and continuity in Central Africa. Philos. Trans. R. Soc. Lond. A317, 111–128.

Delvaux, D., Kervyn, F., Macheyeki, A.S., Temu, E.B., 2012. Geodynamic significance of the TRM segment in the East African Rift (W-Tanzania): Active tectonics and paleostress in the Ufipa plateau and Rukwa basin. Journal of Structural Geology 37, 161-180.

Dickinson, J.L., Brewster, J., Robinson, J., Murphy, C., 2009. Imaging techniques for full tensor gravity gradiometry data, 11th South African Geophysical Association (SAGA) Biennial Technical Meeting and Exhibition. September 2009, Swaziland pp. 84-88.

Duval, J.S., 1983. Composite color images of aerial gamma-ray spectrometric data. Geophysics 48, 722-735.

Ebinger, C.J., Rosendahl, B.R., Reynolds, D.J., 1987. Tectonic model of the Malawi rift, Africa. Tectonophysics 141, 215-235.

Ebinger, C.J., 1989. Tectonic development of the Western Branch of the East African Rift System. Geological Society of America Bulletin 101, 885-903.

Ebinger, C., Casey, M., 2001. Continental breakup in magmatic provinces: An Ethiopian example. Geology 29, 527-530.

Erdi-Krausz, G., Matolin, M., Minty, B., Nicolet, J.-P., Reford, W.S., Schetselaar, E., 2003. Guidelines for Radioelement Mapping Using Gamma-ray Spectrometry Data. International Atomic Energy Agency Publication IAEA-TECDOC-1363, Vienna, Austria (173 pp.).

Fernandez-Alonso, M., Cutten, H., De Waele, B., Tack, L., Tahon, A., Baudet, D., Barritt, S.D., 2012. The Mesoproterozoic Karagwe-Ankole Belt (formerly the NE Kibara Belt): The result of prolonged extensional intracratonic basin development punctuated by two short-lived far-field compressional events. Precambrian Research 216–219, 63-86.

Fraser, S.I., Fraser, A.J., Lentini, M.R., Gawthorpe, R.L., 2007. Return to rifts – the next wave: fresh insights into the petroleum geology of global rift basins. Petroleum Geoscience 13, 99-104.

Fritz, H., Abdelsalam, M.G., Ali, K.A., Bingen, K.A., Collins, A.S., Fowler, A.R., Ghebreab, W.,Hauzenberger, C.A., Johnson, P.R., Kusky, T.M., Macey, P.,Muhongo, S., Stern, R.J.,

Viola,G., 2013. Orogeny style in the East African Orogen: a review of the Neoproterozoic to Cambrian tectonic evolution. J. Afr. Earth Sci. 86, 65–106.

Girdler, R. W., and McConnell, D. A., 1994. The 1990 to 1991 Sudan Earthquake Sequence and the Extent of the East African Rift System. Science 264, 67-70.

Grasty, R., Smith, B., Minty, B., 1997. Developments in the standardization and analysis of airborne gamma ray data. Decennial International Conference on Mineral Exploration, pp. 725-732.

Grasty, R.L., 1997. Radon emanation and soil moisture effects on airborne gamma-ray measurements. Geophysics 62, 1379-1385.

Hayward, N.J., Ebinger, C.J., 1996. Variations in the along-axis segmentation of the Afar Rift system. Tectonics 15, 244-257.

Jakovlev, A., Rümpker, G., Schmeling, H., Koulakov, I., Lindenfeld, M., Wallner, H., 2013. Seismic images of magmatic rifting beneath the western branch of the East African rift. Geochemistry, Geophysics, Geosystems 14, 4906-4920.

Kampunzu, A. B., Bonhomme, M.G. Kanika, M., 1998. Geochronology of volcanic rocks and evolution of the Cenozoic Western Branch of the East African Rift System. Journal of African Earth Sciences 26, 441-46.

Kendall, J.M., Stuart, G.W., Ebinger, C.J., Bastow, I.D., Keir, D., 2005. Magma-assisted rifting in Ethiopia. Nature 433, 146-148.

Keranen, K., Klemperer, S.L., 2008. Discontinuous and diachronous evolution of the Main Ethiopian Rift: Implications for development of continental rifts. Earth and Planetary Science Letters 265, 96-111.

Keranen, K.M., Klemperer, S.L., Julia, J., Lawrence, J.F., Nyblade, A.A., 2009. Low lower crustal velocity across Ethiopia: Is the Main Ethiopian Rift a narrow rift in a hot craton? Geochemistry Geophysics Geosystems 10, Q0AB01, doi: 10.1029/2008GC002293.

King, S.D., Anderson, D.L., 1995. An alternative mechanism of flood basalt formation. Earth and Planetary Science Letters 136, 269-279.

King, S.D., Anderson, D.L., 1998. Edge-driven convection. Earth and Planetary Science Letters 160, 289-296.

King, S.D., Ritsema, J., 2000. African hot spot volcanism: small-scale convection in the upper mantle beneath cratons. Science 290, 1137-1140.

Korme, T., Acocella, V., Abebe, B., 2004. The role of pre-existing structures in the origin, propagation and architecture of faults in the Main Ethiopian Rift. Gondwana Res. 7, 467–479.

Lenoir, J.-L., Liégeois, J.P., Theunissen, K., Klerkx, J., 1994. The Paleoproterozoic Ubendian shear belt in Tanzania: geochronology and structure. J. Afr. Earth Sci. 19, 169–184. McClay, K.R., White, M.J., 1995. Analogue modelling of orthogonal and oblique rifting. Marine and Petroleum Geology 12, 137-151.

McClay, K.R., White, M.J., 1995. Analogue modelling of orthogonal and oblique rifting. Mar. Pet. Geol. 12, 137–151.

McClay, K.R., Dooley, P., Whitehouse, and Mills, M., 2002. 4-D Evolution of rift systems: Insights from scaled physical models. The American Association of Petroleum Geologists Bulletin 8, 935-959.

Minty, B., 1997. Fundamentals of airborne gamma-ray spectrometry. AGSO Journal of Australian Geology and Geophysics 17, 39-50.

Minty, B., McFadden, P., 1998. Improved NASVD smoothing of airborne gamma-ray spectra. Exploration Geophysics 29, 516-523.

Nyakecho, C., Hagemann, S.G., 2014. An overview of gold systems in Uganda. Australian Journal of Earth Sciences, doi: 10.1080/08120099.2013.831773.

Ring, U., 2008. Extreme uplift of the Ruwenzori Mountains in the East African Rift, Uganda: Structural framework and possible role of glaciations, Tectonics, TC4018, doi: 10.1029/2007TC002176.

Roberts, E.M., Stevens, N.J., O'Conner, P.M., Dirks, P.H.G.M., Gottfried, M.D., Clyde, W.C., Armstrong, R.A., Kemp, A.I.S., Hemming, S., 2012. Initiation of the western branch of the East African Rift coeval with the eastern branch, Nature Geoscience 5, 289-294.

Ruotoistenmaki, T., 2014. Geophysical characteristics of the Aswa shear, Nakasongola discontinuity and ring dyke complex in Uganda. J. Afr. Earth Sci. 93, 23–41.

Salem, A., Williams, S., Fairhead, J.D., Ravat, D., Smith, R., 2007. Tilt-depth method: A simple depth estimation method using first-order magnetic derivatives. The Leading Edge 26, 1502-1505.

Saria, E., Calais, E., Stamps, D., Delvaux, D., Hartnady, C., 2014. Present-day kinematics of the East African Rift. Journal of Geophysical Research, Solid Earth 119, 3584-3600.

Sherman, S.I., 1992. Faults and tectonic stresses of the Baikal rift zone. Tectonophysics 208, 297-307.

Smith, R.S., Salem, A., 2005. Imaging depth, structure, and susceptibility from magnetic data: The advanced source-parameter imaging method. Geophysics 70, L31-L38.

Stamps, D.S., Calais, E., Saria, E., Hartnady, C., Nocquet, J.-M., Ebinger, C.J., Fernandes, R.M., 2008. A kinematic model for the East African Rift. Geophysical Research Letters 35, L05304, doi:10.1029/2007GL032781.

Tack, L., Wingate, M.T.D., De Waele, B., Meert, J., Belousova, E., Griffin, B., Tahon, A., Fernandez-Alonso, M., 2010. The 1375 Ma "Kibaran event" in Central Africa: Prominent emplacement of bimodal magmatism under extensional regime. Precambrian Research 180, 63-84.

Tentler, T., 2003. Analogue modeling of overlapping spreading centers: insights into their propagation and coalescence. Tectonophysics 376, 99-115.

Thurston, J., Smith, R., 1997. Automatic conversion of magnetic data to depth, dip, and susceptibility contrast using the SPI (TM) method. Geophysics 62, 807-813.

Upcott, N., Mukasa, R., Ebinger, C., Karner, G., 1996. Along-axis segmentation and isostasy in the Western rift, East Africa. Journal of Geophysical Research 101, 3247-3268.

Vauchez, A., Tommasi, A., Barruol, G., 1998. Rheological heterogeneity, mechanical anisotropy and deformation of the continental lithosphere. Tectonophysics 296, 61-86.

Wölbern, I., Rümpker, G., Link, K., Sodoudi, F., 2012. Melt infiltration of the lower lithosphere beneath the Tanzania craton and the Albertine rift inferred from S receiver functions. Geochemistry, Geophysics, Geosystems 13, doi: 10.1029/2012GC004167.

Wright, T.J., Ebinger, C., Biggs, J., Ayele, A., Yirgu, G., Keir, D., Stork, A., 2006. Magma-maintained rift segmentation at continental rupture in the 2005 Afar diking episode. Nature 442, 291-294.

PAPER II

EXTENT, KINEMATICS AND TECTONIC ORIGIN OF THE PRECAMBRIAN ASWA SHEAR ZONE IN EASTERN AFRICA.

3.0 ABSTRACT

The Aswa Shear Zone (ASZ) is a fundamental Precambrian lithospheric structure that has been shaped by many tectonic events in eastern Africa. It separates the Saharan Metacraton in the northeast from the Northern Uganda Terrane (which represents part of the Northeastern Congo Block of the Congo craton) to the southwest. Nonetheless, its tectonic evolution is not fully understood. We used high-resolution airborne magnetic and radiometric data over Uganda integrated with Shuttle Radar Topography Mission (SRTM) Digital Elevation Model (DEM) in South Sudan to assess the extent, kinematics and contribute to the understanding of the tectonic origin of the ASZ. (1) Our results showed that the ASZ extends in a NW–SE direction for ~550 k in Uganda and South Sudan. (2) The airborne magnetic and radiometric data revealed a much wider (~50 km) deformation belt than the 5-10 km of the exposed surface expression of the ASZ. The deformation belt is defined by three NW-trending sinistral strike-slip shear zones bounding structural domains with magnetic fabric showing splays of secondary shear zones and shear-related folds. These folds are tighter close to the discrete shear zones with their axial traces becoming sub-parallel to the shear zones. A similar fold pattern is observed in South Sudan from the SRTM DEM. We interpreted these folds as due to ENE-WSW contraction associated with the sinistral strike-slip movement. (3) To the northeast, the magnetic patterns and radiometric signatures suggest the

presence of a series of W-verging nappes indicative of strong E–W to NE–SW contraction deformation. (4) We relate the evolution of the ASZ to E–W to NE–SW Neoproterozoic oblique collision between East and West Gondwana. The deformation related to this collision was partitioned into E–W to NE–SW contraction resulting in W-verging thrusts in the east and a sinistral strike-slip movement along the NW-trending ASZ with the strain localized at the boundary between the Saharan Metacraton and the Northern Uganda Terrane.

3.1 INTRODUCTION

The Aswa Shear Zone (ASZ) is a fundamental NW-trending Precambrian structure in the central part of Gondwana (Fig. 1A). Traces of the shear zone have been mapped in eastern and central Africa extending in a NW–SE direction from South Sudan in the northwest through Uganda, Kenya and Tanzania to the southeast and possibly into Madagascar as the Ranotsara shear zone (Fig. 1A; Collins et al., 2003). It has been proposed that the ASZ extends further southeast into south India as the Achankovil shear zone in a Greater Gondwana reconstruction (Fig. 1A; Pradeepkumar and Krishnanath, 2000; Santosh and Collins, 2003). Until recently, only a few generalized studies have attempted to explain the Precambrian evolution of the ASZ and most of these attempts correlated the shear zone to other Neoproterozoic NW-trending strike-slip shear zones in the Arabian–Nubian Shield, the most prominent of which is the Najd fault system which is exposed in northwestern Saudi Arabian and the Eastern Desert of Egypt (Fig. 1A; Berhe, 1990; Stern, 1994). Both Berhe (1990) and Stern (1994) suggested that the development of the ASZ can be linked to the collision

between East and West Gondwana similar to other NW-trending strike-slip shear zones in the Arabian–Nubian Shield.

Besides its importance in understanding the Precambrian evolution of East and West Gondwana and their lithospheric structure, the ASZ is also important for understanding the development of Mesozoic and Cenozoic rifts, seismicity distribution, and controls on the Nile drainage system in eastern Africa. Recent studies in Uganda (Nyakecho and Hagemann, 2014; Ruotoistenmäki, 2014; Westerhof et al., 2014) have highlighted the importance of the ASZ, especially as a major Precambrian structure. However, the lack of geological investigations in the better exposed part of the ASZ in South Sudan hinders full understanding of the geodynamic evolution of this structure.

In this work, we attempt to define the extent and explain the kinematics of the ASZ in Uganda and South Sudan benefiting from the availability of Shuttle Radar Topography Mission (SRTM) Digital Elevation Model (DEM) and the newly acquired high resolution airborne geophysical data from Uganda. Additionally, we propose an origin for the ASZ within the context of East and West Gondwana tectonics.

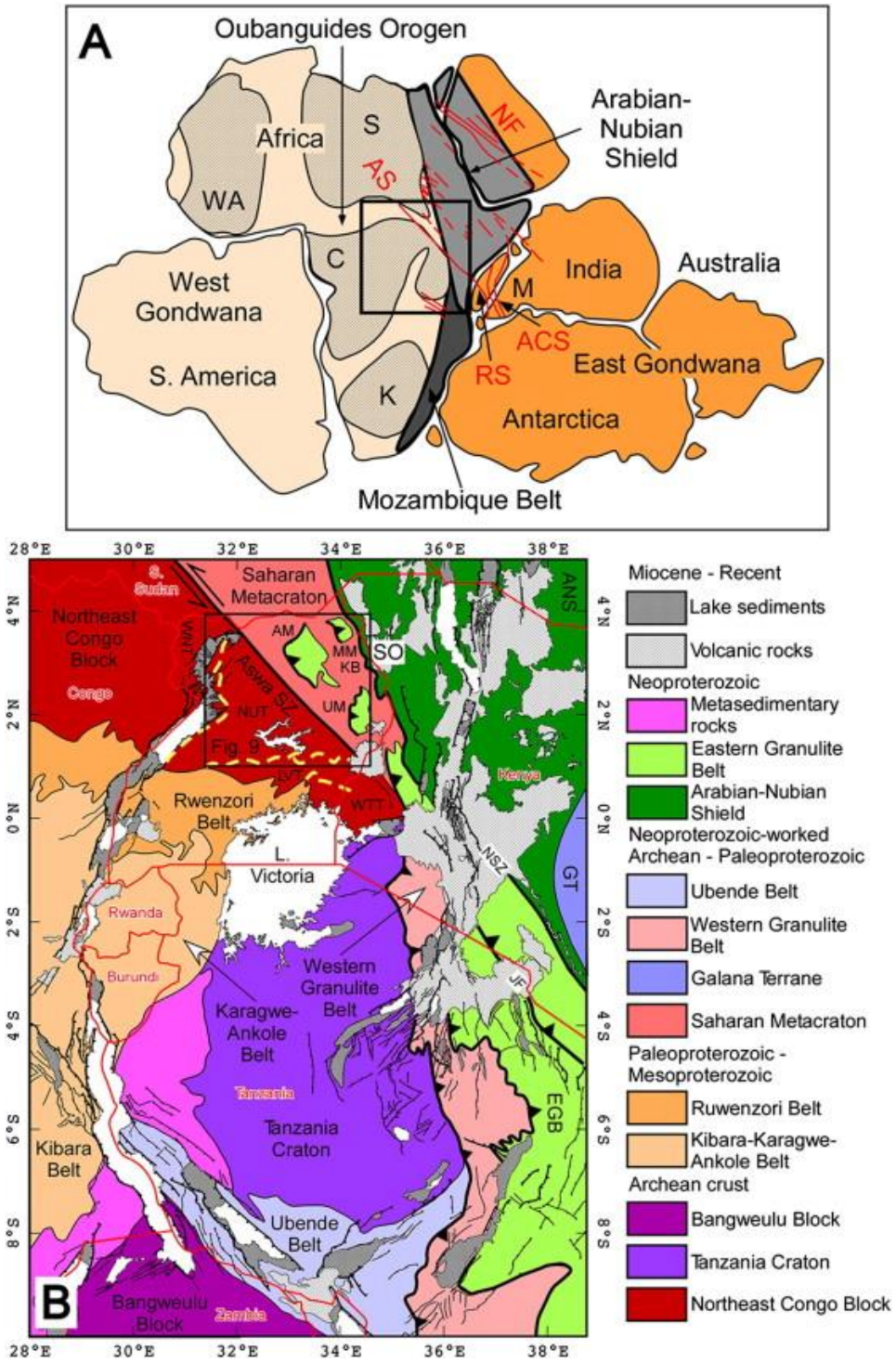

Figure 1: (A) The Arabian–Nubian Shield and the Mozambique belt representing the East African Orogen between East and West Gondwana. Modified after Meert and Lieberman (2008). M =

Madagascar. WA = West Africa Craton. S = Saharan Metacraton. C = Congo Craton. K = Kalahari Craton. AS = Aswa Shear Zone. NF = Najd Fault System. RS = Ranotsara shear zone. ACS=Achankovil shear zone. The NW-trending shear zones are from Berhe (1990) and Stern (1994). (B) Precambrian tectonic map of eastern Africa. Modified from a compilation by Katumwehe et al. (2015). Dotted yellow lines approximate the boundaries suggested by Westerhof et al. (2014) to divide the Northeastern Congo Block in Uganda into the Western Nile Terrane (WNT), Northern Uganda Terrane (NUT), Lake Victoria Terrane (LVT) and West Tanzania Terrane (WTT). ANS = Arabian–Nubian Shield. GT = Galana Terrane. EGB=Eastern Granulite belt. SO=Sekerr ophiolite.MM=Morungole massif. AM=Akurmassif. UM=Ukutatmassif. KB=Karamoja belt. NSZ=Nyangere shear zone. JF=Jailhouse rock fault.

3.1.1. THE ASZ AND GONDWANA TECTONICS

Abdelsalam et al. (2002, 2011) suggested that the ASZ might represent the boundary between the Saharan Metacraton in the northeast and the Congo craton to the southwest (Fig. 1A). The extent of the Congo craton in northeastern Congo and northwestern Uganda is referred to as the Northeastern Congo Block (Fig. 1B; Tack et al., 2010; Fernandez-Alonso et al., 2012). This region has been further divided by Westerhof et al. (2014) into the Northern Uganda Terrane, the West Nile Terrane, the Lake Victoria Terrane, and the West Tanzania Terrane (Fig. 1B). This new sub-division makes the ASZ in Uganda the boundary between the Saharan Metacraton in the northeast and the Northern Uganda Terrane to the southwest (Fig. 1B). However, Westerhof et al. (2014) considered the portion of the Saharan Metacraton immediately northeast of the ASZ to represent the continuation of the Northern Uganda Terrane. Based on geophysical evidence that will be discussed below, we consider the region to the northeast of the ASZ in Uganda and South Sudan as part of the Saharan Metacraton.

The ASZ has been correlated to other NW-trending shear zones (including the Najd fault system) in the Mozambique belt in the south and the Arabian–Nubian Shield to the north that are collectively named the East African Orogeny (Fig. 1; Stern, 1994). Burke and Sengör (1986) and Berhe (1990) postulated that the NW-trending shear zones together with minor NE-trending strike-slip shear zones represent conjugate sets of sinistral and dextral strike-slip fault systems, respectively. Further, Burke and Sengör (1986) and Berhe (1990) proposed that the shear zones were formed as a result of Neoproterozoic oblique collision between East and West Gondwana as escape roots due to northward expulsion of the Arabian–Nubian Shield from the Mozambique belt. However, Abdelsalam and Stern (1991) pointed out that the locations, trends and kinematics of these fault systems do not reconcile with an escape tectonics model as predicted by scaled models and observations from the indentation of India into Eurasia (Tapponnier et al., 1982).

A recent model for the geodynamic evolution of the ASZ by Westerhof et al. (2014) explained the early stages of its development as a sinistral strike-slip shear zone associated with northward escape of the Arabian–Nubian Shield and the northeastern segment of the Northern Uganda Terrane (shown in Fig. 1B as the Saharan Metacraton) because of oblique collision between East and West Gondwana. Further, Westerhof et al. (2014) proposed that the ASZ subsequently witnessed an E–W extension triggered by N–S collision between the proto-Congo craton and the Saharan Metacraton (Fig. 1A) and that the final assembly of Gondwana allowed for northwest and southeast propagation of the shear zone.

3. 1.2. THE LITHOSPHERIC STRUCTURE OF THE ASWA SHEAR ZONE

It has been suggested that the ASZ represents the boundary between the Congo craton in the southwest (represented in Uganda by the Northern Uganda Terrane of Westerhof et al. (2014)) and the Saharan Metacraton to the northeast (Fig. 1B; Abdelsalam et al., 2002, 2011).Seismic

tomography results suggested that the Saharan Metacraton has a lithospheric thickness of ~100 km compared to the Congo craton which has a lithospheric thickness of ~175–250 km Abdelsalam et al., 2011). Southwest of the ASZ, in the upper 100 km of the lithospheric column, the S-wave velocity is 2 to 6% faster relative to the Primary Reference Earth Model (PREM) while it is 2% slower relative to PREM northeast of the shear zone (Fig. 2A; Abdelsalam et al., 2011). A similar pattern is also present in the 100–175 km depth interval of the lithosphere (Fig. 2B). Additionally, from the N–S S-wave velocity profile, Abdelsalam et al. (2011) have shown that the northwestern continuation of the ASZ, which intersects the Oubanguide Orogen (Fig. 1A), as a much slower S-wave velocity compared to both the Congo craton and the Saharan Metacraton (Fig. 2C). In addition, Craig et al. (2011) have shown that there is a sharp transition in earthquake focal depths across the ASZ where the seismogenic thickness is less than 20 km northeast of the shear zone and it is greater than 20 km southwest of it (Fig. 2D). Craig et al. (2011) also observed that this sharp transition from shallow to deep seismogenic thickness coincides with a change from thin (~100 km) lithosphere northeast of the ASZ to a thick (~175 km) lithosphere southwest of the shear zone (Fig. 2E).

3.1.3. THE ASWA SHEAR ZONE AND EVOLUTION OF MESOZOIC AND CENOZOIC RIFTS IN EASTERN AFRICA

Although no detailed information is available, the parallelism between the NW-trending ASZ and the NW-trending Mesozoic rifts in eastern Africa, especially in South Sudan, led Daly et al. (1989) to consider strain localization during the Mesozoic rifting event as being facilitated by the ASZ and other related NW-trending shear zones. By contrast, relatively more research has been carried out to explain the influence of the ASZ on the evolution of the Cenozoic-aged East African Rift System, especially its bifurcation into an Eastern and a Western Branch and the apparent termination of the

Western Branch against the shear zone (Fig. 3A). The bifurcation of the East African Rift System southwest of the ASZ led Chorowicz (2005) to suggest that the shear zone has been reactivated as a "continental transform fault" where WNW–ESE extension exerted by the east–southeast motion of the Somali plate relative to the Nubian plate (Calais et al., 2006; Stamps et al., 2008; Saria et al., 2014) has been accommodated as a strike-slip motion along the shear zone.

The northern segment of the Western Branch of the East African Rift System represented by the Albertine–Rhino Grabens sharply terminates against the ASZ (Fig. 3B). However, the 1990–1991 earthquake events of South Sudan have been interpreted as an indication of the continuation of the Western Branch further northeast beyond the Albertine–Rhino Grabens (Girdler and McConnell, 1994). Contrary to this suggestion, Katumwehe et al. (2015) have shown from airborne magnetic data that the Albertine–Rhino Grabens do not extend in a northeast direction beyond the ASZ. Further, Katumwehe et al. (2015) suggested that the presence of the heterogeneous and thinned lithosphere of the Saharan Metacraton that lacks well-developed pre-existing lithospheric fabric might have prevented strain localization during the onset of rifting, hence leading to the apparent termination of the Western Branch against the ASZ.

Some of the Cenozoic shield volcanoes associated with the development of the Eastern Branch of the East African Rift System are found at or close to the intersection of the ASZ with the Cenozoic structure. For example, Mt Elgon, which is found in the Elgon depression to the west of the main trend of the Eastern Branch, is located along the trace of the ASZ (Fig. 3A). Similarly, Mt Kilimanjaro is located at the intersection of the ASZ with NE-trending structures related to the Eastern Branch (Fig. 3A). This led Fairhead (1980) to refer to the ASZ as the "leaky transform fault".

3.1.4. THE ASWA SHEAR ZONE AND SEISMICITY IN EASTERN AFRICA

The vicinity of the ASZ has been the site of seismic activities in eastern Africa (Fig. 3A and C; Gaulon et al., 1992; Girdler and McConnell, 1994; Moussa, 2008; Craig et al., 2011), especially the 1990–1991 earthquakes in South Sudan. A significant number of earthquakes with magnitudes 7.2 and focal depth of 20–50 km were reported in 1990–1991 in South Sudan. Fault plane solutions from these earthquakes suggest sinistral strike-slip movement along NW-trending planes, normal-slip movement within WNW-trending planes, and oblique-slip movement within WNW-trending planes (Fig. 3C; Moussa, 2008; Craig et al., 2011).

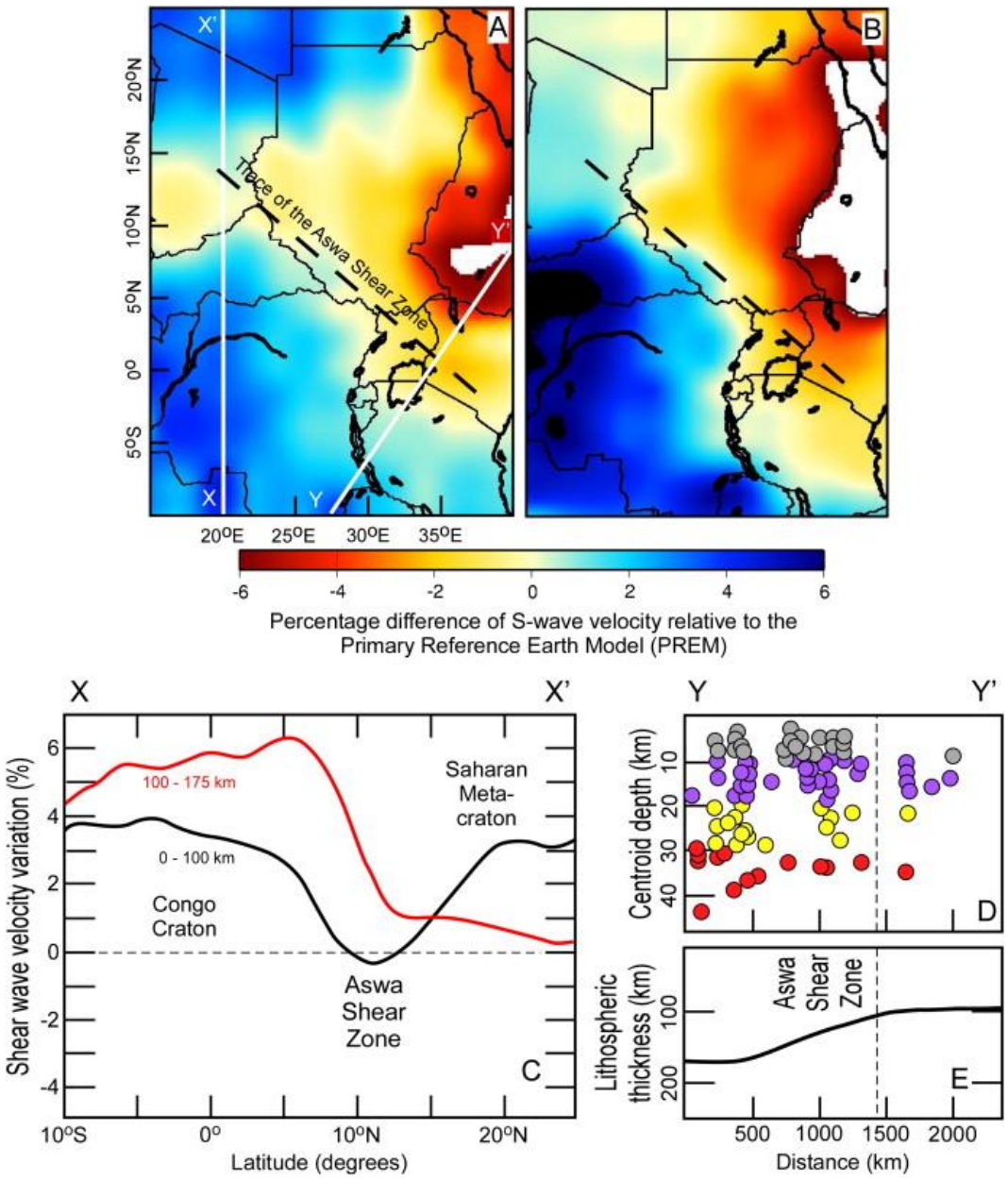

Figure 2: Lithospheric structure of the Aswa Shear Zone. (A) and (B) Shear wave velocity anomalies beneath eastern and central Africa at 0–100 km and 100–175 km depth, respectively.(C) N–S S-wave velocity profiles across the Aswa Shear Zone along longitude 20°E at 0–100 and 100–175 km depth. (A) (B) and (C) are adopted from Abdelsalam et al. (2011). (D) Depth distribution of earthquake foci across the Aswa Shear Zone. Grey= 0–9 km. Violet = 10–19 km. Yellow= 20–

29 km. Red = Greater than 30 km. (E) Lithospheric thickness variation across the Aswa Shear Zone. Figures (D) and (E) are adopted from Craig et al. (2011).

The normal-slip movement was considered to indicate northward continuation of the East African Rift System to the northeast of the ASZ (Gaulon et al., 1992; Girdler and McConnell, 1994) whereas the strike-slip movement was interpreted to be associated with the reactivation of the ASZ into sinistral strike-slip fault due to east-southeast movement of the Somali plate away from the stationary Nubian plate (Moussa, 2008). The reactivation of the ASZ from ductile Precambrian structure to younger brittle NW-trending fractures is also apparent in remote sensing data where morphologically-defined structures are observed to coincide with the trace of the shear zone (Fig. 4). This part of the shear zone has influenced the evolution of the Nile drainage system where the NE-flowing Albert Nile shifted its flow direction by making a sharp left turn when it encountered the ASZ to become the NW-flowing Bahr el Jabal (Fig. 4).

3.2. REGIONAL GEOLOGY OF THE ASWA SHEAR ZONE

The ASZ occupies an important region in the East African Orogeny since it is exposed close to the interface between the Arabian–Nubian Shield in the north and the Eastern Granulite belt to the south which represent part of the Mozambique belt (Fig. 1B). The exposed part of the shear zone in Uganda seems to separate Precambrian regions that differ in their characters. The region to the southwest of the shear zone is dominated by the Northern Uganda Terrane (Fig. 1B) which is composed of Mesoarchean granulites and Neoarchean gneisses, migmatites, and granitoids (Nyakecho and Hagemann, 2014; Westerhof et al., 2014). The northern part of this Terrane is intruded by a largely un-deformed Neoproterozoic granitic body. Differently, the region to the northeast of the ASZ is characterized by the presence of Neoproterozoic exposures of banded granulites–charnockites complexes together with highly sheared Neoproterozoic gneisses and

granitoids, and Archean– The ASZ occupies an important region in the East African Orogeny since it is exposed close to the interface between the Arabian–Nubian Shield in the north and the Eastern Granulite belt to the south which represent part of the Mozambique belt (Fig. 1B). The exposed part of the shear zone in Uganda seems to separate Precambrian regions that differ in their characters. The region to the southwest of the shear zone is dominated by the Northern Uganda Terrane (Fig. 1B) which is composed of Mesoarchean granulites and Neoarchean gneisses, migmatites, and granitoids (Nyakecho and Hagemann, 2014; Westerhof et al., 2014). The northern part of this Terrane is intruded by a largely un-deformed Neoproterozoic granitic body. Differently, the region to the northeast of the ASZ is characterized by the presence of Neoproterozoic exposures of banded granulites–charnockites complexes together with highly sheared Neoproterozoic gneisses and granitoids, and Archean– Paleoproterozoic gneisses (Nyakecho and Hagemann, 2014;Westerhof et al., 2014). Westerhof et al. (2014) concluded that the Neoproterozoic granulites–charnockites complexes are tectonically emplaced and they represent three allochthonous sheets referred to as the Morungole, Akur and Ukatat massif (Fig. 1B). These allochthonous sheets were thrust above the Archean–Paleoproterozoic gneisses. Further, Westerhof et al. (2014) proposed that the source of the Neoproterozoic banded granulites–charnockites allochthonous sheets is the deeper roots of the suture between East and West Gondwana.

Fritz et al. (2013), Westerhof et al. (2014) and Nyakecho and Hagemann (2014) agreed that the Neoproterozoic rocks in the northeastern-most part of Uganda belong to the East African Orogen. Westerhof et al. (2014) referred to these exposures as the Pan-African Karamoja belt (Fig. 1B). Fritz et al. (2013) linked the evolution of the ASZ to that of the Nyangere shear zone, which marks the western boundary of the Arabian–Nubian Shield (Fig. 1B). Also, Fritz et al. (2013) suggested that the ASZ continues to the southeast into Tanzania and merges into a NW-trending sinistral strike slip fault referred to as the 'Jailhouse rock fault' (Fig. 1B). Based on regional correlation between the ASZ and the Nyangere shear zone, Fritz et al. (2013) suggested that sinistral strike-

slip activities in the ASZ might have commenced prior to ~590 Ma. This is based on cross-cutting relationships where the Nyangere shear zone is cut by an un-deformed granitic body which gave a whole rock Rb/Sr isochron age of 593+/−50 Ma (Ries et al., 1992). Recently, Westerhof et al. (2014) reported U–Pb zircon ages of ~2660 Ma and ~690 Ma from a migmatite granitic body that is deformed by the ASZ and interpreted the younger age as due to overprint of blasto-mylonite peak metamorphism associated with the onset of the ASZ activities. Further, Westerhof et al. (2014) interpreted a U–Pb zircon age of 659+/−15Ma obtained from an elongated granitic body (2–4 km wide and ~75 km long) that intrudes the northwestern part of the ASZ to indicate the age of an extensional activity in the shear zone exerted by N– S collision between the proto-Congo craton and the Saharan Metacraton.

Almond (1962) described the ASZ as a ~6 km wide zone of sinistral strike-slip shearing characterized by the development of mylonitic fabric that deforms older gneissic layering. Almond (1962) pointed out that the gneisses across the shear zone are of different character because the sinistral strike-slip movement along the shear zone brought different rock types to juxtaposition. Recent observations by Ruotoistenmäki (2014) from airborne magnetic data have shown that the ASZ is wider than what has been mapped from the surface geology. Westerhof et al. (2014) described the ASZ as a complex zone of steeply NE and SW-dipping ductile-brittle sinistral strike-slip fabric characterized by the presence of discrete blasto-mylonite high-strain zones that enclose lenses which are relatively not affected by the shearing. Westerhof et al. (2014) also observed that in many places, the planar fabric of the ASZ deforms the gneisses of the North Uganda Terrane resulting in the transposition of the older gneissic banding leading to the formation of rootless isoclinal folds. Westerhof et al. (2014) documented in some outcrops the transitioning of the blasto-mylonite fabric into pseudotachylite as well as the formation of boudinage structure due to the deformation of a pre-existing dolerite dike by the sinistral strike-slip movement of the ASZ.

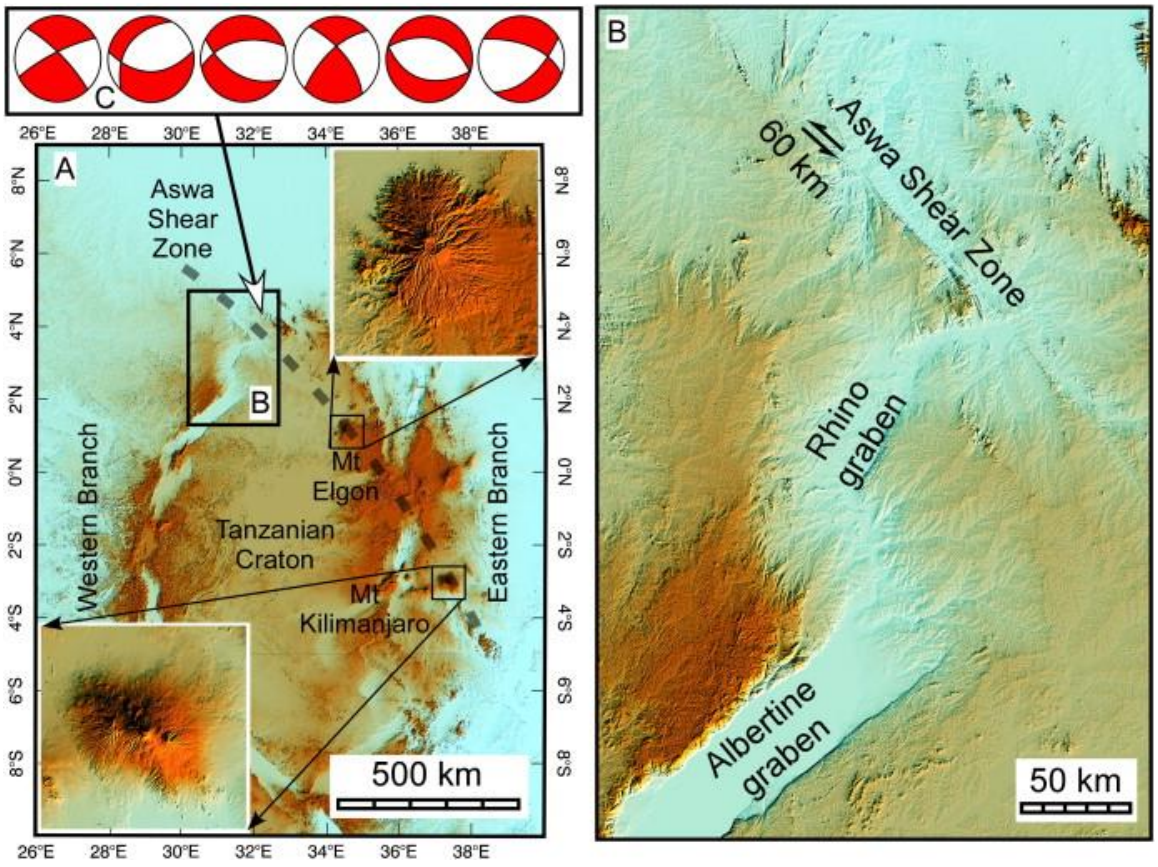

Figure 3: (A) Shuttle Radar Topography Mission (SRTM) Digital Elevation Model (DEM) showing the bifurcation of the East African Rift System into the Eastern and Western Branches southwest of the Aswa Shear Zone. (B) SRTMDEM showing the Western Branch represented by the Albertine–Rhino Grabens terminating against the Aswa Shear Zone. (C) Fault plane solutions of earthquakes occurred along the Aswa Shear Zone from Moussa (2008) and Craig et al. (2011). Red = Compressional stress. White= Tensile stress.

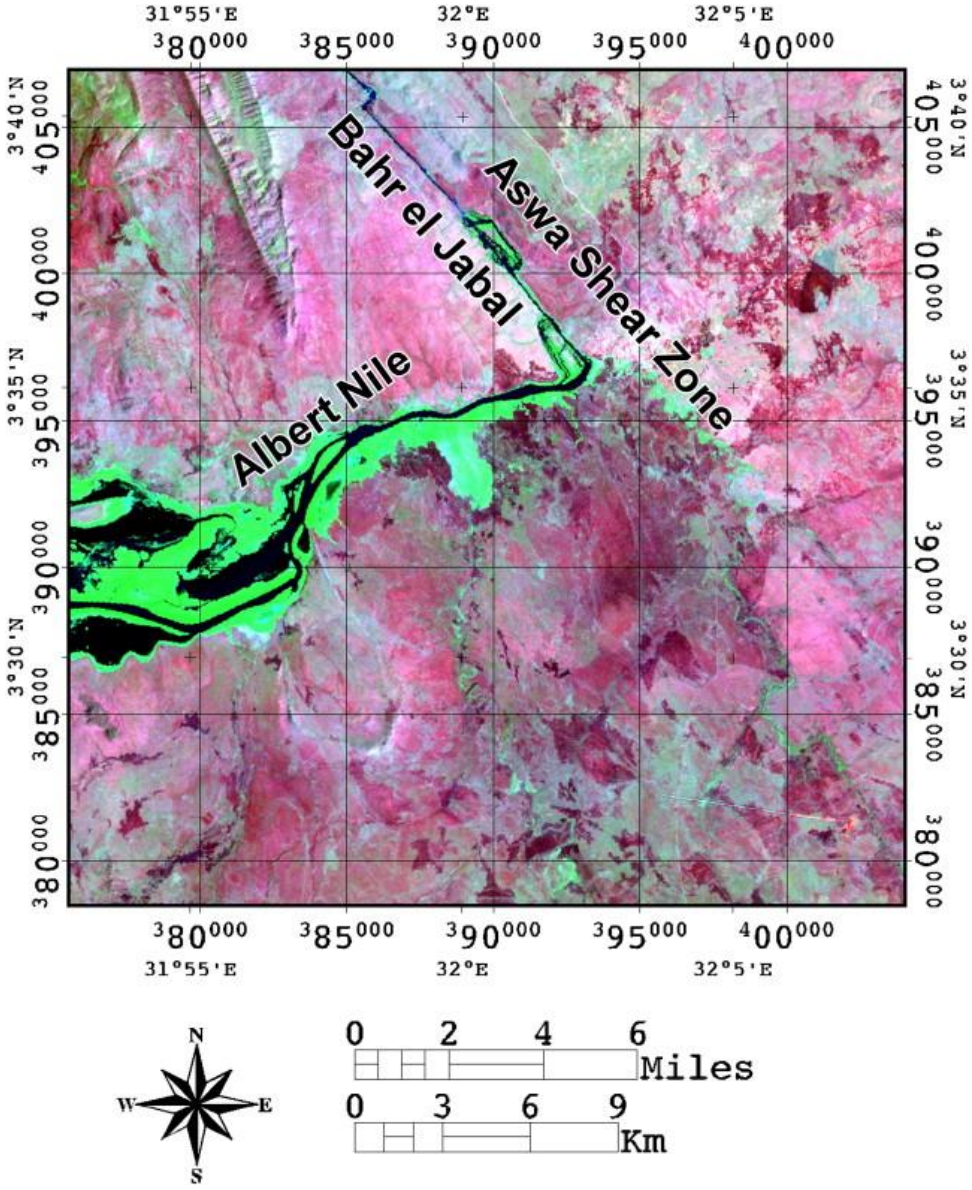

Figure 4: A 7-4-2 Landsat Thematic Mapper (TM) image showing the reactivation of the Precambrian ductile structure of Aswa Shear Zone to younger brittle and morphologically-defined fractures that changed the flow direction of the Nile from northeast (Albert Nile) to northwest (Bahr el Jabal).

3.3. DATA AND METHODS

3.3.1. AIRBORNE MAGNETIC DATA

The airborne total field magnetic data we used in this study (Fig. 5A) were part of a 2006–2009 data acquisition campaign by the Ugandan Department of Geological Survey and Mines (DGSM) that covered 80% of the country. The data were collected with a flight altitude of ~80 m, line spacing of ~500 m, and a flight orientation of ~N55°. The low magnetic inclination in the study area that ranges between−14° and−22° did not allow us to identify the sources of the magnetic anomalies using conventional methods such as the reduction to the pole. Alternatively, to highlight the general trends of the Precambrian structures through the magnetic anomalies, we have extracted a horizontal derivative map from the total field magnetic data (Fig. 5B). The results of this edge detection filtering technique are not affected by the magnetic inclination, declination or remanence (Thurston and Smith, 1997; Smith and Salem, 2005). Hence, because the horizontal derivative map images the edges of the magnetized bodies, we were able to use the resulting magnetic fabric (Fig. 5B) as a proxy for mapping regional Precambrian structures.

We have developed a new method to measure the orientation of the strike and the dip amount and direction of the regional Precambrian structures from the airborne magnetic data. First, we used the magnetic fabric defined by the horizontal derivative map to measure the strike of the regional Precambrian structures in specific locations of the study area. Second, using the technique established by Thurston and Smith (1997), Verduzco et al. (2004), Smith and Salem (2005) and Salem et al. (2007) we developed a tilt derivative image by obtaining the ratio of the vertical derivative to the horizontal derivative of the total field airborne magnetic data (Fig. 5C). In this image, the tilt distribution defines the contacts between geological materials that have alternating high and low magnetic susceptibility (Salem et al., 2007). The calculated tilt angles range between +90° and −90° with the angle values with (+) sign represent the tilt of the magnetic source towards

the northeast and southeast quadrants. The angle values with (−) sign indicate tilt direction towards the southwest and northwest quadrants. Third, we extracted the tilt angles and directions from the tilt derivative image for the same locations where we used the horizontal derivative image to measure the strike of the magnetic fabric. This allowed us to establish strike and dip datasets for the study area.

3.3.2. AIRBORNE RADIOMETRIC DATA

The airborne radiometric data we used in this study (Fig. 5D) were simultaneously acquired with the airborne magnetic data. The emission of gamma rays through radioactive decay of naturally occurring radioisotopes has proven useful for mapping the boundaries of geological units (Duval, 1983; Minty, 1997). Hence, gamma ray surveys have been used to image the geochemical characteristics of the Earth surface and near surface to a depth of 30 cm (Erdi-Krausz et al., 2003). The three radioisotopes that have been traditionally used for geological mapping include Potassium (K), Uranium (U) and Thorium (Th). The emission of gamma rays during the decay of ^{40}K to the stable isotope Argon (40Ar) can be used to estimate the amount of K in the geological unit. Radioisotopes ^{238}U and ^{235}U decay to stable Lead isotope (^{206}Pb) and (^{207}Pb), respectively. The naturally occurring radioisotope ^{232}Th decay series ends in producing isotope ^{208}Pb.

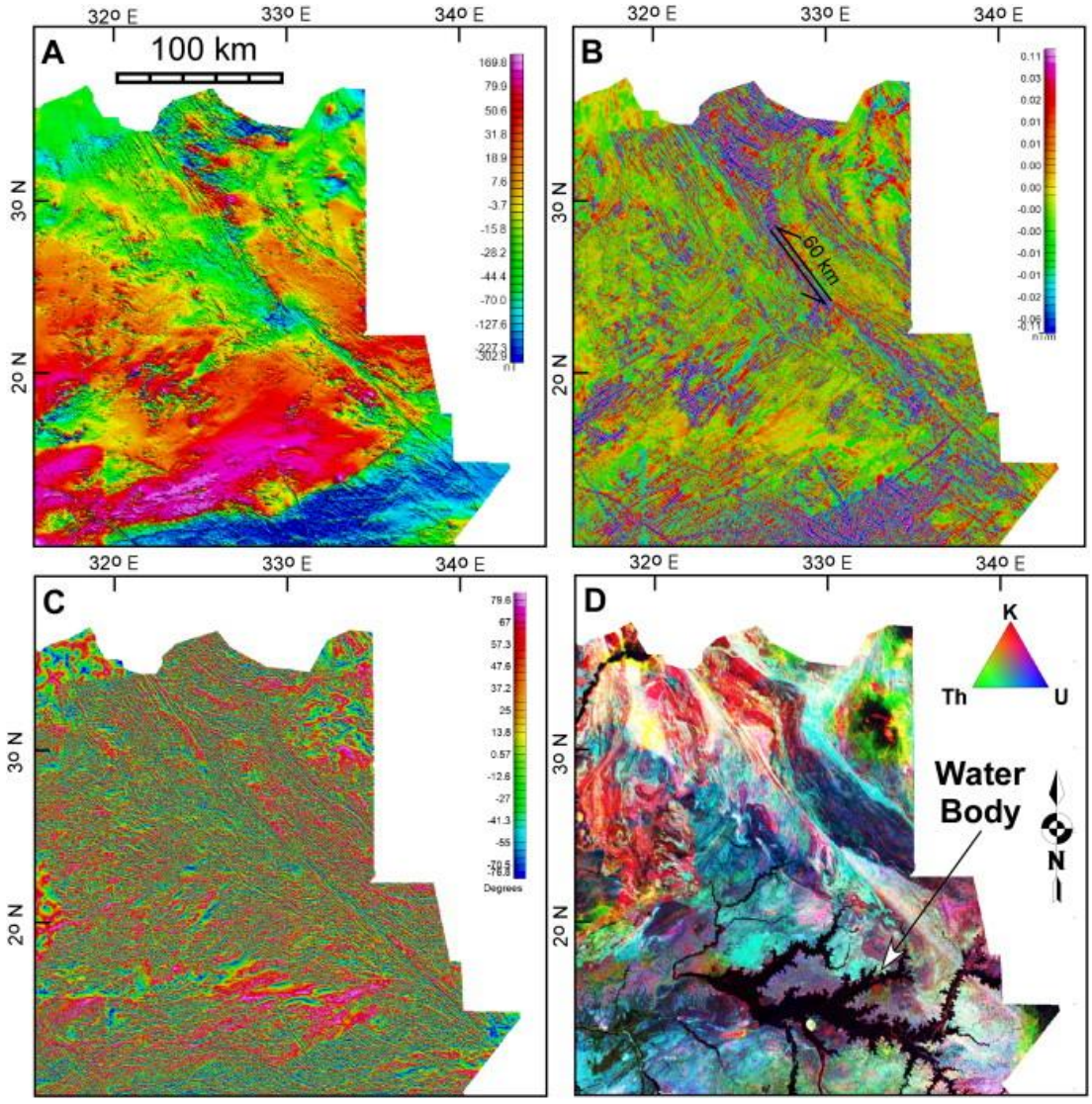

Figure 5: Airborne geophysical data of northeastern Uganda. (A) Total field magnetic image. (B) Horizontal derivative magnetic image. (C) Tilt derivative magnetic image. (D) Ternary radiometric image.

The concentration of radioisotopes 238U and 232Th in any geological unit can be indirectly estimated from the gamma ray emission of their radioactive daughter products. This is because these radioisotopes do not emit gamma ray in their initial radioactive decay process. Assuming that the radioactive daughter products of radioisotopes 238U and 232Th are under equilibrium, the

concentration of the two radioisotopes can be estimated as the equivalents eU and eTh in parts per million (ppm).

After removing the noise from the airborne radiometric data using the noise-adjusted value decomposition method, we used the minimum curvature gridding algorithm (Briggs, 1974; Grasty, 1997; Minty and McFadden, 1998) to obtain K, eTh, and eU concentrations from the airborne radiometric data with a grid cell spatial resolution of 50 m. Subsequently, we created a ternary image by assigning the K concentration to red, the eTh concentration to green, and the eU concentration to blue (Fig. 5D). Areas with high concentration of all three radioisotopes appear white in the ternary image. Differently, areas that lack concentration of all radioisotopes appear black as in the case of water bodies (Fig. 5D). The color yellow in the ternary image is indicative of high K and Th concentration, magenta reflects high concentration of K and U, whereas cyan manifests high Th and U concentration.

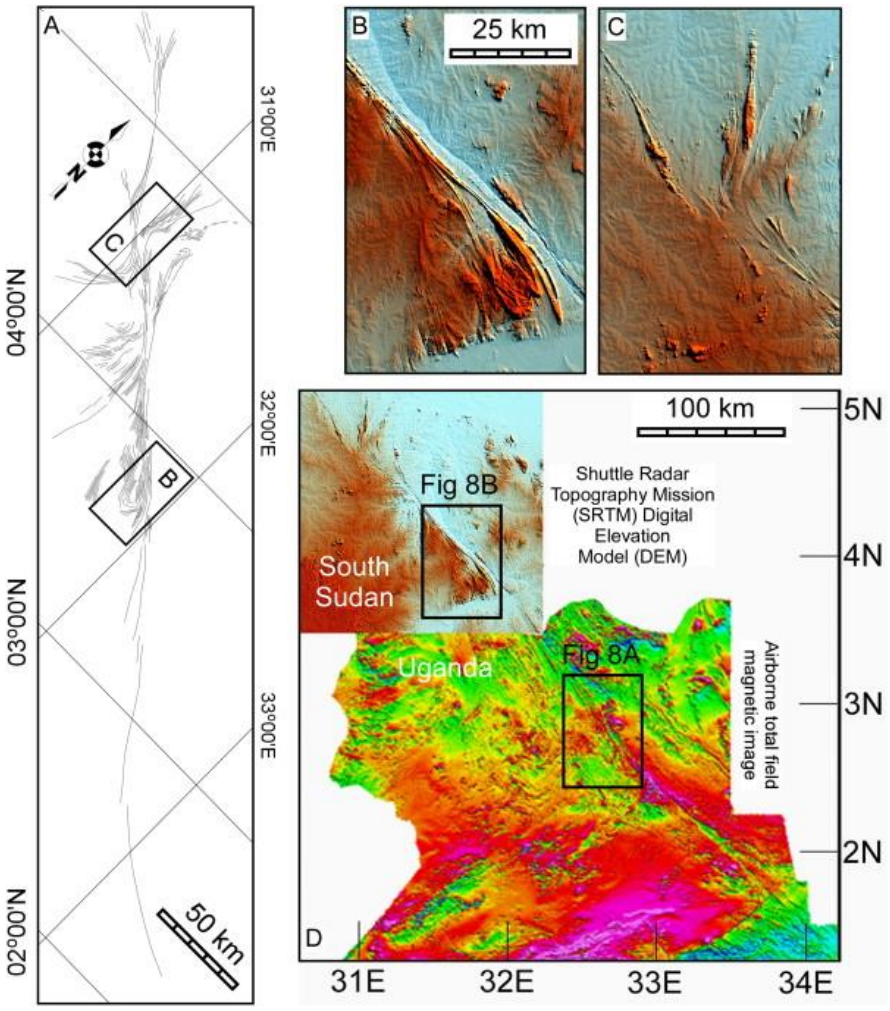

Figure 6. (A) Trajectories of the main structural trends of the Aswa Shear Zone in Uganda and South Sudan extracted from the interpretation of Shuttle Radar Topography Mission (SRTM) Digital Elevation Model (DEM). (B) SRTM DEM showing tight NW–SE trending folds related to the Aswa Shear Zone. (C) SRTMDEM showing N and NE-trending structural splays related to the Aswa Shear Zone. (D) Integration of SRTM DEM from South Sudan and airborne total field magnetic image from Uganda showing the extent and structural complexity of the Aswa Shear Zone

3.4. RESULTS

3.4.1. THE EXTENT OF THE ASWA SHEAR ZONE

The SRTM DEM enabled us to map the extent of the ASZ in Uganda and South Sudan for over ~550 km extending from longitude 30° 20′E and latitude 5° 20′N in the northwest to longitude 33° 30′E and latitude 2° 10′N in the southeast (Fig. 6A). In the northwest, the shear zone bifurcates into a number of NW-trending splays before disappearing under what seems to be unconsolidated sediments (Fig. 6A). To the southeast, in Uganda the trace of the shear zone disappears under the volcanic pile of Mt Elgon (Fig. 3A). In Uganda, the SRTM DEM shows the shear as a single linear trend that persists in a NW–SE direction for ~250 km (Fig. 6A).

The surface expression of the ASZ is more apparent in South Sudan where the southeastern end of the shear zone is dominated by what appears to be tight folds that lie sub-parallel to the prominent trend of the shear zone itself (Fig. 6B). The central part of the shear zone in South Sudan is characterized by the presence of splays of regional fabric originating from the main trace of the shear zone resulting in the presence of N and NE-trending structures (Fig. 6C). Although the ASZ in Uganda has a limited surface expression observable in the SRTM DEM, the airborne total field magnetic image revealed it as a much wider structure similar to its extent in South Sudan (Fig. 6D).

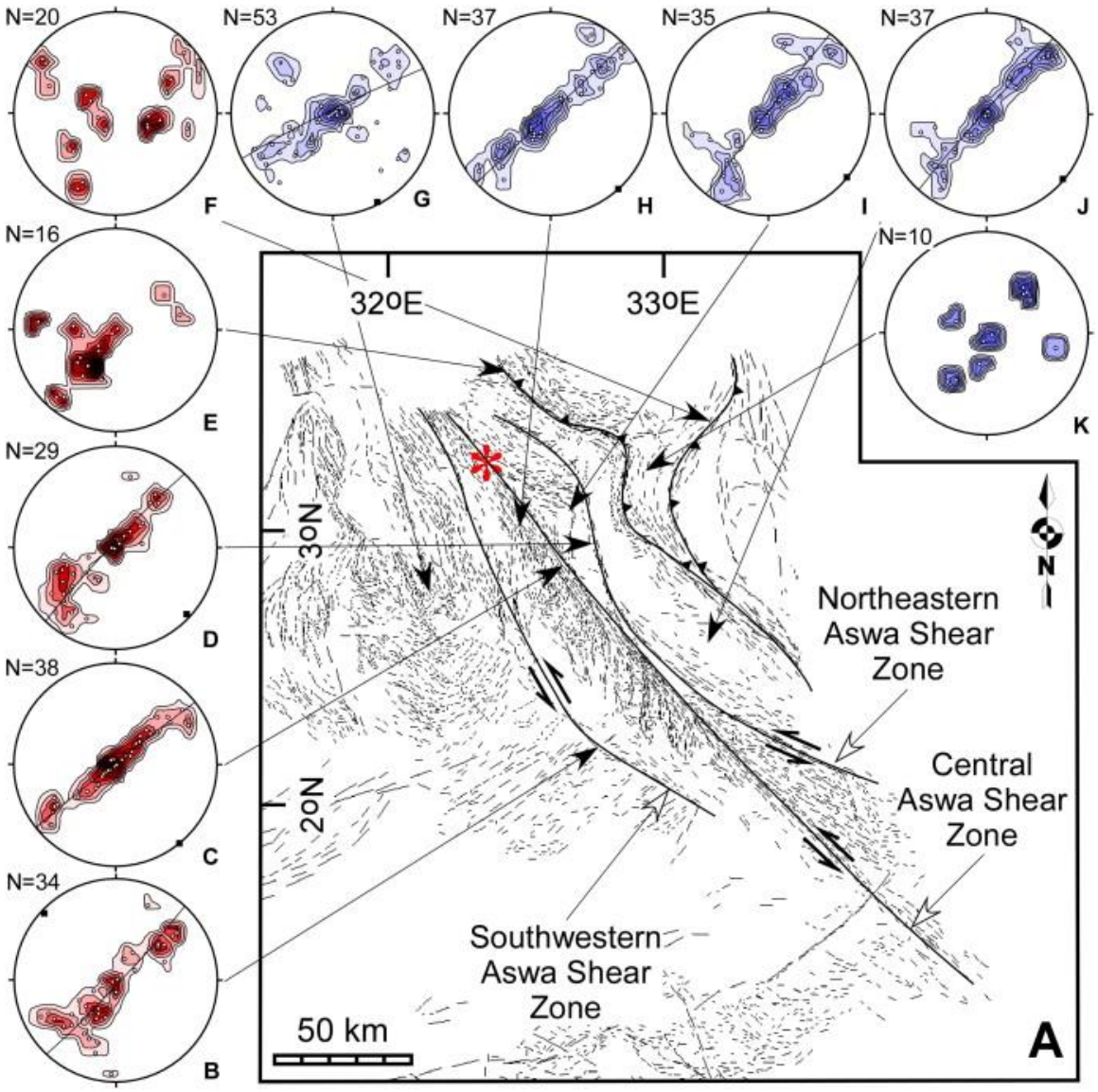

Figure 7: (A) Structural trajectories of the Aswa Shear Zone and surrounding domains and deformation belts in Uganda extracted from the horizontal derivative image in Fig. 5B. (B–K) Plot of poles to magnetic fabric in equal area stereonets with contouring interval at 1% per unit area. (B–D) π-diagrams from the three branches of the Aswa Shear Zone showing folding around NW–SE trending axis. (E) Plot of planar magnetic fabric from the deformation belt northeast of the Aswa Shear Zone indicating shallowly-dipping to the northeast planar fabric. (F) Plot of magnetic fabric from the deformation belt in the far northeastern part of the study area showing the lack of any preferred orientation of the planar fabric. (G) π-diagram of the domain southwest of the Aswa Shear

Zone showing folding about SSE-plunging axis. (H–J) π-diagrams of the domains bounded by the three branches of the Aswa Shear Zone and the one to the northeast showing folding about NW–SE trending axes. (K) Plot of planar magnetic fabric from the domain bounded by the two thrusts showing no obvious preferred orientation of the planar fabric. The red star indicates the location of folded mylonite fabric reported by Almond (1962).

The Extraction of structural lineation from the horizontal derivative (Fig. 5B) and the ternary image (Fig. 5D) revealed a more complicated picture of the ASZ in Uganda (Fig. 7A) than what is apparent in the SRTMDEM. This image shows that the ASZ is characterized by the presence of three branches that are separated from each other with distances ranging between 5 and 30 km (Fig. 7A). Here, we refer to these branches as the northeastern ASZ, central ASZ, and southwestern ASZ (Fig. 7A). The central ASZ corresponds to the exposed part of the shear zone that is traced from the SRTM DEM as a single linear feature (Fig. 6A). This branch of the shear zone is also distinct in the ternary image by its bright to white color indicating high K, Th and U concentrations (Fig. 5D). The northeastern ASZ exhibits a curvilinear pattern by changing orientation from NW-trending in the northwest to N-trending in the central part and back to NW-trending in its southeastern end (Fig. 7A). This branch seems to separate a domain of variable K, Th and U concentrations in the southwest from a domain with no specific radiometric concentration in the northeast (Fig. 5D). The southwestern ASZ is less obvious in the ternary image suggesting that it does not separate two distinct lithologies (Fig. 5D). However, this branch is more apparent in the horizontal derivative image because it separates domains with different orientations of the magnetic fabric (Figs. 5B and 7A). The domain in the southwest is dominated by magnetic lineation that defines N-trending broad open folds (Figs. 5B and 7A). On the other hand, the domain that is bounded by the southwestern and the central ASZ is characterized by sigmoidal N-S-trending magnetic fabric sometimes defined by what appears to be tight folds (Figs. 5B and 7A).

The region to the northeast of the ASZ is dominated by well-defined and strong linear magnetic fabric that we interpret as indicating the presence of at least two major structural boundaries (Figs. 5B and 7A). These two boundaries bound a funnel-shaped region shown by cyan color in the ternary image indicative of high Th and U concentration (Fig. 5D). This is followed further northeast by a domain that lacks any significant magnetic fabric (Fig. 5B) with either Th or no radioisotopes.

3.4.2. KINEMATICS OF THE ASWA SHEAR ZONE

3.4.2.1. SENSE AND AMOUNT OF DISPLACEMENT ALONG THE ASWA SHEAR ZONE

Ruotoistenmäki (2014) used offsets of magnetic anomaly to suggest ~60 km horizontal sinistral strike-slip movement along the ASZ. The displacement of a similar magnetic anomaly to the northwest of the one that was measured by Ruotoistenmäki (2014) also gave ~60 km horizontal displacement (Fig. 5B). Additionally, a similar amount of horizontal sinistral strike-slip displacement has been observed from drag features related to the shear zone that appear in the SRTM DEM in South Sudan (Fig. 3B).

3.4.2.2. STRUCTURAL COMPLEXITY OF THE ASWA SHEAR ZONE

The strike and dip of the magnetic fabric defining the ASZ and surrounding structures extracted from the airborne magnetic data were used to outline the three-dimensional (3D) geometry of these structures. For this, we established a number of structural domains that are separated by the three branches of ASZ as well as the two additional localized deformation zones to the northeast (Fig. 7A). Subsequently, to analyze the dominant orientation of the deformation zones, the strike and dip of the magnetic fabric along the entire length of each boundary were plotted as poles to planar fabric in equal area stereonet (Fig. 7B–F). Additionally, to analyze the geometry of the structures

dominating the domains between the deformation zones, the magnetic fabric from these domains were plotted as poles to planar fabric in equal area stereonet (Fig. 7G–K).

We drew the following observations from these plots:

1) The three branches of the ASZ (Fig. 5A) show a consistent pattern of stereonets indicative of the presence of sub-horizontal NW–SE trending fold axes (Fig. 7B–D). Assuming that the magnetic fabric defines the regional NW-trending, steeply NE and SW-dipping mylonitic fabric associated with the sinistral strike-slip shearing of the ASZ as observed by Westerhof et al. (2014), our results suggest that the mylonitic planar fabric itself has been subsequently folded. This is consistent with field observations from outcrops where refolding of the mylonitic fabric is apparent (Fig. 7A; Almond, 1962). This in turn suggests a strong role of an E–W to NE–SW contraction component in the development of the ASZ.

2) The stereonet plot in the localized deformation zone to the northeast of the northeastern ASZ does not support the presence of NW–SE trending folding of the magnetic fabric (Fig. 7E). Rather, the plot suggests the presence of shallow to moderately dipping to the northeast planar fabric within the localized deformation zone. Farther to the northeast, the magnetic fabric from the northeastern-most deformation zone produced a stereonet plot that lacks clear presence of any preferred orientation of the planar fabric. (Fig. 7F). This deformation zone bounds a region in the east that lacks obvious magnetic lineation possibly due to the presence of sub-horizontal magnetic fabric (Fig. 5B). Comparing the airborne magnetic images with the geological map of Westerhof et al. (2014) and Nyakecho and Hagemann (2014) revealed that this region is dominated by one of the Neoproterozoic banded granulites–charnockites complexes that is structurally underlain by the highly-sheared Neoproterozoic gneisses and granitoids. The Neoproterozoic banded granulites–charnockites complex fall within the northwestern along-strike continuation of the Eastern Granulite belt which is better defined in Tanzania and Kenya (Fig. 1B). This belt is interpreted as

dominantly W-verging nappe (Fritz et al., 2013). As initially proposed by Westerhof et al. (2014), we consider the two deformation zones to the northeast of the ASZ to represent W-verging thrusts where the highly-sheared Neoproterozoic gneisses and granitoids on the one hand and the granulites–charnockites complex on the other hand were thrust westward over the Archean–Paleoproterozoic gneisses. This observation further reinforces the notion that a strong E–W to NE–SW contraction component played a significant role in the final architecture of the ASZ.

3) The domain to the southwest of the southwestern ASZ is characterized by the presence of open folds defined by NW and NE-trending magnetic fabric (Figs. 5B and 7A). Plotting the poles of the magnetic fabric in equal area stereonet indicates that the fold axis is shallowly plunging to the south-southeast (Fig. 7G). Westerhof et al. (2014) documented that these open folds are younger Neoproterozoic structure that refolded the planar fabric and isoclinal folds of the older Archean rocks of the Northern Uganda Terrane.

4) The stereonets of the domains bounded by the three branches of the ASZ show a common pattern indicating folding about NW–SE trending axes (Fig. 7H–J). One example of these folds is found within the domain that is bounded by the southwestern and central ASZ where the magnetic fabric defines what appears to be a tight NW–SE trending fold (Fig. 8A). This is similar to the fold geometry observed in the SRTM DEM ~150 km to the northwest (Fig. 8B). The axial traces of these folds (as estimated from the magnetic fabric and SRTM DEM) are at slight angle to the NW-trend of the ASZ. This suggests the development of these folds as due to secondary ENE-WSW contraction component associated with the overall sinistral strike-slip movement on the NW-trending planes of the shear zone.

5) The plot of poles to the magnetic fabric from the domain to the northeast of the ASZ does not seem to define any particular π- circle in the equal area stereonet (Fig. 7K). This might be due

to superimposition of more than one folding event since this domain is bounded by curved boundaries that have been interpreted as W verging thrusts.

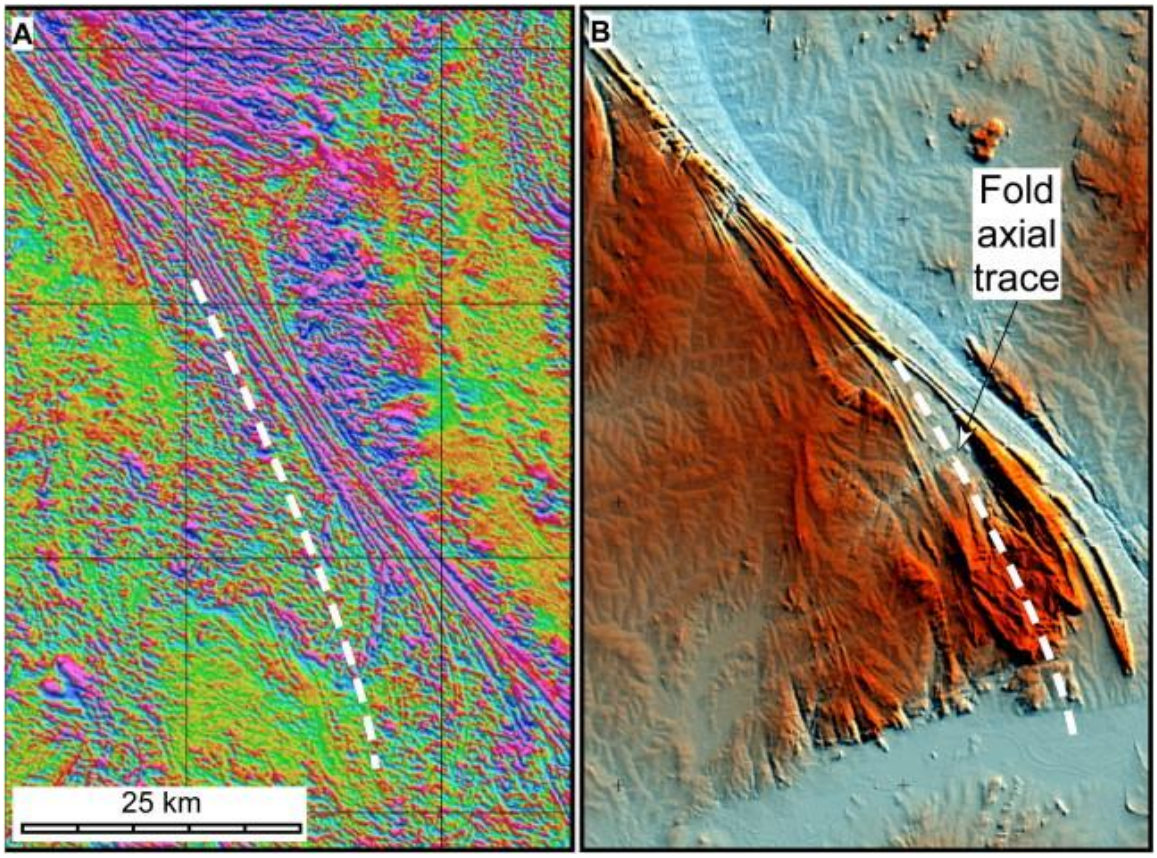

Figure 8. Horizontal derivative image from the domain bounded by the central and southwestern branches of the Aswa Shear Zone in Uganda (A) and Shuttle Radar Topography Mission (SRTM) Digital Elevation Model (DEM) from Aswa Shear Zone in South Sudan (B) showing NW–SE trending folds. See Fig. 6 for location.

3.5. DISCUSSION

3.5.1 UNDERSTANDING THE TECTONIC ORIGIN OF THE ASZ

We outline observations that are important for understanding the tectonic origin of the ASZ. (1) Our results show that the mylonitic fabric which was developed due to sinistral strike-slip shearing was subsequently refolded (Fig. 7B–D). The stereonets in Fig. 7B–D show folding of the planar fabric about NW–SE axes indicating that an E–W to NE– SW contraction component is recorded throughout the region. (2) Our results also show that the domains bounded by the three branches of the ASZ are dominated by NW–SE trending folds (Fig. 7G–J). (3) Our observations agree with those of Westerhof et al. (2014) in that the region to the northeast of the ASZ is dominated by W-verging thrusts where Neoproterozoic banded granulites–charnockites complexes form allochthonous units overlying highly-sheared Neoproterozoic gneisses and granitoids which themselves overly Archean–Paleoproterozoic gneisses. (4) Farther east, along the Uganda–Kenya border, previous studies documented the presence of a heterogeneous W-verging nappe consisting of Neoproterozoic granulites, granitic gneisses, amphibolite, quartzites and marbles (Fig. 9A) and these lithologies have been referred to by Westerhof et al. (2014) as the Pan-African Karamoja belt. This nappe represents the western margin of the Arabian–Nubian Shield as evidenced by the presence of Sekerr ophiolite found in Kenya just to the east (Fig. 1B; Fritz et al., 2013).

The observations above indicate the presence of a strong E–W to NE–SW contraction component that has affected this part of the East African Orogen, the Saharan Metacraton, and the Northern Uganda Terrane. We attribute this contraction to E–W to NE–SW oblique collision between East and West Gondwana. This interpretation is in good agreement with a model previously proposed by Westerhof et al. (2014) to explain the early stages of the development of the ASZ. The collision obliquity must have contributed to the partitioning of strain into E–W to NE–SW contraction and NW-trending sinistral strike-slip component.

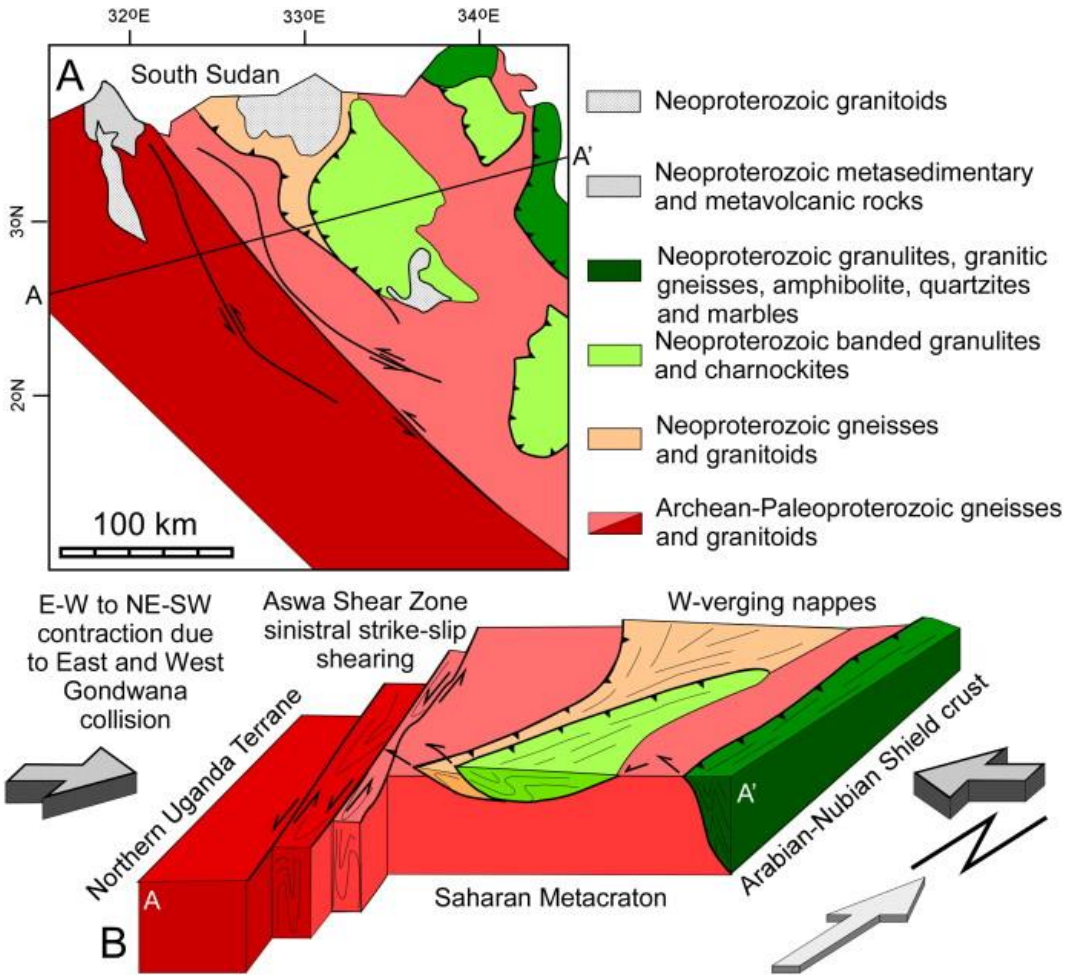

Figure 9: (A) Geological map of the Aswa Shear Zone and the surrounding structures in northeast Uganda generated from the structural analysis of airborne geophysical data and geological maps published by Westerhof et al. (2014) and Nyakecho and Hagemann (2014) showing distribution of different lithological units. (B) Three-dimensional (3D) diagram illustrating the evolution of the Aswa Shear Zone as a NW-trending sinistral strike-slip shear zone due to E–W to NE–W contraction that accompanied Neoproterozoic oblique collision between East and West Gondwana.

Hence, we suggest that the oblique collision resulted in the development of W-verging nappes on the eastern edge of the Saharan Metacraton, and these nappes represent part of the Arabian–Nubian Shield (Fig. 9B). The collision also resulted in the westward emplacement of the Neoproterozoic banded granulites–charnockites complexes onto the Archean–Paleoproterozoic gneisses of the

Saharan Metacraton (Fig. 9B). To the west, the collision was accommodated as dominantly sinistral strike-slip movement accompanied by E–W to NE–SW contraction. It is possible that the strain localization within the ASZ was facilitated by the presence of a pre-existing boundary between the Saharan Metacraton and the Northern Uganda Terrane. Gondwana based on the orientation and kinematic similarities between the ASZ and the Najd fault systems (both are regional NW-trending sinistral strike-slip shear zones), the age difference suggests separate evolutionary development for both of them.

3.6. CONCLUSIONS

The analysis of airborne magnetic and radiometric data over Uganda and SRTM DEM covering Uganda and South Sudan allowed tracing the Precambrian ASZ for over 550 km in a NW–SE direction with a width of ~50 km in Uganda. Unlike its exposed part in Uganda, the airborne geophysical data revealed three branches of the shear zone which bound structural domains characterized by the presence of secondary shear zones and shear-related folds. The shear-related folds are also apparent in the SRTM DEM covering South Sudan. Both the airborne geophysical data and the SRTM DEM indicate that the ASZ is a sinistral strike-slip system with ~60 km horizontal displacement. The region to the northeast of the shear zone in Uganda is dominated by magnetic fabric indicating the presence of W-verging nappes. The folding of magnetic fabric defining the ASZ about NW–SE trending axis, presence of NW–SE folds within the structural terrains bounded by the shear zone branches, and the presence of W-verging nappes to the northeast of the shear zone all indicate a strong E–W to NE–SW contraction component that played an important role in the evolution of the shear zone. This contraction component is possibly related to Neoproterozoic E–W to NE–SW oblique collision between East and West Gondwana. This collision resulted in the development of the ASZ as a NW-trending sinistral strike-slip and E–W to

NE–SW contraction belt between the Archean–Paleoproterozoic crusts of the Saharan Metacraton in the northeast and the Northern Uganda Terrane to the southwest. This collision also resulted in the emplacement of the W-verging nappes of the Arabian–Nubian Shield and the Eastern Granulite belt on the eastern edge and atop the Saharan Metacraton, respectively.

Fritz et al. (2013), from regional geologic correlation, considered the ASZ to be active prior to ~590 Ma. However, U–Pb zircon ages obtained by Westerhof et al. (2014) suggest that the Neoproterozoic activities of the ASZ might have been between ~690 and ~660Ma. The 690–660Ma age of the ASZ activities seems to be older than the 640–560 Ma timing of activities of the Najd fault system in the northern part of the Arabian– Nubian Shield (Stern, 1994). Hence, although it is tempting to suggest a common origin for the two structures within the Neoproterozoic collisional tectonics between East and West.

3.7 ACKNOWLEDGMENTS

We thank the Government of Uganda for allowing us free access to the airborne magnetic and radiometric data. This study was financially supported by the National Science Foundation Continental Dynamics grant # EAR 1255233.We thank two anonymous reviewers for their detailed comments and associate Editor A. Collins for handling the manuscript. This is Oklahoma State University Boone Pickens School of Geology contribution number 2015–21.

3.8 REFERENCES

Abdelsalam, M. G., Stern, R. J., 1991. Comments and Reply on “Ophiolites in northeast and east Africa: implication for Proterozoic crustal growth”. Journal of the Geological Society, London 148, 600-606.

Abdelsalam, M.G., Liégeois, J.P., Stern, R.J., 2002. The Saharan Metacraton. Journal of African Earth Sciences 34, 119-136.

Abdelsalam, M.G., Gao S.S., Liegeois J.P., 2011. Upper mantle structure of the Saharan Metacraton, Journal of African Earth Sciences 60, 328-336.

Almond D. C., 1962. Explanation of the Geology of Sheet 15 (Kitgum). Geological Survey of Uganda Report number 8, 55p.

Berhe, S.M., 1990. Ophiolites in Northeast and East Africa: implications for Proterozoic crustal growth. Journal of the Geological Society, London 147, 41-57.

Briggs, I.C., 1974. Machine contouring using minimum curvature. Geophysics 39, 39-48.

Burke, K., Sengör, C., 1986. Tectonic escape in the evolution of the continental crust. Geodynamics Series 14, 41-53.

Calais, E., Ebinger C., Hartnady C., Nocquet J.M., 2006. Kinematics of the East African Rift from GPS and earthquake slip vector data. Geological Society of London Special Publications 259, 9-22.

Chorowicz, J., 2005. The East African Rift System. Journal of African Earth Sciences 43, 379-410.

Collins, A.S., Fitzsimons, I.C.W., Hulscher, B., Razakamanana, T., 2003. Structure of the eastern margin of the East African Orogen in central Madagascar. Precambrain Reseaarch 123, 111-133.

Craig, T. J., Jackson, J. A., Priestley, K., McKenzie, D., 2011. Earthquake distribution patterns in Africa: their relationship to variations in lithospheric and geological structure, and their rheological implications. Geophysical Journal International 185, 403-434.

Daly, M., Chorowicz, J., Fairhead, J., 1989. Rift basin evolution in Africa: the influence of reactivated steep basement shear zones. Geological Society of London Special Publications 44, 309-334.

Duval, J., 1983. Composite color images of aerial gamma-ray spectrometric data. Geophysics 48, 722-735.

Erdi-Krausz, G., Matolin, M., Minty, B., Nicolet, J.-P., Reford, W.S., Schetselaar, E., 2003. Guidelines for radioelement mapping using gamma-ray spectrometry data. International Atomic Energy Agency Publication IAEA-TECDOC-1363, Vienna, Austria, 173 p.

Fairhead, J.D., 1980. The structure of the cross-cutting volcanic chain of northern Tanzania and its relation to the East African Rift System.Tectonophysics 65, 193–208.

Fernandez-Alonso,M., Cutten, H., DeWaele, B., Tack, L., Tahona, A., Baudet, D., Barritt, S.D., 2012. The Mesoproterozoic Karagwe-Ankole Belt (formerly the NE Kibara Belt): the result of prolonged extensional intracratonic basin development punctuated by two short-lived far-field compressional events. Precambrian Research 216, 63–86.

Fritz, H., Abdelsalam, M.G., Ali, K.A., Bingen, K.A., Collins, A.S., Fowler, A.R., Ghebreab, W., Hauzenberger, C.A., Johnson, P.R., Kusky, T.M., Macey, P., Muhongo, S., Stern, R.J., and Viola, G., 2013. Orogeny style in the East African Orogen: A review of the Neoproterozoic to Cambrian tectonic evolution. Journal of African Earth Sciences 86, 65-106.

Gaulon, R., Chorowicz, J., Vidal, G., Romanowicz, B., Rouit, G., 1992. Regional geodynamic implications of the May–July 1990 earthquake sequence in southern Sudan. Tectonophysics 209, 87-103.

Girdler, R. W., McConnell, D. A., 1994. The 1990 to 1991 Sudan Earthquake Sequence and the Extent of the East African Rift System. Science 264, 67-70.

Grasty, R.L., 1997. Radon emanation and soil moisture effects on airborne gamma-ray measurements. Geophysics 62, 1379-1385.

Katumwehe, A. B., Abdelsalam, M.G., and Atekwana, E.A., (in press). The Role of Pre-existing Precambrian Structures in Rift Evolution: The Albertine and Rhino Grabens, Uganda. Tectonophysics.

Meert, J.G., Lieberman, B.S., 2008. The Neoproterozoic assembly of Gondwana and its relationship to the Ediacaran-Cambrian radiation. Gondwana Research 14, 5-21.

Minty, B., 1997. Fundamentals of airborne gamma-ray spectrometry. AGSO Journal of Australian Geology and Geophysics 17, 39-50.

Minty, B., McFadden, P., 1998. Improved Noise adjusted singular deconvolution (NASVD) smoothing of airborne gamma-ray spectra. Exploration Geophysics 29, 516-523.

Moussa, H.H.M., 2008. Spectral P-wave magnitudes, magnitude spectra and other source parameters for the 1990 southern Sudan and the 2005 Lake Tanganyika earthquakes. Journal of African Earth Sciences 52, 89-96.

Nyakecho, C., Hagemann S., 2014. An overview of gold systems in Uganda. Australian Journal of Earth Sciences 61, 59-88.

Pradeepkumar, A. R. Krishnanath (2000). A Pan-African 'humite epoch'in East Gondwana: implications for Neoproterozoic Gondwana geometry. Journal of Geodynamics 29, 43-62.

Ries, A., Vearncombe, J., Price R.C., Shackleton R.M., 1992. Geochronology and geochemistry of the rocks associated with a late Proterozoic ophiolite in West Pokot, NW Kenya. Journal of African Earth Sciences 14, 25-35

Ruotoistenmäki, T., 2014. Geophysical characteristics of Aswa shear, Nakasongola discontinuity and ring dyke complex in Uganda. Journal of African Earth Sciences 93, 23-41.

Salem, A., Williams, S., Fairhead, J.D., Ravat, D., Smith, R., 2007. Tilt-depth method: A simple depth estimation method using first-order magnetic derivatives. The Leading Edge 26, 1502-1505.

Santosh, M., Collins, A.S., 2003. Gemstone mineralization in the Palghat-Cauvery Shear Zone System (Karur-Kangayam Belt), southern India. Gondwana Research 6, 911-918.

Saria, E., Calais, E., Stamps, D.S., Delvaux, D., Hartnady, C., 2014. Present-day kinematics of the East African Rift. Journal of Geophysical Research — Solid Earth 119, 3584–3600.

Smith, R.S., Salem, A., 2005. Imaging depth, structure, and susceptibility from magnetic data: The advanced source-parameter imaging method. Geophysics 70, 31-38.

Stamps, D.S., Calais, E., Saria, E., Hartnady, C., Nocquet, J.-M., Ebinger, C.J., Fernandes, R.M., 2008. A kinematic model for the East African Rift. Geophysical Research Letters 35, L05304.

Stern, R.J., 1994. Arc-assembly and continental collision in the Neoproterozoic African orogen: implications for the consolidation of Gondwanaland. Annual Review of Earth and Planetary Sciences 22, 319-351.

Tack, L., Wingate, M.T.D., De Waele, B., Meert, J., Belousova, E., Griffin, B., Tahon, A., Fernandez-Alonso, M., 2010. The 1375 Ma "Kibaran Event" in Central Africa: prominent emplacement of bimodal magmatism under extensional regime. Precambrian.

Tapponnier, P., Peltzer, G., Le Dain, A., Armijo, R., Cobbold, P., 1982. Propagating extrusion tectonics in Asia: New insights from simple experiments with plasticine. Geology 10, 611-616.

Thurston, J., Smith, R., 1997. Automatic conversion of magnetic data to depth, dip, and susceptibility contrast using the Source parameter imaging method. Geophysics 62, 807-813.

Verduzco, B., J. D. Fairhead, C. M. Green, C. MacKenzie, 2004. New insights into magnetic derivatives for structural mapping: The Leading Edge 23, 116–119.

Westerhof, P A.B., Paavo, H., Isabirye, E., Katto, E., Koistinen, T., Kuosmanen, E., Lehto, T., Matti, I., Lehtonen, Mäkitie, H., Manninen,T., Mänttäri, I., Pekkala, Y., Pokki,J., Saalmann, K., Virransalo, P. 2014. Geology and Geodynamic Development of Uganda with Explanation of the 1:1,000,000 Scale Geological Map. Geological Survey of Finland Special Paper 55, 387 pp.

PAPER III

EVOLUTION OF THE MAGMA-POOR ALBERTINE-RHINO GRABEN AND EDWARD-GEORGE RIFT, EAST AFRICAN RIFT SYSTEM THROUGH MANTLE DELAMINATION, MELTING AND PRECAMBRIAN SUTURE ZONE GUIDED FLUID MIGRATION.

4.0 ABSTRACT

We used two-dimensional (2D) radially-averaged power spectral analysis and 2D forward modeling of aeromagnetic and satellite gravity data to investigate the thermal (Curie Point Depth (CPD) and heat flow) and crustal (Moho depth) structure beneath the Albertine-Rhino Graben and the Edward-George Rift. These extensional structures represent the northern segments of the Western Branch of the East African Rift System and they are separated by the ~5 km high Rwenzori Mountains. The northern part of the Albertine-Rhino Graben extends between the Archean-Paleoproterozoic North Uganda Terrane in the east and the West Nile Block to the west (together they represent the Northeast Congo Block which is the Congo craton in northwest Uganda and northeast Congo). The two cratonic blocks are separated by Mesoproterozoic-Neoproterozoic Madi-Igisi Fold and Thrust Belt. The southwestern part of the Albertine-Rhino Graben and the Edward-George Rift extends within the Paleoproterozoic-Mesoproterozoic Rwenzori and Kibara-Karagwe Ankole orogenic belts.

No surface expression of volcanic activities is found at the vicinity of the Albertine-Rhino Graben but the Toro-Ankole volcanic field is found at the northeastern tip of the Edward-George Rift. We found shallow CPD (~19-22±1 km) and high heat flow (~62-79±0.2 mWm^{-2}) beneath the Edward-George Rift, the Rwenzori Mountains, the southwestern part of the Albertine Graben, the northwestern margin of the Albertine Graben (Bunia Border Fault characterized by ~3 km high escarpments), and the transitional region between the Albertine and Rhino Graben. We also found thin crust (~25-30 km) beneath these regions. Based on these observations and those of previous studies we propose that strain localization during the initiation of rifting in the northern segments of the Western Branch was facilitated by sub-continental lithospheric mantle delamination beneath the Edward-George Rift, the Rwenzori Mountains and the Bunia escarpment of the Albertine Graben that resulted in rapid uplift of these regions. This delamination was accompanied by mantle melting that produced the Toro-Ankole volcanic field. Hot fluids generated from the mantle melt were channelized northeastward guided by Madi-Igisi "suture zone", hence allowing for the Albertine-Rhino Graben to initiate between the two cratonic Blocks represented by the North Uganda Terrane and West Nile Block.

Key words: East African Rift System, Albertine-Rhino Rift, Lake Edward-George Rift, Rwenzori Mountains, Curie point depth, Crustal thickness, Heat flow, Channelized fluids, delamination.

Highlights

- We investigated crustal and thermal structures beneath the Albertine-Rhino Rift.

- We found higher heat flow and thinner crust beneath the rift compared to surrounding Precambrian basement.
- We also found south to north decrease in heat flow beneath the rift, thinned crust beneath the Rwenzori Mountains, the Lakes George- Edward-rift and beneath the Bunia escarpments.
- We propose a lithospheric mantle delamination beneath these thinned crust that resulted into accelerated uplift in these regions
- Delamination led to mantle melting resulting in the Ankole-Toro Volcanic Fields, and a northward movement of channelized hot fluids.
- The hot mantle fluids were guided by pre-existing lithospheric structures represented by Madi Igisi Fold and Thrust Belt.
- The fluid migration allowed for strain localization between the two cratonic blocks leading to initiation of the Albertine-Rhino Graben between two cratonic blocks of the Northern Uganda Terrane and the northeastern Congo Block.

4.1 INTRODUCTION

Continental rifts are widespread extensional structures that were formed throughout the Earth's geological history and their spatial distribution generally suggests their formation as being localized within relatively thin continental lithosphere of orogenic belts at the margins of thicker lithosphere of cratons. In Africa, the spatial association between continental rifts of different Phanerozoic ages and Precambrian orogenic belts led to the general acceptance that the presence of lithospheric-scale pre-existing structures might be one of the most important factors leading to strain localization during the onset of rifting in both magma-rich and magma-poor settings [*Birt et al*., 1997; *Vauchez et al*., 1997;

Wilson et al., 2005; *Korme et al*., 2004]. This is further supported by centrifuge models which show that the presence of weak zones such as suture zones strongly localize strain resulting in the development of continental rifts [*Van Wijk 2005*; *Agostini et al*., 2009; *Corti et al*., 2013].

Impressive examples of the spatial association between Phanerozoic rifts in Africa and Precambrian orogenic belts include: (1) The NE-trending Karoo Permian-Triassic (~300 – 200 Ma) amagmatic Luangwa Rift (Figure 1A) which extends within the Mesoproterozoic-Neoproterozoic Irumide orogenic belt between the Bangweulu cratonic block and the Niassa craton [*Daly et al*., 1989; *De Waele et al*., 2006a and b] (2) The N-trending Neogene (~20 – 5 Ma) magma-rich Eastern Branch of the East African Rift System (EARS) (Figure 1A) which follows the traces of the Neoproterozoic East African Orogen represented by the Mozambique orogenic belt at the eastern margin of the Tanzania craton [*Daly et al*., 1989], (3) The NW-trending Neogene (~20 Ma) magma-poor Rukwa rift (representing the central part of the Western Branch of the EARS) (Figure 1A) which stretches within the Paleoproterozoic Ubendian orogenic belt sandwiched between the Tanzanian craton in the northeast and the Bangweulu cratonic block to the southwest [*Rosendaht et al*., 1992; *Delvaux*, 2001] and (4) The NE-trending Quaternary (< 1 Ma) amagmatic Okavango rift zone (representing the terminal segment of the Southwestern Branch of the EARS) (Figure 1A) which is actively developing within the Paleoproterozoic-Neoproterozoic Ghanzi-Chobe-Damara orogenic belt which is bounded by the Congo craton in the northwest and the Kaapvaal-Zimbabwe craton to the southeast [Figure 1*; Kampunzu et al*., 1998; *Modisi et al*., 2000; *Leseane et al*., 2015].

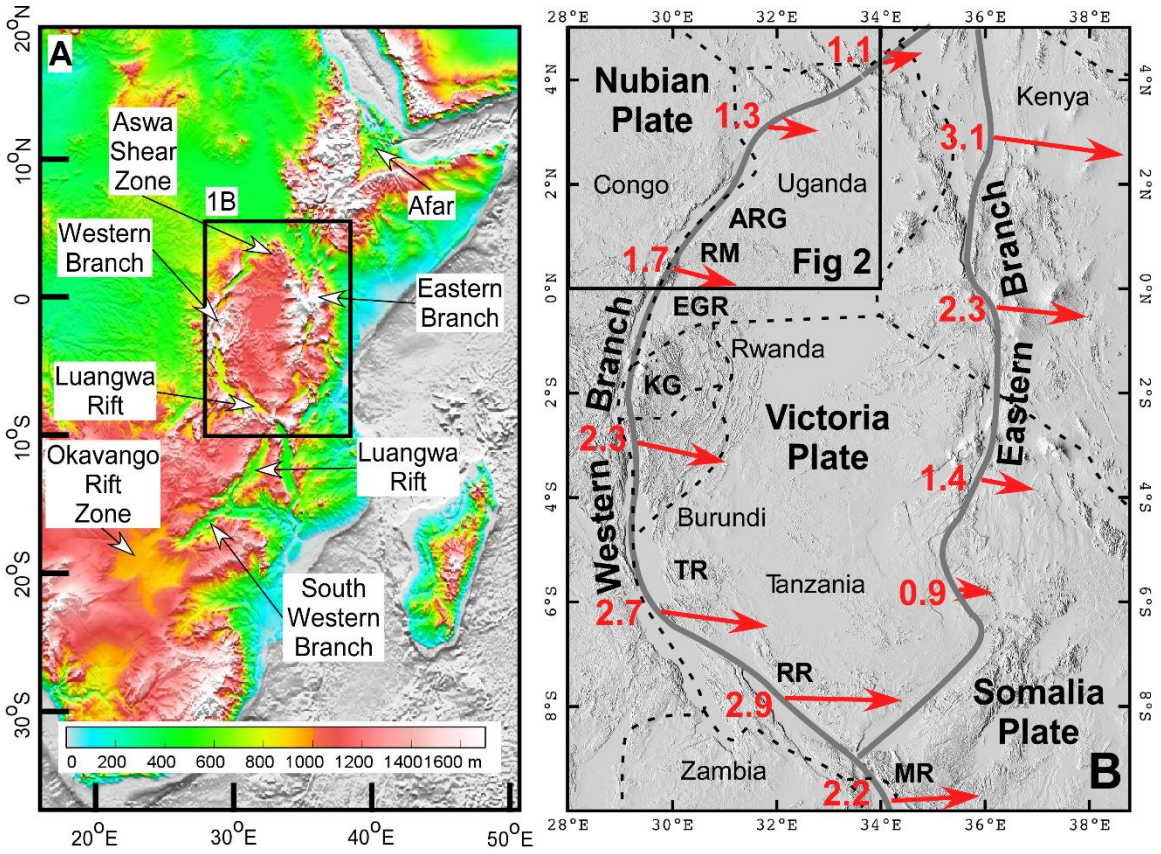

Figure 1: Global 30 arc second elevation data (GTOPO30) DEM showing the East African Rift System (EARS) and Karoo basins (A) and the Eastern and Western Branches of the EARS (B). Red vectors represent surface motions (mm/year) of the Somalia and Victoria plates relative to the Nubian Plate as reported by *Saria et al.* [2014]. ARG = Albertine-Rhino Graben. RM = Rwenzori Mountains. EGR = Edward-George Rift. KG = Kivu Graben. TR = Tanganyika rift. RR = Rukwa rift. MR = Malawi rift.

In magma-rich continental rifts, thermal softening of the lithosphere during the initiation of rifts is thought to be achieved through the injection of magmatic dikes sourced from shallow (~5 km deep) magma chambers which themselves are fed from a deeper source represented by an ascending asthenosphere or a mantle plume in what is referred to as magma-assisted rifting model [*Ebinger and Casey, 2001*; *Kendall et al*., 2005; *Wilson*

et al., 2005; *Sigmundsson*, 2006; *Wright et al*., 2006; *Valentine et al*., 2006; *Hammond et al*., 2013]. In the EARS, the magma-assisted rifting model is best supported by observations from the northern part of the Afar Depression (Figure 1A) where numerous dike emplacement events have been observed beneath the rift since 2005 [*Sigmundsson*, 2006; *Wright et al*. 2006; *Ebinger et al*., 2008; *Bastow et al*. 2010; *Keir et al*., 2011].

In magma-poor continental rifts, it is argued that the lack of a surface expression due to volcanic activities does not mean the absence of subsurface magma sources beneath these rifts. For example, using passive seismic data *Jakovlev et al.* [2013] concluded from P-wave tomography that reservoirs of molten material exist beneath the southwestern end of the Albertine-Rhino Graben beneath the Edward-George Rift (Figure 1B). In addition, using S-wave receiver functions, *Wolbern et al.* [2012] also presented evidence from passive seismic study for the presence of melt infiltration resulting in an elevated mid-lithospheric discontinuity beneath the rift.

In a more recent study in the amagmatic Okavango rift zone (Figure 1A), *Leseane et al.*, [2015] provided evidence for elevated heat flow and advanced a new model whereby thermal softening of the lithosphere during the onset of continental rifting is achieved without the need for the presence of subsurface magma source beneath the rift. In this model they considered hot mantle fluids concentrated by the presence of a lithospheric-scale pre-existing structure (the fluid domain) to be the primary driver of the thermal softening of the lithosphere leading to strain localization and rift initiation. Similarly, *Hyunwoo et al*., [2016] based on the mantle derived carbon isotope study that reaches the earth surface through diffusion and the ratio of V_p/V_s to suggested that fluids were involved in the initiation of continental rifting in the northern Tanzania divergence zone.

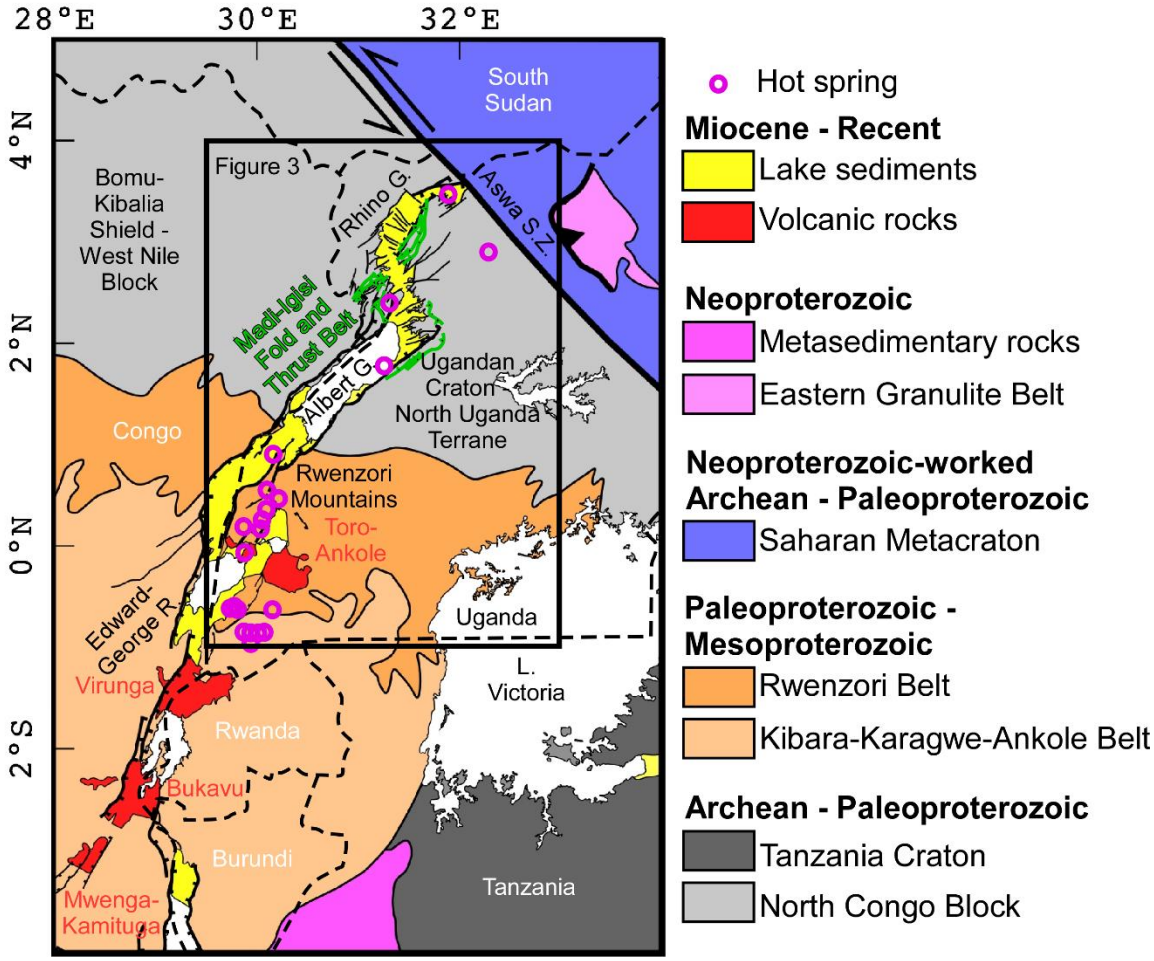

Figure 2: Geological map of the northern segment of the Western Branches of the East African Rift System (EARS). The normal faults and lake sediments are interpreted from Shuttle Radar Topography Mission (SRTM) Digital Elevation Model (DEM). The spatial extent of the Miocene – Recent volcanic rocks are modified from *Kampunzu et al.* (1998) and *Nyakecho and Hagemann* [2014]. Boundaries of different Precambrian entities are modified from *Tack et al.* [2010], *Fernandez-Alonso et al.* [2012], and *Westerhof et al.* [2014].

Although the examples above support the notion that Phanerozoic continental rifts follow the thinner lithosphere of the Precambrian orogenic belts and do not develop within

thicker cratonic lithosphere, there seems to be a number of examples, especially in the EARS, that defy this norm. For example, the Neogene (~10 Ma) N-trending magma-poor Malawi rift (which forms the southern segment of the Western Branch of the EARS) (Figure 1A) extends at oblique angle to the dominantly NE-trending structural grain of the Mesoproterozoic-Neoproterozoic Irumide and southern Irumide orogenic belts and it crosses the NE-trending Mwembeshi-Macaloge shear zone which represent the boundary between the two orogenic belts [Figure 1; *Lao-Davila et al*., 2015]. Also, the Neogene (~20 Ma) magma-poor Albertine-Rhino Graben which represents the northern end of the Western Branch of the EARS extends for ~200 km in a NE-SW direction within the Archean-Paleoproterozoic Northeast Congo Block which represents the northeastern extension of the Congo craton [Figure 2; *Katumwehe et al*., 2015]. Additionally, at its southeastern end, the Albertine-Rhino Graben crosses the boundary between the Northeast Congo Block and the Paleoproterozoic-Mesoproterozoic Rwenzori orogenic belt [Figure 2; *Katumwehe et al.*, 2015; *Koehn et al*., 2015].

North of the Rwenzori Mountains, the Albertine-Rhino Graben shows no evidence of surface volcanism and it extends within what appears to be the thick cratonic lithosphere of the North Congo Block along the Madi-Igisi Fold and Thrust Belt [Figure 2; *Westerhof et al.,* 2014]. It therefore represents an ideal locality for examining processes leading to strain localization during the initiation of magma-poor "cratonic" rifts. Studies by *Wölbern et al.,* [2012] and *Jakovlev et al.,* [2011; 2013] resolved the crust and sub-continental lithospheric mantle structure beneath the Rwenzori Mountains and the Edward-George Rift. In this work, we extend the work of *Jakovlev* et al., [2011; 2013] north of the Rwenzori Mountains to include the Albertine-Rhino Graben until its termination against the

Precambrian Aswa Shear Zone. We use two-dimensional (2D) radially-averaged power spectral analysis of aeromagnetic and satellite gravity data in order to resolve the thermal (Curie Point Depth (CPD) and heat flow) and crustal (Moho Depth) structure beneath the Albertine-Rhino Graben as well as the northeastern part of the Edward-George Rift and the Rwenzori Mountains [Figure 1B]. We integrate our results with those of *Wölbern et al.*, [2012] and *Jakovlev et al.*, [2011; 2013] to advocate for a geodynamic model that involves: (1) sub-continental lithospheric mantle delamination beneath the southwestern part of the Albertine Graben, the Edward-George Rift, the Rwenzori Mountains and the northwestern escarpment of the Albertine Graben (the Bunia Escarpment), (2) delamination was accompanied by mantle melting that produced the Toro-Ankole volcanic field and resulted in rapid uplift of the Rwenzori Mountains and the Bunia Escarpment, (3) hot fluids generated from the mantle melt were channelized northeastward guided by the Mesoproterozoic-Neoproterozoic Madi-Igisi Fold and Thrust Belt, hence allowing for the Albertine-Rhino Graben to localize between the Archean-Paleoproterozoic North Uganda Terrane and West Nile Block (Figure 2).

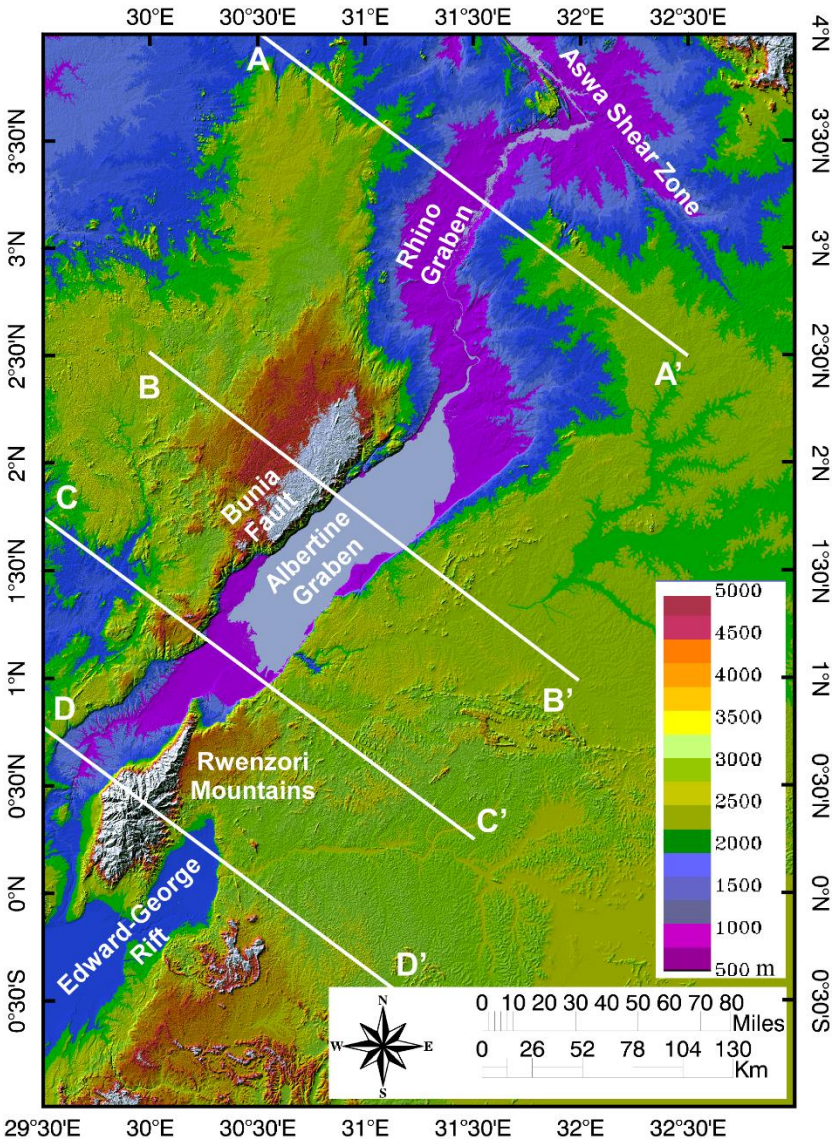

Figure 3: Shuttle Radar Topography Mission (SRTM) Digital Elevation Model (DEM) showing the Albertine-Rhino Graben, the Edward-George Rift and the Rwenzori Mountains. Profiles A-A', B-B', C-C' and D-D' represent location for the two (2D) dimensional gravity models where profile A-A' is across the Rhino Graben, profile (B-B' and C-C' are across the central and southwestern parts of the Albertine Graben, and profile D-D' is across the Rwenzori Mountains which is the overlap zone between the Albertine Graben and the Edward-George Rift.

4.2. TECTONIC SETTING

The ~4000 km Cenozoic EARS comprises the magma-rich Eastern Branch and the largely magma-poor Western Branch [Figure 1A; *Lindenfeld et al*., 2012]. The Albertine-Rhino Graben, the focus of this study, represents the northern segment of the Western Branch (Figure 1A). South of the Albertine-Rhino Graben, the Western Branch continues as a series of rift segments which include from north to south, the NE-trending Edward-George Rift, the N-trending Kivu rift, the NNW-trending Tanganyika rift, the NW-trending Rukwa rift, and the N-trending Malawi rift (Figure 1B). Building on previous studies by *Calais et al*. [2006] and *Stamps et al*., [2008], *Saria et al*. [2014] presented a refined kinematic model for the Western Branch based on Global Position System (GPS) measurements, earthquakes slip vectors and transform fault azimuth data. They found that the best fit model of the data favors an eastward movement of the Victoria plate away from the Nubian plate with the plate's relative velocity increasing from 1.1 mm/year in the north around the Rhino Graben to 2.9 mm/year to the south around the Rukwa rift (Figure 1B).

Rift initiation in the Western Branch is thought to have started ~12 Ma ago, later than the ~20 Ma rift initiation of the Eastern Branch [*Ebinger,* 1989; *Cohen et al*., 1993]. However, in a recent study of the Rukwa rift (Figure 1A) using $^{40}Ar/^{39}Ar$ and U–Pb age dating of volcanic tuffs, detrital zircons for sediments provenance, change in sedimentological depositional environment and flow direction of ancient rivers found that by 26–25 Ma the Rukwa rift was a well-developed basin bounded by border faults and uplifted shoulders [*Roberts et al*., 2012]. Numerical modeling study by *Koptev et al*. [2015] provides insights into how the magmatic Eastern Branch and magma-poor Western Branch could develop synchronously from possibly a single mantle plume. In this model the

deflection of the mantle plume to the east of the Tanzania craton (Figure 1A) allowed for more melt resulting in the development of the Eastern Branch as magmatic continental rift and leaving the Western Branch as a magma-poor rift. The model also advocated for thinning of the lithosphere to create channels that served as conduits for transporting the mantle plume material. This model is consistent with data from Neogene volcanic rocks in the region that support a single plume model [*Rooney et al*., 2012].

The Albertine-Rhino Graben strikes in a NE-SW direction from west of the Rwenzori Mountains (which represents a ~5 km high uplifted horst block of Precambrian basement between the Albertine Graben in the west and the Edward-George Rift to the east (Figure 3) as the Albertine Graben and further northeast as the Rhino Graben before terminating against the Precambrian Aswa Shear Zone (Figure 3). The asymmetrical full Albertine Graben maintains a uniform width of 60 to 80 km with well-developed topographic escarpments defining the border faults (Figure 3). The northwestern escarpment of the Graben represents the surface expression of the Bunia fault with escarpment significantly higher than the southeastern escarpment, reaching in places ~1,300 meters compared to the ~400 meters height of the southeastern escarpment (Figure 3). The Albertine Graben is filled with early Miocene-late Pleistocene sedimentary rocks dominated by lacustrine sandstone, shaley sandstone, sandstone and conglomerates, calcareous sandstone, calcareous shale, siltstone and organic rich shales [*Karp et al*., 2012]. These sedimentary rocks are thicker in the northwestern part of the Graben reaching ~5,400 meters compared to ~1,250 meters in the southeastern side of the Graben [*Upcott et al.*, 1996; *Ring*, 2008]. This, together with the escarpment heights (Figure 3), suggests a maximum vertical throw of ~6,700 meters in the northwestern border fault of the Albertine

Graben and 1,650 meters in its southeastern border fault. The Rhino Graben narrows from a ~40 km width in the southwest to a ~10 km width to the northeast (Figure 3). Its surface topographic expression suggests that the southwestern part of the Rhino is a SE-dipping half-Graben whereas it is a NW-dipping half-Graben in the northeast [Figures 3; *Katumwehe et al.,* 2015].

The Albertine-Rhino Graben extends, for the most part within the Archean-Paleoproterozoic Northeast Congo block with the exception of its southwestern-most part where the Paleoproterozoic-Mesoproterozoic Rwenzori orogenic belt is exposed [Figure 2; *Tack et al*., 2010; *Fernandez-Alonso et al*., 2012; *Nyakecho and Hagemann*, 2014] and this Northeast Congo Block represents the exposures of the Congo craton in northeastern Congo and northwestern Uganda. Based on synthesis of published geological data, *Begg et al*., [2009] divided the Northeast Congo Block into the Bomu-Kibalian shield in the west and the Ugandan craton to the east. Also, based on geological and geochronological studies, *Westerhof et al*. [2014] proposed dividing the Northeast Congo Block into the North Uganda Terrane east of the Albertine-Rhino Graben and the West Nile Block west of the Graben (Figure 4). *Begg et al*. [2009] stated that Archean granulites that experienced ultra-high pressure metamorphism at ~2.4 Ga are present within the Ugandan craton, hence this cratonic block must be fundamentally different from the Bomu-Kibalian shield west of the Albertine-Rhino Graben. Both *Begg et al*. [2009] and *Westerhof et al*. [2014] suggested that the boundary between the Ugandan craton - North Uganda Terrane and the Bomu-Kibalian shield –West Nile Block might be found beneath the Western Branch of the EARS (Figure 2). Further, *Westerhof et al*. [2014] mapped a number of SE and NW-

verging Precambrian thrust faults (the Mesoproterozoic-Neoproterozoic Madi-Igisi Belt) that coincides with the proposed boundary between the two cratonic blocks (Figure 2).

To the south, the Albertine-Rhino Graben overlaps with the Edward-George Rift separated by the Rwenzori Mountains (Figure 3) which extends into the Paleoproterozoic-Mesoproterozoic Rwenzori and the Kibara-Karagwe-Ankole orogenic belts [Figure 2; *Begg et al*., 2009; *Tack et al*., 2010; *Link et al*., 2010; *Aanyu and Koehn*, 2011, *Westerhof et al*., 2014]. The Edward-George Rift is represented by two half-Grabens with the main border fault located to the west and these half-Grabens are separated by a NW-SE accommodation zone [*Lærdal* and *Talbot*, 2002].

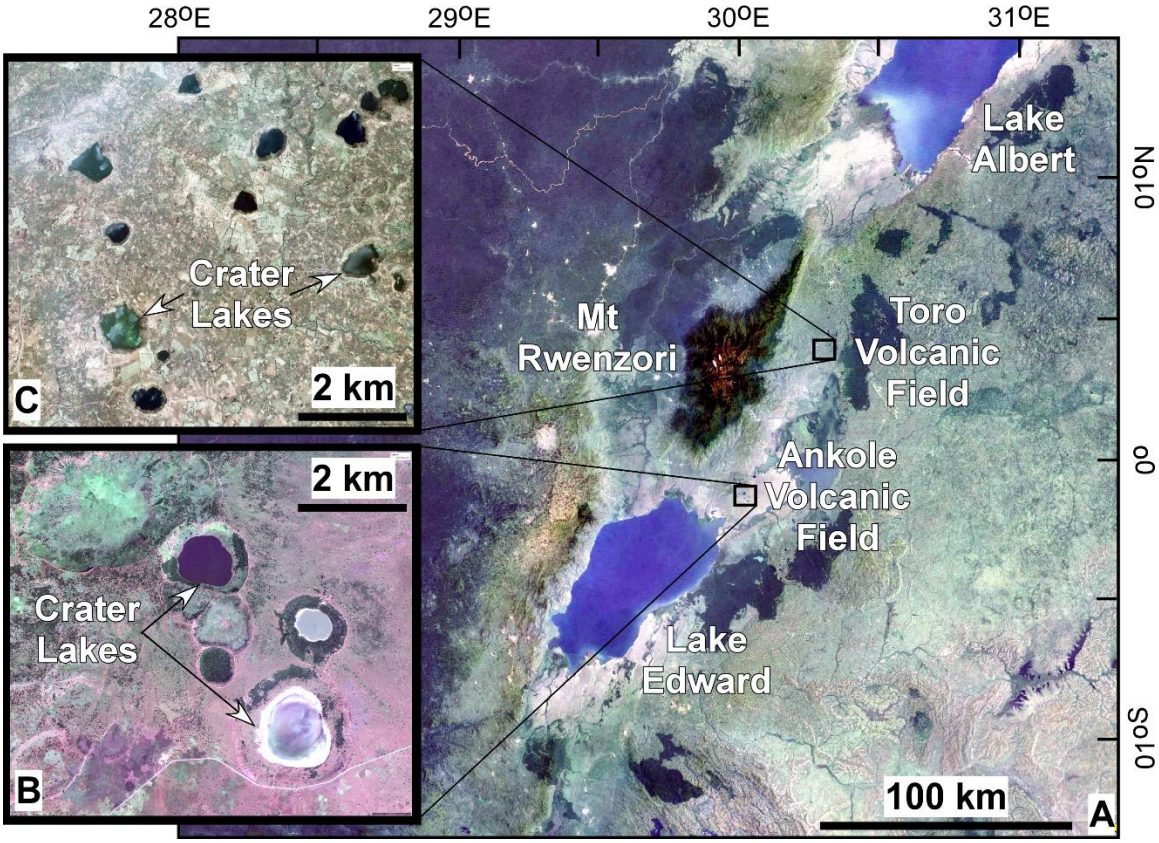

Figure 4: (A) Landsat Thematic Mapper (TM) image covering the southern part of the Albertine-Rhino Graben (represented by Lake Albert), the northeastern part of the Edward-George Rift, the Rwenzori Mountains and Ankole-Toro Volcanic Fields. (B) and

(C) Digital Globe images of volcanic crater lakes associated with the Toro and Ankole volcanic fields, respectively.

Whereas volcanic rocks are not found around in and surrounding the Albertine-Rhino Graben, the Edward-George Rift is characterized by the presence of the Toro-Ankole volcanic field at its northeastern tip and the Virunga volcanic field at its southwestern tip [Figures 2 and 4; *Lærdal and Talbo*t, 2002]. It is suggested that these volcanic fields were erupted in two separate phases. The older volcanism initiated during the early stages of rifting and this volcanism lies parallel to the NW-SE accommodation zones and Precambrian faults. Differently, the younger phase which formed the Pleistocene explosive volcanic craters accompanied the later stages of rifting and these volcanic craters are aligned parallel to the NE-SW-trending border faults [*Lærdal and Talbot*, 2002, *Corti et al*., 2004]. Some of the volcanic craters in the Toro-Ankole volcanic field are characterized by the presence of hot springs [*Bahati et al*., 2005] where isotopic studies of the highly-alkaline volcanic rocks have suggested a mantle origin [*Muravyeva and Belyatsky*, 2009] due to possible magma mixing within the Precambrian basement [*Rosenthal et al*., 2009].

Recent geophysical studies in the Western Branch have been focused on the Rwenzori Mountains, the Edward-George Rift and the Toro-Ankole Volcanic Field (Figures 2 and 3). Based on seismic receiver functions and shear wave splitting results from the Edward-George Rift [*Wolbern et al*., [2010, 2012]; *Jakovlev et al*., [2013] and Batte et al. [2014] suggested the presence of melt infiltration beneath the Rwenzori Mountains. Additionally, *Lindenfeld et al*. [2012] demonstrated by using passive seismic data that the presence of vertical fluid migration within fault systems due to extensional forces will

eventually lead to the Rwenzori Block to break away from the Victoria plate. Similarly, *Häuserer,* and *Junge*, [2011] using magnetotelluric data have identified NE-SW trending conductive anomalies at a depth of ~15-20 km that may be related to partial melt connected to the Toro-Ankole volcanic field.

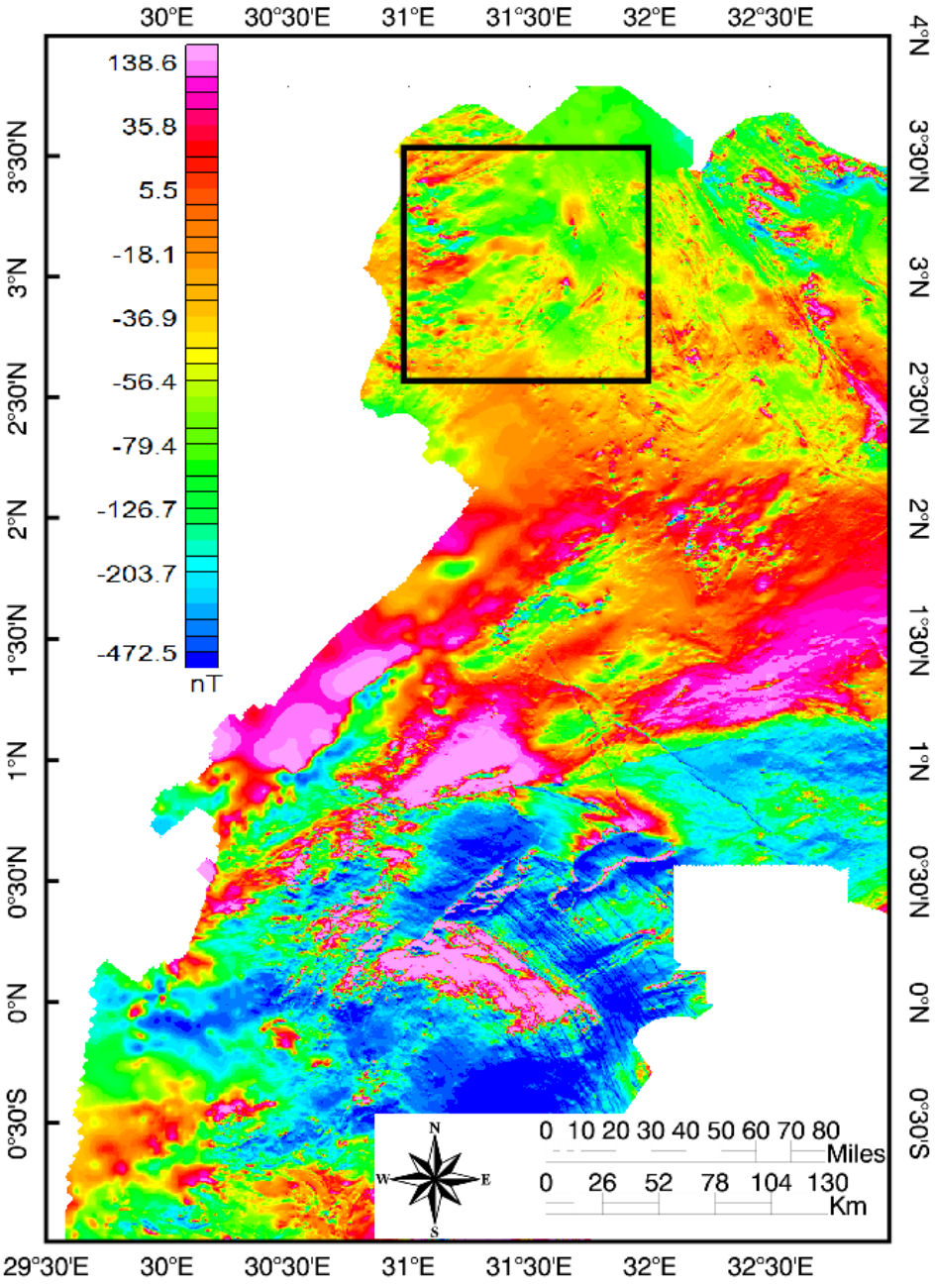

Figure 5: Total magnetic field data of northwestern Uganda used in the estimation of Curie Point Depth (CPD) in Figure 9. The black square shows an example of the 1^o x 1^o (110 km x 110 km) sub-region window used for the extraction of the 2D radially-averaged power specral curves shown in figures 6A and B.

4.3. METHODOLOGY

4.3.1. AEROMAGNETIC DATA

The aeromagnetic data used in this study (Figure 5) were acquired between 2006 and 2009 by the Ugandan Government through the Geological Survey and Mineral Department. The data were acquired at a terrain clearance of ~80 meters and flight line spacing of ~200 meters with an orientation of ~N55^{o}E. The aeromagnetic data have the International Geomagnetic Reference Field (IGRF) of 2010 removed from the total magnetic field. In this study we used the original magnetic field to calculate the CPD using the 2D radially-averaged power spectral analysis for the Albertine-Rhino Graben, the Edward-George Rift, the Rwenzori Mountains and the surrounding Precambrian basement. Subsequently, we used the CPD to estimate the heat flow for these regions. Because of lack of aeromagnetic data over Congo, our CPD and heat flow calculations are limited to Uganda.

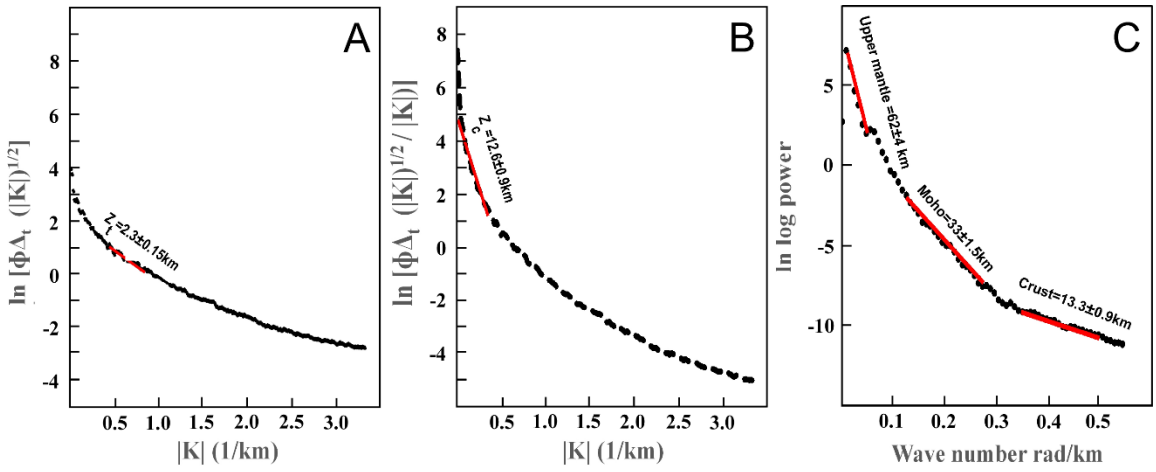

Figure 6: (A) Plot of natural logarithm of the radial magnetic spectral analysis showing the natural log power against wave number denoting the depth (Z_t) to top of the magnetic source. (B) Plot of natural logarithim of the radial magnetic spectral analysis showing the natural log power against wave number denoting the depth to the centroid (Z_c) of the magnetic source. (C) Plot of power density spectral analysis showing the natural log power against wave number denoting the mid lithospheric discontinuity, crustal thickness (Moho) and upper crust.

4.3.1.1. CURIE POINT DEPTH (CPD)

The CPD can provide an approximation to the depth to the bottom of the magnetized crust that defines the depth to which ferrimagnetic minerals lose their magnetization. This depends on the magnetic mineralogy of the crust which is usually magnetite which has a Curie temperature of ~580^{o}C [*Spector and Grant* 1970; *Haggerty, 1978*; *Maus et al*., 1997]. However, this value changes depending on the magnetic mineral composition within the rocks [*Chiozzi et al*., 2005]. The presence of elevated temperature in the lithosphere affects the magnetization of different minerals and this can be used to image the thermal structure of the lithosphere [*Chiozzi et al*., 2005]. Different approaches

were developed to determine the depth to the base of the magnetized sources using spectral analysis of the magnetic data. For example, *Spector and Grant* [1970] developed the spectral peak method by transforming the spatial data into frequency domain where the position of the spectral peak is a function of the depths to the base (Z_b) and depth to top (Z_t) of causative sources. Subsequently, *Bhattacharyya and Leu*, [1975] suggested the use of the centroid method of the power density spectrum which was later modified and used by various authors [e.g. *Ravat et al*., 2007; *Tanaka et al*., 1999; *Hussein et al*., 2013; *Arnaiz-Rodríguez and Orihuela*, 2013; *Leseane et al*., 2015]. The centroid method is a function of the slopes for the curve that results from plotting the power spectrum of the magnetic anomalies against the wave numbers. The power spectrum is a combination of both the short and long wavelength information that reflect shallow and deeper sources, respectively [*Spector and Grant*, 1970]. The depth of the magnetized layer is related to the CPD while the depth variations are related to heat flow and temperature gradient [*Arnaiz-Rodrigues* and *Orihuela*, 2013]. Previous studies [*Ravat et al*., 2007; *Bouligand et al.*, 2009; *Hussein et al*., 2013] have suggested that the sub-area window size from which the 2D radially-averaged power spectrum curve is extracted should at least be three to four times larger than the depth of the magnetized source being studied.

We used the 2D radially-average power spectral analysis to calculate the CPD from the IGRF corrected airborne magnetic data (Figure 5). Owing to the narrow width of continental rifts (10 to 80 km in the case of the Albertine-Rhino Graben and the Edward-George Rift) a large sub-area window will result in a mixed signature representing the magnetic anomalies of the rifts and the surrounding Precambrian basement. For this reason, smaller window sizes of 1^o x 1^o to 0.5^o x 0.5^o (110 km x 100 km to 55 km x 55 km) were

used to minimize this effect [*Ross et al*., 2006]. A total of 81 sub-area windows with sizes of ~1^o by 1^o and 0.5^o x 0.5^o and 25% to 50% overlap were used to obtain a better lateral coverage and to minimize the ringing artefacts (fading signal) near the edges.

The grids of the total magnetic grids field were converted into the Fourier domain by calculating the radially-average power spectrum in the wave number domain. The natural logarithmic of the power spectrum (E) was plotted against the wave number (radian/distance) and the depth to source was approximated based on 10 point moving averages using a straight line on the slope that indicated different depth estimates. The radially-average spectrum for the magnetic data that shows the depth to the centroid (Z_c) of magnetic source is:

$$Z_c = \ln [\Phi\Delta_T (|k|)^{1/2}/|k|] \quad 1$$

Where $\Phi\Delta_T$ is the radially-average power spectrum of the total magnetic field and k is the wave number (*Okubo et al*., 1985).

The depth to the top (Z_t) of magnetic source is:

$$Z_t = \ln [\Phi_{\Delta T} (|k|)^{1/2}] \quad 2$$

We obtained Z_c by using wave numbers ranging between 0.01and 0.44 rad km^{-1} while Z_t was obtained using with wave numbers ranging between 0.5 and 0.8 rad km^{-1}. An example of this analysis is shown in Figures 6A and B. The slopes of different curve segments are related to different potential field signatures from subsurface sources at differing depth where the mean depth is proportional to the slope of the line [*Tanaka et al*., 1999].

The depth (Z_b) to the base of the magnetized crust (CPD) was then calculated from the difference between twice the depth to the centroid and depth to the top of the magnetic

source [*Maus et al*., 1997; *Tanaka et al., 1999*; *Ravat et al., 2007*; *Hussein et al*., 2013; *Arnaiz et al*., 2013; *Leseane et al*., 2015].

$$Z_b = 2Z_c - Z_t \quad (3)$$

The calculation of the CDP is based on the clarity of the change in slopes between the higher and lower wave numbers of the 2D radially-averaged power spectrum curve. We estimated the statistical error using the Linest function in Excel based on the least squares best fit method. The least squares best fit method is found effective since it removes the ambiguity of where to place the slope when calculating the depth to the centroid to distinguish it from the low wave number segment. The statistical error was then calculated from the ratio between the standard deviation and the range of the radial frequency used in the determination of Z_t and Z_c [*Chiozzi et al., 2005*]. Our results from all sub-area windows had a mean error of ±2 km.

4.3.1.2. HEAT FLOW CALCULATIONS FROM THE CURIE POINT DEPTH (CPD)

Since the depth to the base of the magnetized body may be directly related to the Curie isothermal point, it has an indirect relationship with the regional heat flow [*Tanaka et al*., 1999]. To calculate the regional heat flow from the CPD, the one-dimensional (1D) Fournier's law of conductive heat flow was used. The Fournier's law is given by:

$$q = k\,(dT/dz) \quad (4)$$

Where *dT/dz*, *q* and *k* represent the temperature gradient, heat flux and the thermal conductivity, respectively. Based on studies by *Tanaka et al.* [1999], the Curie temperature, *C*, can be obtained using:

$$C = (dT/dz)D \quad (5)$$

Where D is the CPD. This assumes that there are no other heat sources between the Earth surface and the CPD, no convective heat sources and the temperature gradient dT/dz is constant. Given these assumptions, equations 4 and 5 can be reduced to:

$$D = kC/q \quad (6)$$

Where k is the thermal conductivity and is a geological dependent variable [*Okubo* et al., 1989]. Previous studies by *Okubo* et al., [1989] suggested a range of k values for granitic rocks ranging from ~2.4-3.8 $Wm^{-1}K^{-1}$ and the Curie temperature of 580^{o} C for magnetite which is taken to be the most predominant magnetic mineral [*Hunt et al., 1995; Mullins, 1977*].

According to Equation 6, heat flow estimates from CPD are strongly influenced by the k value used which is different for different rock types. In the absence of measured thermal conductivity from borehole data, our heat flow results were obtained using an average k value of 2.17 $Wm^{-1}K^{-1}$, this is generally due to different k values 1.67 (sandstone, shale and limestone), 1.9 $Wm^{-1}K^{-1}$ (sandstone, shale and limestone and, 2.3 $Wm^{-1}K^{-1}$ (limestone shale, silt) [*Jorand et al*., 2015]. These formations form the main sedimentary units within the borehole information from the Albertine rift [*Karp et al*., 2012]. Similarly, heat flow for basement geology was estimated using an average of 2.5 $Wm^{-1}K^{-1}$ due to different k values ranging from 1.9 $Wm^{-1}K^{-1}$ (limestone), 2.3 $Wm^{-1}K^{-1}$ (gneiss) and gneissic complex 2.77 $Wm^{-1}K^{-1}$.

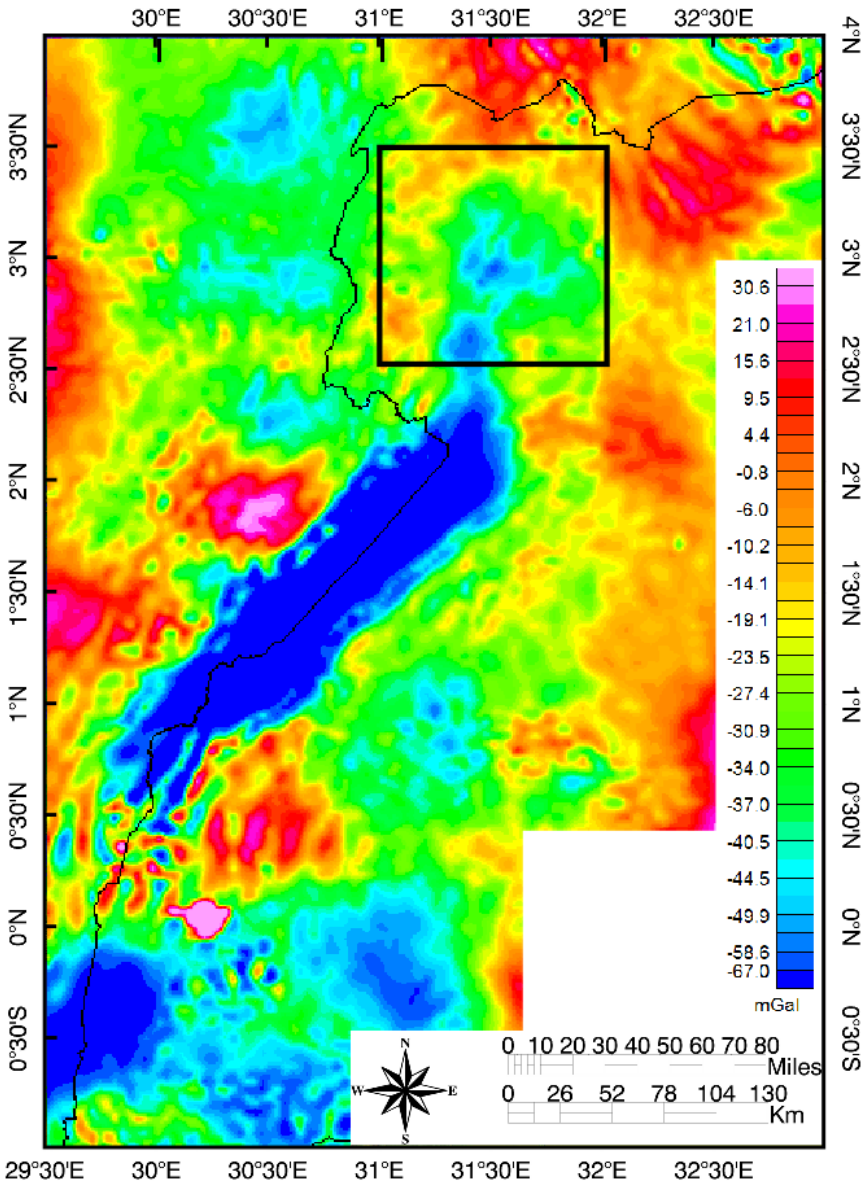

Figure 7: Gravity Bouguer anomaly from the World Gravity Map 2012 (WGM2012) satellite gravity data covering northwestern Uganda and northeastern Congo. The data are used to estimate the Moho depth shown in figure 10. The black box shows an example of the 1^o x 1^o (110 km x 110 km) sub-region window used for the extraction of the 2D radially-averaged power specral curves shown in Figure 6C.

4.3.2. MOHO DEPTH CALCULATIONS

The satellite gravity data used in this study is based on the World Gravity Map project 2012 (WGM 2012) model [Figures 7; *Balmino et al*., 2012]. The WGM2012 satellite gravity data have a spatial resolution of 9 km and is computed using a spherical harmonic approach [*Balmino et al*., 2012]. This data are based on the Earth global models (EGM 2008) that uses combined gravity data from land, sea, marine, airborne surveys as well as long wavelength Gravity Recovery and Climate Experiment (GRACE) satellite model to compute a 5 arc-minute equiangular Free Air grid gravity anomaly [*Kuhn et al*., 2009; *Pavlis et al*., 2012; *Balmino et al*., 2012]. The WGM2012 data also include the global 30 arc-second elevation data (GTOPO30) to remove the influence of the terrain and subsequently this is used to calculate the complete spherical Bouguer anomaly.

Additionally, to investigate the gravity anomalies within the crust, Bouguer gravity anomalies were created by applying a band-pass filter where wavelength between 5 and 175 km (Figure 7B) were applied to remove high and low wavelength anomalies, respectively. The relationship between the gravity 2D radially-averaged power spectrum and depth is log-linear and the slope of the curve provides an estimate of the depth to gravity anomaly source [*Russo and Speed*, 1994; *Tselentis et al*., 1988; *Sanchez-Rojas and Palma*, 2014]. The 2D radially-averaged power spectrum curves (Figure 6C) are the plot of log power against the wave number. We calculated the 2D radially-averaged power spectral curves for areas within the Albertine-Rhino Graben, the Edward-George Rift and the surrounding Precambrian basement using sub-area window sizes of 1^{o} by 1^{o} and overlap of 50%. An example of the 2D radially-averaged power spectral curve extracted from a sub-area window is shown in Figure 6C. In this curve, the first linear slope corresponding

to wave numbers ranging between 0.0 and 0.09 represents the mid-continental lithospheric discontinuity. The second linear slope corresponding to wave numbers ranging between 0.2 and 0.29 is taken to be associated with the crust and sub-continental lithospheric mantle boundary (the Moho depth). The third linear slope corresponding to wave numbers ranging between 0.3 and 0.39 represents density boundaries within the crust or noise. Similarly, the best fit and the statistical error of the slopes representing the Moho depths are calculated based on the *Morrison* [2014] method as in CPD calculation.

4.3.3. TWO-DIMENSIONAL (2D) FORWARD MODELING

To verify the Moho depth results obtained from the 2D radially-average power spectral analysis and to establish the cross-sectional view of the lithospheric structure across the study area we constructed four NW-SE -2D lithospheric-scale forward gravity models (Figure 3). From northeast to southwest these are across the Rhino Graben (A-A' in Figure 3), across the central and southwestern parts of the Albertine Graben (B-B' and C-C' in Figure 3), and across the Rwenzori Mountains representing the overlap zone between the Albertine Graben and the Edward-George Rift (D-D' in Figure 3). For each model, the upper crust has a density of 2.87 gm/cm^3, lower crust has a density of 2.95 gm/cm^3 and the sub-continental lithospheric mantle has a density of 3.20 gm/cm^3. These density values are in agreement with values used in previous studies [Maguire et al., 1994; Tesha et al., 1997; Simiyu and Keller, 2001]. When available, as in the case of the profiles that crosses the southwestern part of the Albertine Graben and the overlap between the Albertine Graben and the Edward-George Rift (C-C' and D-D' in Figure 3), the initial

depth to Moho used in the 2D forward gravity models is constrained by passive seismic results [*Wolbern et a*l., 2010].

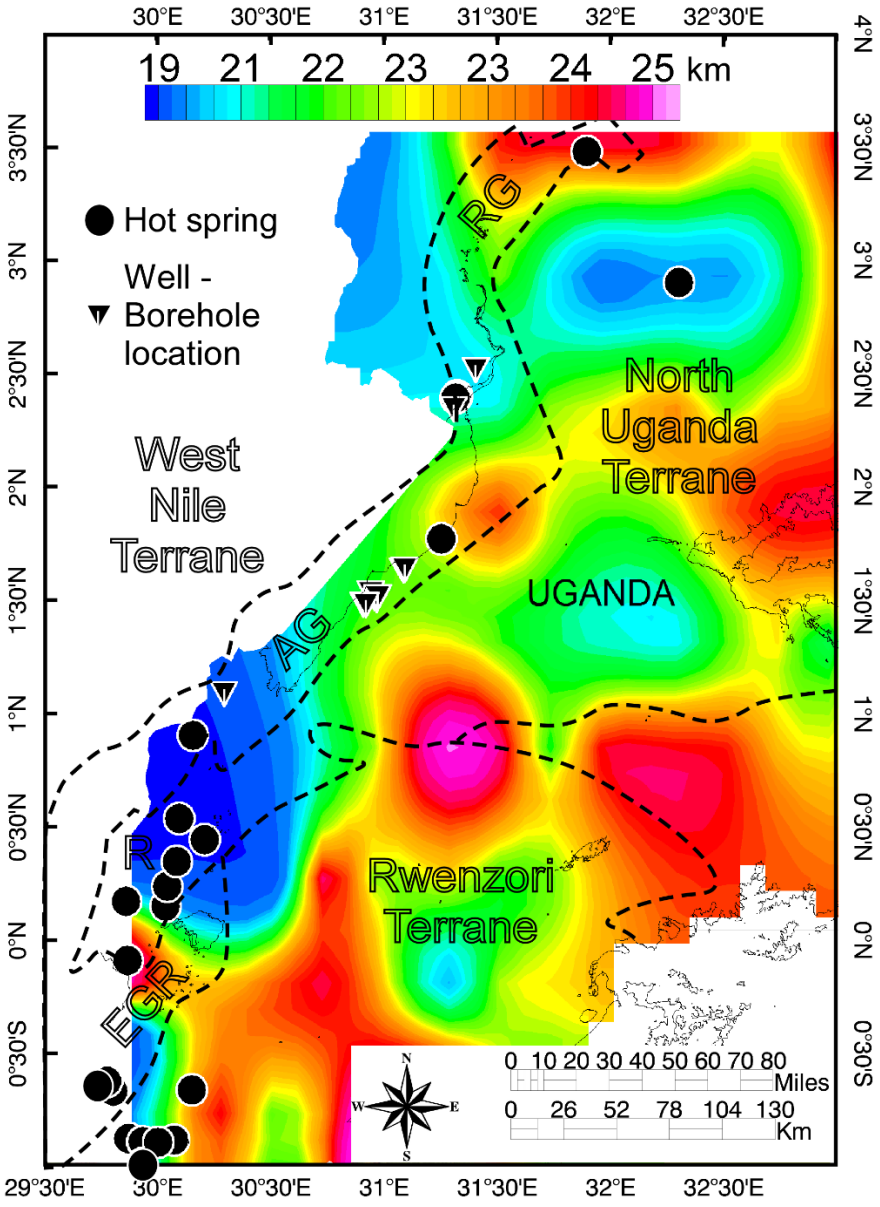

Figure 8: Curie Point Depth (CPD) estimates beneath the Albertine-Rhino Graben, the Edward-George Rift and the Rwenzori Mountains based on the two-dimensional (2D) radially averaged power spectral analysis of the aeromagnetic data shown in Figure 5. RG = Rhino Graben. AG = Albertine Graben. R = Rwenzori Mountains. EGR = Edward-George Rift.

4.4. RESULTS

4.4.1. CURIE POINT DEPTH (CPD) AND HEAT FLOW

Figures 8 and 9 show the CPD values and heat flow, respectively beneath the Albertine-Rhino Graben, the Edward-Gorge rift, the Rwenzori Mountains and the surrounding Precambrian basement. Generally, the CPD ranges between 23 - 26 km and the heat flow values range between 52 - 70 mWm^{-2}. The shallowest CPD and the highest heat flow values associated with the rift structure occur in three regions. These structures are from south to north: (1) The Edward-George Rift, and the Toro-Ankole volcanic field (Figures 8 and 9). In this region the CPD reaches a depth of ~20 km and the heat flow values of ~70 mWm^{-2}. This region (Figures 8 and 9) is also characterized by the presence of numerous hot springs [*Bahati et al*., 2005]. (2) The region to the northeast of the Rwenzori Mountains and the southwestern part of the Albertine Graben which also shows the presence of many hot springs (Figures 8 and 9). In this region, we report CPD that reaches the shallowest depth of 19 km and heat flow values as high as 70 mWm^{-2}. (3) The zone between the Albertine and the Rhino Grabens at approximately latitude 3N where the CPD shallows to 21 km and the heat flow values increase to 65 mWm^{-2} (Figures 8 and 9). This zone of shallow CPD extends eastward into the Precambrian basement of the North Uganda Terrane**.** It is worth noting here that the northeastern tip of the Rhino Graben where it terminates against the Precambrian Aswa Shear Zone does not show any anomalously shallower CPD or higher heat flow values. Here, the CPD and heat flow values are indistinguishable from those of the surrounding Precambrian basement (Figure 8)**.**

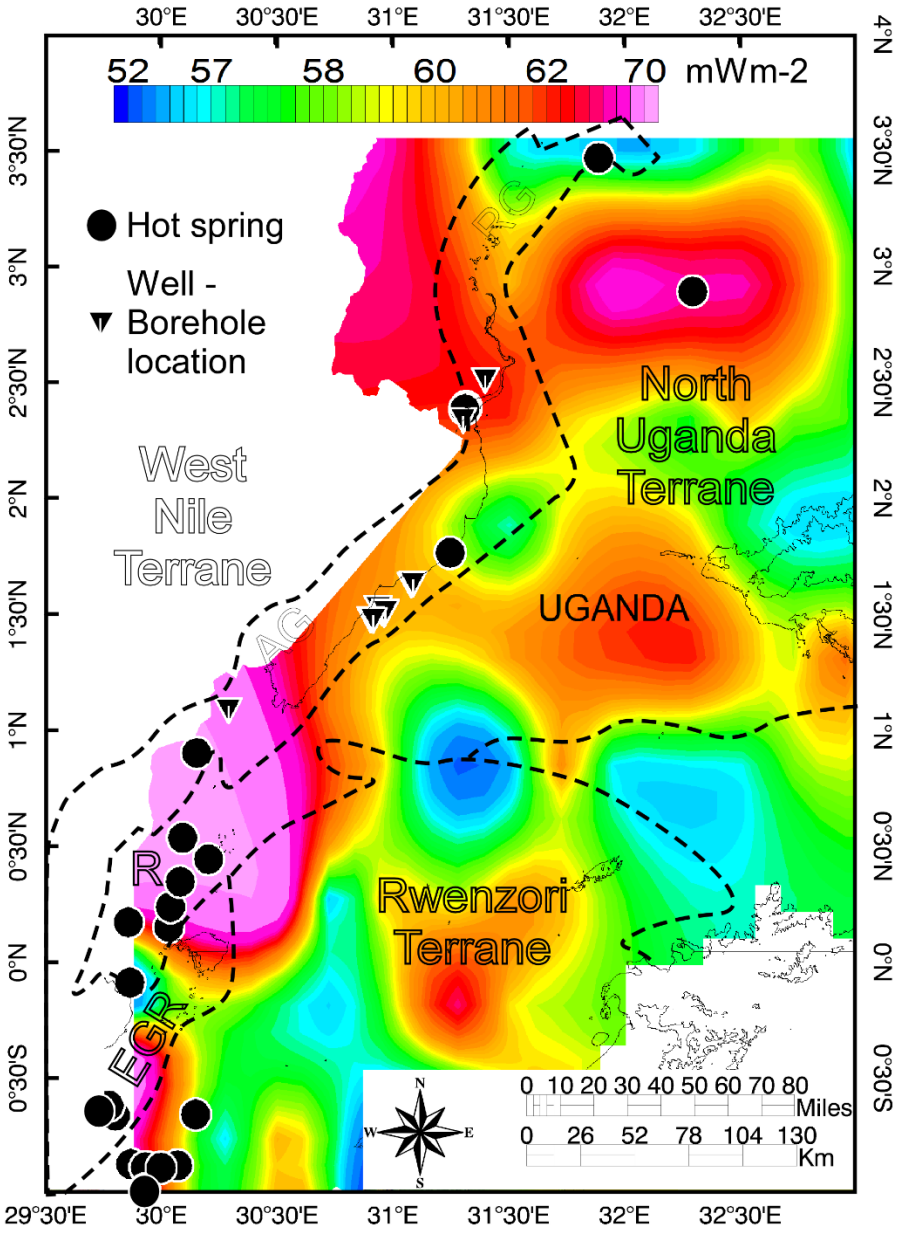

Figure 9: Heat flow estimated for the Albertine-Rhino Graben, the Edward-George Rift and the Rwenzori Mountains based on the Curie Point Depth (CPD) data shown in figure 8. RG = Rhino Graben. AG = Albertine Graben. R = Rwenzori Mountains. EGR = Edward-George Rift.

Other areas where shallow CPD and high heat flow values are found away from the rift structures include the southwestern part of the North Uganda Terrane and the north-

central part of the Rwenzori Terrane (Figures 8 and 9). The CPD is anomalously shallower and the heat flow values are higher for such an Archean-Paleoproterozoic cratonic block (the North Uganda Terrane) and a Paleoproterozoic-Mesoproterozoic orogenic belt (the Rwenzori Terrane). The lithospheric thermal structure of the Precambrian basement is beyond the scope of this work, and future work can be focused on understanding the source of these anomalies.

4.4.2. CORRELATION OF HEAT FLOW RESULTS FROM AEROMAGNETIC DATA WITH BOREHOLE GEOTHERMAL MEASUREMENTS

To evaluate the accuracy of heat flow results obtained from the CPD that is calculated from the aeromagnetic data, we compared these results with heat flow results calculated from the geothermal gradient measured in 12 wells in the Albertine Graben and 2 wells in the Rhino Graben (Figure 9). The calculations are based on equation 4-6 above. The heat flow results obtained from the CPD calculated from the aeromagnetic data is in good agreement with those calculated from the borehole geothermal gradient data (Table 1). The correlation coefficient (r) between results from the two methods is ~0.94 and the Root Mean Square Error (RMSE) is 4.6 mWm^{-2}.

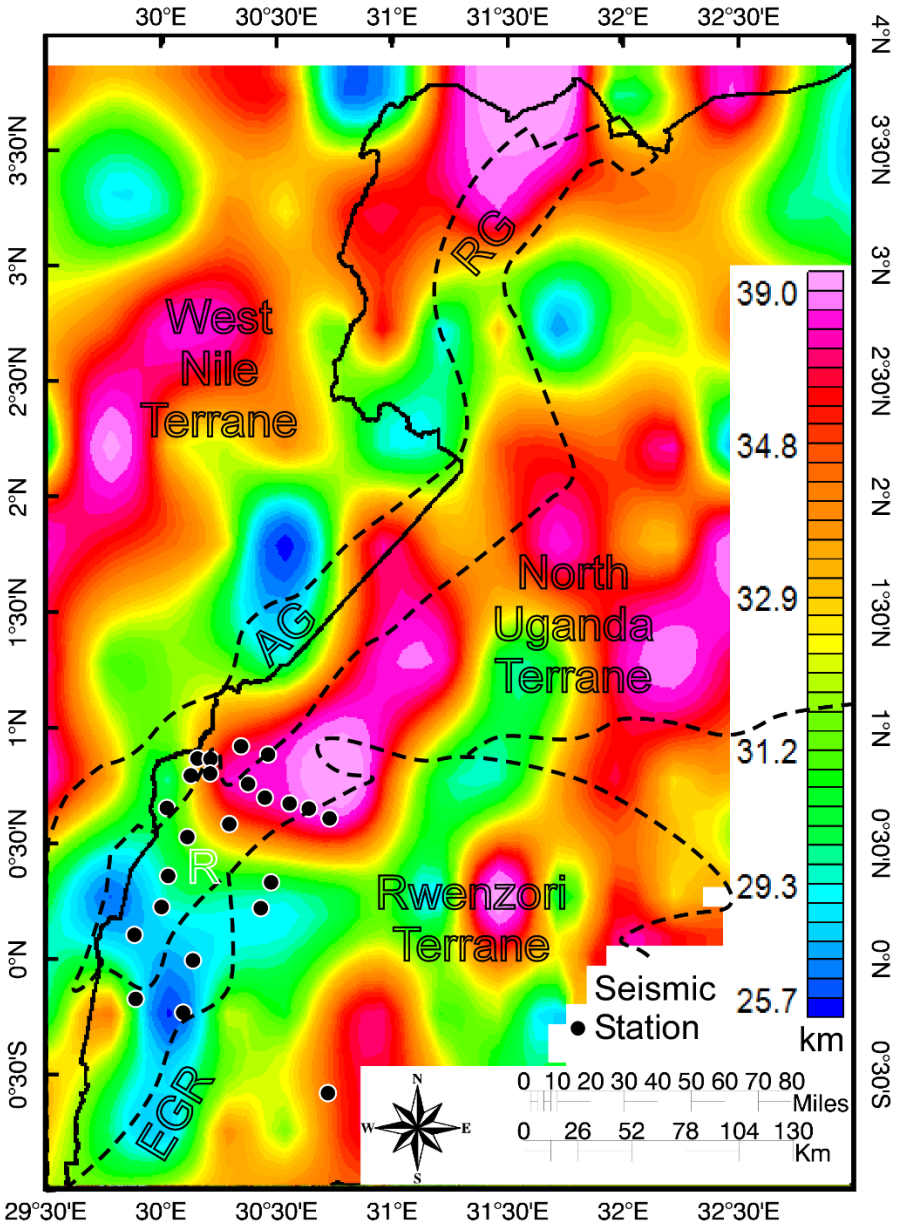

Figure 10: Crustal thickness estimated beneath the Albertine-Rhino Graben, the Edward-George Rift and the Rwenzori Mountains based on the two-dimensional (2D) radially averaged power spectral analysis of the World Gravity Map 2012 (WGM2012) staellite gravity data shown in Figure 7A. RG = Rhino Graben. AG = Albertine Graben. R = Rwenzori Mountains. EGR = Edward-George Rift.

4.4.3. CRUSTAL THICKNESS FROM SATELLITE GRAVITY DATA

Figure 10 shows the Moho depths based on the 2D radially-averaged power spectrum analysis of the gravity data beneath the Albertine-Rhino Graben, the Edward-George Rift, the Rwenzori Mountains and the surrounding Precambrian basement. The depth to Moho in the region ranges between 25 -39 km. There are two regions of elevated (shallow) Moho that are associated with the rift structures: (1) the Edward-George Rift and the southwestern part of the Rwenzori Mountains are underlain by elevated Moho reaching a shallow depth of ~ 25 km (Figure 10). (2) We observe an elevated Moho depths of 27 km to the southwestern part of the Albertine Graben areas around the northwestern border fault. However, northeast of this latter area, the elevated Moho departs from beneath the Albertine topographic trough to the western rift shoulder. Here, the shallow Moho of ~ 25 km is found beneath the ~2 km high topographic escarpment associated with the Bunia fault, which represents the northwestern border fault of the Albertine Graben. This zone of thin crust seems to extend northeastward parallel to the Albertine Graben until the transitional zone between the Albertine and Rhino Grabens. It then extends eastwards across the rift to the Precambrian basement beneath the North Ugandan Terrane. Interestingly, the northeastern part of the Rhino Graben (north of 3^{o}N) is characterized by Moho depths that ranges from 35-39 km which is indistinguishable from the Moho depths beneath the Precambrian basement (Figure 10)**.**

There is a region of elevated Moho (~30 km) that occurs outside the rift structures and extends in the southwestern part of the North Uganda Terrane and the north-central part of the Rwenzori Terrane (Figure 10). This region is also characterized by elevated CPD's and high heat flow values (Figures 8 and 9). This thinner crust is unusual for

Archean-Paleoproterozoic cratonic blocks (the North Uganda Terrane) and a Paleoproterozoic-Mesoproterozoic orogenic belts (the Rwenzori Terrane). The crustal structure of the Precambrian basement is beyond the scope of this work, and future work can be focused on understanding the source of these anomalies.

4.4.4. CORRELATION OF RESULTS OF CRUSTAL THICKNESS FROM TWO-DIMENSIONAL (2D) RADIALLY-AVERAGED POWER SPECTRUM ANALYSIS OF WORLD GRAVITY MODEL 2012 (WGM 2012) SATELLITE GRAVITY DATA WITH RESULTS FROM PASSIVE SEISMIC DATA

Figure 10 shows the locations of 24 temporary broadband seismic stations deployed to study crustal and upper mantle structure beneath the Edward-George Rift, the eastern edge of Rwenzori Mountains and the southern part of the Albertine Graben [*Wolbern et a*l., 2010]. The Moho depths obtained from the 2D radially-average power spectrum analysis of the WGM 2012 satellite gravity data are generally in good agreement with results obtained from passive seismic data (Table 2). The correlation coefficient (r) between results from the two methods is ~0.8 and the Root Mean Square (RMS) error is 3.72 km. Seventy five percent of the passive seismic stations reported Moho depths results that are within ±4 km with results obtained using the satellite gravity data (Table 2). This difference is indistinguishable from the combined statistical error of the two methods (Table 2). The largest difference in Moho depths (8-6 km) between the two methods came from stations that are located in the eastern side of the Rwenzori Mountains (stations ITOJ, KARU and KINY in Table 2). Although both methods reported thinner crust in this region

the passive seismic method reported shallower Moho depths compared to those from the 2D radially-average power spectral analysis of the WGM2012 data (Table 2). It is possible that the additional material presented by the Rwenzori Mountains might have contributed to the estimation of the long wavelength density anomaly (Moho) at deeper depth. Differently, only one passive seismic station (Station RUGA in Table 2) reported results showing a deeper (38 km) Moho depth compared to the gravity results (32 km). The location of this site coincides with the Toro-Ankole volcanic field (Figure 3) and a deeper Moho at this location has been suggested to be due to magma underplating [*Wolbern et al*., 2010]. The specific details of the seismic locations can be found in the *Wolbern et al*., [2010].

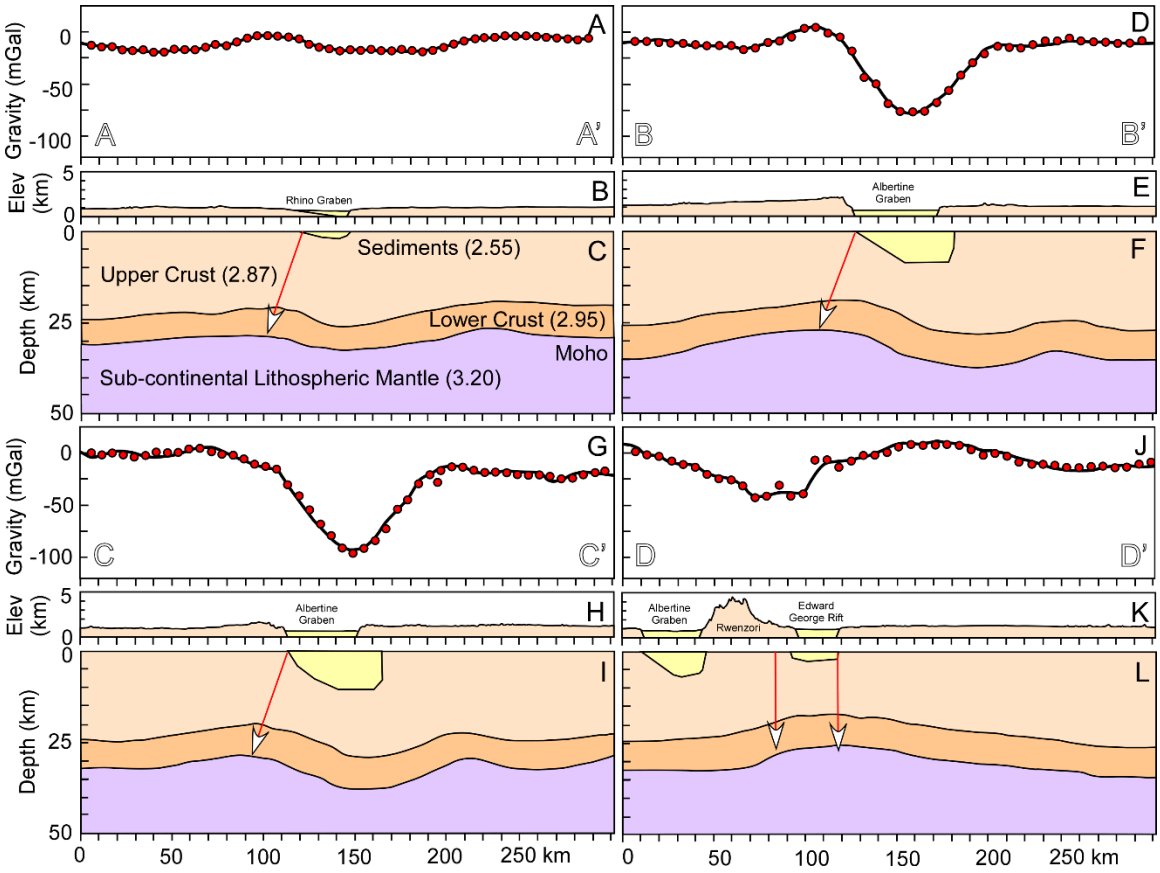

Figure 11: Northwest-southeast trending Bouguer anomaly profiles, simplified cross-sections and lithospheric-scale two-dimensional (2D) forward models across the Rhino Graben (A-C), the central part of the Albertine Graben (D-F), the southwestern part of the Albertine Graben (G-I), and the southwestern-most part of the Albertine Graben, the Edward-George Rift, and the Rwenzori Mountains (J-L).

4.4.5. TWO-DIMENSIONAL (2D) FORWARD MODELLING OF GRAVITY DATA

There are three important observations from the 2D forward modeling of gravity data: (1) There is no crustal thinning observed directly beneath the surface expression of the Rhino Graben (Figure 11C), the central part of the Albertine Graben (Figure 11F), or the southwestern part of the Albertine Graben (Figure 11H). Rather, the 2D forward models in all three profiles suggest that the maximum crustal thinning, where the Moho is elevated to a shallow depth of ~28 km, occurs ~20 km northwest of the northwestern edges of the Grabens (Figures 11C, F and H). (2) There is crustal thinning beneath the surface expression of the Edward-George Rift and the southeastern part of the Rwenzori Mountains where the Moho is elevated to a shallow depth of ~25 km (Figure 11L). (3) There is no crustal thinning beneath the southwestern-most extension of the Albertine Graben (Figure 11L).

4.5. DISCUSSION – MECHANISM FOR STRAIN LOCALIZATION DURING THE INITIATION OF THE ALBERTINE-RHINO GRABEN AND EDWARD-GEORGE RIFT

Our results show shallow CPDs, high heat flow values and thinner crust beneath the southwestern part of Albertine Graben, the Edward-George Rift, and the Rwenzori Mountains (Figures 8-10). Similarly, the northwestern margin of the Albertine Graben is characterized by shallow CPDs, high heat flow values and thinner Moho (Figures 8-10). The Rwenzori Mountains and the northwestern margin of the Albertine Graben are characterized by anomalously high topography reaching ~5 km and 3 km, respectively (Figure 3). The transition zone between the Albertine and Rhino Graben is also characterized by shallow CPDs, high heat flow values and thinner crust. However, comparing the CPD and the heat flow values of this region with those from the Edward-George Rift-Rwenzori Mountains-southwestern Albertine Graben indicates shallower CPD, higher heat flow values and shallower Moho beneath the latter. This suggests a possible northeastward deepening of the CPD and decrease in the heat flow values.

Studies carried out in the more magma-rich Eastern Branch of the EARS using borehole and silica geo-temperature data [*Wheildon et al*., 1994] show more elevated heat flow values compared to those we obtained for the Albertine-Rhino Graben and the Edward-George Rift. *Wheildon et al* (1994] reported heat flow values of 144±20 mWm^{-2} in the rift axis of the Eastern Branch, 139±21 mWm^{-2} in the western flank of the rift, and 129±23 mWm^{-2} in the rift eastern flank. This comparison suggests possible absence of magma directly beneath the Albertine-Rhino Graben and the presence of much smaller

magma volume beneath the Edward-George Rift where scattered lava flows are found within the Toro-Ankole volcanic fields (Figures 2 and 4).

The absence of surface manifestation of volcanic activity in the Albertine Graben north of the Rwenzori Mountains suggests that other factors might have facilitated strain localization during rift initiation of the Albertine-Rhino Graben. Studies from the amagmatic Okavango rift zone (Figure 1) have suggested the role of fluids migration within lithospheric-scale Precambrian pre-existing structures forming enough pressure to initiate rifting [*Leseane et al*., 2015]. Similarly, recent isotopic studies from mantle derived carbon emissions and Vp/Vs ratios from the northern Tanzanian Divergent Zone [*Hyunwoo et al*., 2016] have suggested the role of mantle fluids in rift initiation. Additionally, isotopic studies from the Albertine Graben and the surrounding Precambrian basement suggest that the source of water within the hot springs is from deeper source that migrated to the surface through a series of cross-cutting faults and joints in the Precambrian basement [*Bahati et al*., 2010].

Previous studies on the southeastern edge of the Rwenzori Mountains and the northeastern part of the Edward-George Rift have explained the presence of a thinned crust to be associated with partial melting accompanying sub-continental lithospheric mantle delamination [*Wallner and Schmeling*, 2010; *Wolbern et al*., 2010; *Häuserer and Junge*, 2011]. Sub-continental lithospheric mantle delamination has also been used to explain the extreme elevation of the Rwenzori Mountains [*Wallner and Schmeling*, 2010]. Moreover, isotopic studies on the highly alkaline volcanic materials of the Toro-Ankole volcanic field have pointed to a mantle origin [*Muravyeva and Belyatsky*, 2009].

Here, we suggest a model that involves ascendance of magma from a deeper source beneath the southwestern part of the Albertine Graben, the Edward-George Rift and the Rwenzori Mountains aided by the delamination of sub-continental lithospheric mantle. Small amount of this magma reached the surface to form the Toro-Ankole volcanic field. Sub-continental lithospheric mantle delamination is supported by the presence of considerable crustal thinning beneath the anomalously elevated Rwenzori Mountains and the northwestern side of the Albertine Graben (Figure 3). Previous studies suggested that phase change and compositional difference at the lithospheric-asthenosphere boundary can cause instability in density and gravitational balance leading to sinking of the denser sub-continental lithospheric mantle into the asthenosphere [*Schott and Schmeling*, 1998; *Wallner and Schmeling*, 2010; *Johnson et al*., 2014]. As a result, the mountain root will delaminate and will be replaced by upwelling asthenosphere followed by lateral shortening, isostatic unloading and accelerated uplift.

The presence of magmatic activities might have thermally softened the lithosphere, hence allowing for extensional strain localization to initiate the Edward-George Rift and the southwestern part of the Albertine Graben across the pre-existing structure of the Paleoproterozoic-Mesoproterozoic Rwenzori orogenic belt (*Koehn et al., 2015*) and the Kibara-Karagwe-Ankole orogenic belt (Figure 2). Differently, hot mantle fluids associated with the Toro-Ankole "hot spot" might have migrated northeastward assisted by the presence of the Mesoproterozoic-Neoproterozoic "suture zone". The concentration of these fluids might have led to softening of the lithosphere, hence enabling extensional strain localization and the development of the northeastern part of the Albertine Graben and the entire Rhino Graben as an amagmatic cratonic rift localized between the Archean-

Paleoproterozoic North Uganda Terrane and West Nile Block which form the North Congo Block that represent the northeastern extension of the Congo craton. The northeastward fluids migration could explain the apparent northeastward rift migration from the southwestern part of the Albertine Graben (which is ~80 km wide and where the Victoria plate is moving by 1.7 mm/year relative to the stationery Nubia plate) to the northeastern part of the Rhino Graben (which is ~10 km wide and where the Victoria plate is moving by 1.1 mm/year relative to the Nubia plate) [Figure 1B; *Saria et al*., 2014].

4.6. CONCLUSIONS

Imaging of the thermal (CPD and heat flow) and crustal structure (Moho depth) beneath the Albertine-Rhino Graben, the Edward-George Rift and the Rwenzori Mountains within the western branch of the EARS based on the 2D radially-averaged power spectral analysis and 2D forward modeling of the aeromagnetic and satellite gravity data revealed that the southwestern part of the Albertine Graben, the Edward-George Rift (which extends within the Paleoproterozoic-Mesoproterozoic Rwenzori and Kibara-Karagwe-Ankole orogenic belts) and the Rwenzori Mountains are characterized by shallow CPDs, high heat flow values, and generally thinner lithosphere. Shallow CPDs, high heat flow values and thinner crust are also found beneath the northwestern margin (Bunia Escarpment) of the Albertine Graben. Rwenzori Mountains and the Bunia Escarpments are characterized by anomalously high (5 km and 3 km, respectively) elevation.

No shallow CPDs, high heat flow values, or shallow Moho are observed beneath the entire length of the northeastern part of the Albertine-Rhino Graben which extends between the Archean-Paleoproterozoic North Uganda Terrane and West Nile Block

(constituting the Northeast Congo Block which represents the continuation of the Congo craton in northwestern Uganda and northeastern Congo) separated by the Mesoproterozoic-Neoproterozoic Madi-Igisi Fold and Thrust Belt.

We interpreted this thermal and crustal structure as due to northward migration of hot fluids from the magma chambers that sourced Toro-Ankole volcanic field in the south guided by the lithospheric-scale Madi-Igisi Fold and Thrust Belt which is possibly a suture between the North Uganda Terrane and West Nile Terrane. The Toro-Ankole volcanic field might be associated with sub-continental lithospheric mantle delamination that resulted in strain localization within the southwestern part of the Albertine Graben and the Edward-George Rift and rapid uplift of the Rwenzori Mountains.

We recommend the acquisition of long period magnetotelluric (MT) data across the Albertine-Rhino Graben to better understand the depth extent of the thermal anomaly and its relationship with the Precambrian structure.

Acknowledgements

We thank the Government of Uganda for allowing us free access to the airborne magnetic. This study was financially supported by the National Science Foundation – Continental Dynamics grant # EAR 1255233. This is Oklahoma State University Boone Pickens School of Geology contribution number 2016- xx.

4.7 REFERENCES

Aanyu, K, and D. Koehn (2011). Influence of pre-existing fabrics on fault kinematics and rift geometry of interacting segments: Analogue models based on the Albertine Rift (Uganda), Western Branch-East African Rift System. *Journal of African Earth Sciences 59,* 168-184, doi:10.1016/j.jafrearsci.2010.10.003.

Agostini, A., G. Corti, A. Zeoli, and G. Mulugeta (2009). Evolution, pattern, and partitioning of deformation during oblique continental rifting: Inferences from lithospheric-scale centrifuge models. *Geochemistry, Geophysics, Geosystems 10,* doi: 10.1029/2009GC002676.

Arnaiz-Rodríguez, and M.S., N.Orihuela (2013). Curie point depth in Venezuela and the Eastern Caribbean. *Tectonophysics 590,* 38-51, doi:10.1016/j.tecto.2013.01.004.

Bahati, G., Pang, Z., H. Ármannsson, E.M. Isabirye, and V. Kato (2005). Hydrology and reservoir characteristics of three geothermal systems in western Uganda. *Geothermics 34*, 568-591, doi:10.1016/j.geothermics.2005.06.005.

Bahati, G., V. Kato, and C. Nyakecho (2010). Geochemistry of Katwe-Kikorongo, Buranga and Kibiro geothermal areas, Uganda. Proceedings of the *World Geothermal Congress*, Bali, Indonesia, 25-29.

Balmino, G., N.Vales, S. Bonvalot, and A. Briais (2012). Spherical harmonic modelling to ultra-high degree of Bouguer and isostatic anomalies. *Journal of Geodesy 86*, 499-520, doi: 10.1007/s00190-011-0533-4.

Bastow, I. D., D. Keir, and E. Daly (2011). The Ethiopia Afar Geoscientific Lithospheric Experiment (EAGLE): probing the transition from continental rifting to incipient seafloor spreading. *Geological Society of America Special Papers 478*, 51-76, doi: 10.1130/2011.2478 (04).

Batte, A., G. Rümpker, M. Lindenfeld, and A. Schumann (2014). Structurally controlled seismic anisotropy above small earthquakes in crustal rocks beneath the Rwenzori region, Albertine Rift, Uganda. *Journal of African Earth Sciences*, doi:10.1016/j.jafrearsci.2014.08.001.

Begg, G., W. Griffin, L. Natapov, S.Y. O'Reilly, S. Grand, C. O'Neill, J. Hronsky, Y.P. Djomani, C. Swain, and T. Deen (2009). The lithospheric architecture of Africa: seismic tomography, mantle petrology, and tectonic evolution. *Geosphere 5*, 23-50, doi: 10.1130/GES00179.1.

Bhattacharyya, B. K., and L.K Leu (1975). Analysis of magnetic anomalies over Yellowstone National Park: mapping of Curie point isothermal surface for geothermal reconnaissance, *Journal of Geophysical Research, 80*, 4461-4465.

Birt, C., P. Maguire, M. Khan, H. Thybo, G. Keller, and J. Patel (1997). The influence of pre-existing structures on the evolution of the southern Kenya Rift Valley—evidence from seismic and gravity studies. *Tectonophysics 278,* 211-242, doi: 10.1016/S0040-1951(97)00105-4.

Bouligand, C., J. M. Glen, and R.J. Blakely (2009). Mapping Curie temperature depth in the western United States with a fractal model for crustal magnetization. *Journal of Geophysical Research: Solid Earth (1978–2012) 114*, doi: 10.1029/2009JB006494.

Calais, E., C. Ebinger, C. Hartnady, and J .M. Nocquet (2006). Kinematics of the East African Rift from GPS and earthquake slip vector data. *Geological Society of London Special Publications 259*, 9-22, doi: 10.1144/GSL.SP.2006.259.01.03

Chiozzi, P., J. Matsushima, Y. Okubo, V. Pasquale, and M. Verdoya (2005). Curie-point depth from spectral analysis of magnetic data in central–southern Europe. *Physics of the Earth and Planetary Interiors 152, 267-276*, doi:10.1016/j.pepi.2005.04.005.

Cohen, A.S., M. J. Soreghan, and C.A. Scholz (1993). Estimating the age of formation of lakes: An example from Lake Tanganyika, East African Rift System. *Geology 21, 511-514*.

Corti, G., I. Iandelli, and M. Cerca (2013). Experimental modeling of rifting at craton margins. *Geosphere 9, 138-154*, doi: 10.1130/GES00863.1.

Corti, G (2004). Centrifuge modelling of the influence of crustal fabrics on the development of transfer zones: insights into the mechanics of continental rifting architecture. *Tectonophysics 384*, 191-208, doi:10.1016/j.tecto.2004.03.014.

Daly, M., J. Chorowicz, and J. Fairhead (1989). Rift basin evolution in Africa: the influence of reactivated steep basement shear zones. *Geological Society, London, Special Publications 44*, 309-334, doi: 10.1144/GSL.SP.1989.044.01.17.

Delvaux, D., (2001). Tectonic and paleostress evolution of the Tanganyika-Rukwa-Malawi rift segment, East African rift System. *Peri-Tethys Memoir 6*, 545-567.

De Waele, B., A.B. Kampunzu, B.S.E.Mapani, and F.Tembo (2006a). The Mesoproterozoic Irumide belt of Zambia. *Journal of African Earth Sciences 46*, 36-70, doi:10.1016/j.jafrearsci.2006.01.018

De Waele, B., J.P. Liégeois, A.A. Nemchin, and F.Tembo (2006b). Isotopic and geochemical evidence of Proterozoic episodic crustal reworking within the Irumide Belt of south-central Africa, the southern metacratonic boundary of an Archaean Bangweulu Craton. *Precambrian Research 148,* 225-256, doi:10.1016/j.precamres.2006.05.006.

Ebinger, C.J (1989). Tectonic development of the Western Branch of the East African Rift System. *Geological Society of America Bulletin 101, 885-903,* doi: 10.1130/0016-7606(1989)101<0885: TDOTWB >2.3.CO; 2.

Ebinger, C, and M. Casey (2001). Continental breakup in magmatic provinces: An Ethiopian example. *Geology 29,* 527-530, doi: 10.1130/0091-7613(2001) 029<0527:CBIMPA>2.0.CO;2

Ebinger, C., Keir, D., Ayele, A., Calais, E., Wright, T., Belachew, M., Hammond, J., Campbell, E., Buck, W., 2008. Capturing magma intrusion and faulting processes during continental rupture: seismicity of the Dabbahu (Afar) rift. *Geophysical Journal International 174,* 1138-1152, doi: 10.1111/j.1365-246X.2008.03877.x.

Fernandez-Alonso, M., H. Cutten, B. De Waele, L. Tack., A. Tahon, D. Baudet, and S.D. Barritt (2012). The Mesoproterozoic Karagwe-Ankole Belt (formerly the NE Kibara Belt): The result of prolonged extensional intracratonic basin development punctuated by two short-lived far-field compressional events. *Precambrian Research 216–219,* 63-86, doi:10.1016/j.precamres.2012.06.007.

Haggerty, S, (1978). Mineralogical constraints on Curie isotherms in deep crustal magnetic anomalies, *Geophysical Research Letters 5,* 105-108, doi: 10.1029/GL005i002p00105.

Hammond, J., J.M. Kendall, G. Stuart, C. Ebinger, I. Bastow, D. Keir, A. Ayele, M. Belachew, B. Goitom, and G. Ogubazghi (2013). Mantle upwelling and initiation of rift segmentation beneath the Afar Depression. *Geology 41,* 635-638, doi: 10.1130/G33925.1.

Häuserer, M., and A. Junge (2011). Electrical mantle anisotropy and crustal conductor: a 3-D conductivity model of the Rwenzori Region in western Uganda. *Geophysical Journal International 185,* 1235-1242, doi: 10.1111/j.1365-246X.2011.05006.x.

Hunt, C.P., B.M Moskowitz, and S.K Banerjee (1995). Magnetic properties of rocks and minerals. Rock physics & phase relations: a *handbook of physical constants, 189-204*, doi: 10.1029/RF003p0189.

Hussein, M., K. Mickus, and L.F Serpa (2013). Curie Point Depth Estimates from Aeromagnetic Data from Death Valley and Surrounding Regions, California. *Pure and Applied Geophysics 170,* 617-632, doi: 10.1007/s00024-012-0557-6.

Hyunwoo, L., J.D. Muirhead, T.P. Fischer, C. Ebinger, S.A. Kattenhorn, Z.D. Sharp, and G. Kianji (2016). Massive and prolonged deep carbon emissions associated with continental rifting. *Nature Geoscience,* doi: 10.1038/NGEO2622.

Jakovlev, A., G. Rümpker, M. Lindenfeld, I. Koulakov, A. Schumann and N. Ochmann (2011). Crustal seismic velocities of the Rwenzori Region, East African Rift, from local travel-time tomography: Evidence for low velocity anomalies beneath mountain range. *Bulletin of the Seismological Society of America 101*, 848-858.

Jakovlev, A., G. Rümpker, H. Schmeling, I. Koulakov, M. Lindenfeld, and H. Wallner (2013). Seismic images of magmatic rifting beneath the western branch of the East

African rift. *Geochemistry, Geophysics, Geosystems 14*, 4906-4920, doi: 10.1002/2013GC004939.

Jorand, R., C. Clauser, G. Marquart, and R. Pechnig (2015). Statistically reliable petrophysical properties of potential reservoir rocks for geothermal energy use and their relation to lithostratigraphy and rock composition: The NE Rhenish Massif and the Lower Rhine Embayment (Germany). *Geothermics 53*, 413-428, doi:10.1016/j.geothermics.2014.08.008.

Karp, T., C.A. Scholz, and M.M McGlue (2012). Structure and stratigraphy of the Lake Albert Rift, East Africa: Observations from seismic reflection and gravity data. *Association of American Geologists, Memoir 95*, p.299-318, doi: 10.1306/13291394M952903.

Katumwehe, A.B., M.G. Abdelsalam, and E.A. Atekwana (2015). The role of pre-existing Precambrian structures in rift evolution: The Albertine and Rhino Grabens, Uganda. *Tectonophysics 646*, 117-129, doi:10.1016/j.tecto.2015.01.022.

Kendall, J.M., G.W. Stuart, C. Ebinger, I.D. Bastow, D. Keir (2005). Magma-assisted rifting in Ethiopia. *Nature 433*, 146-148, doi: 10.1038/nature03161.

Keir, D., C. Pagli, I.D. Bastow, and A. Ayele (2011). The magma-assisted removal of Arabia in Afar: Evidence from dike injuction in the Ethiopian rift captured using InSAR and seismicity. *Tectonics 30*, TC2008, DOI:10.1029/2010TC002785.

Koehn, D., K. Link, T. Sachau, C.W. Passchier, K. Aanyu, A. Spikings, R. Harbinson (2015). The Rwenzori Mountains, a Paleoproterozoic crustal shear belt crossing the Albertine rift system. *International Journal of Earth Sciences*, DOI 10.1007/s00531-015-1167-1.

Koptev, A., E. Calais, E. Burov, S.Leroy, and T. Gerya (2015). Dual continental rift systems generated by plume-lithosphere interaction. *Nature Geoscience*, doi: 10.1038/ngeo2401.

Korme, T., V. Acocella, and B. Abebe (2004). The role of pre-existing structures in the origin, propagation and architecture of faults in the Main Ethiopian Rift. *Gondwana Research 7*, 467-479, doi: 10.1016/S1342-937X (05)70798-X.

Kuhn, M., W. Featherstone, and J. Kirby (2009). Complete spherical Bouguer gravity anomalies over Australia. *Australian journal of Earth sciences 56*, 213-223, doi: 10.1080/08120090802547041.

Lærdal, T, and M.R. Talbot (2002). Basin neotectonics of Lakes Edward and George, East African Rift. *Paleogeography, Paleoclimatology, Paleoecology 187*, 213-232, doi: 10.1016/S0031-0182(02)00478-9.

Lao-Davila, D.A., H. Al-Salmi, M.G. Abdelsalam, and E.A. Atekwana (2015). Hierarchical segmentation of the Malawi rift: The influence of inherited lithospheric heterogeneity and kinematics in the evolution of continental rift. *Tectonics 3*, 2399-2417, doi: 10.1002/2015TC003953

Leseane, K., E.A. Atekwana, K. Mickus, M.G. Abdelsalam, E.M. Shemang, and E.A. Atekwana (2015). Thermal perturbations beneath the incipient Okavango Rift Zone, northwest Botswana. *Journal of Geophysical Research: Solid Earth*, doi: 10.1002/2014JB011029.

Lindenfeld, M., G. Rümpker, K. Link, D. Koehn, and A. Batte (2012). Fluid-triggered earthquake swarms in the Rwenzori region, East African Rift—Evidence for rift initiation. *Tectonophysics 566–567*, 95-104, doi:10.1016/j.tecto.2012.07.010.

Link, K., D. Koehn, M.G. Barth, J.V. Tiberindwa, E. Barifaijo, K. Aanyu, and S.F. Foley (2010). Continuous cratonic crust between the Congo and Tanzania Blocks in western Uganda. *International Journal of Earth Sciences 99*, 1559-1573, doi: 10.1007/s00531-010-0548-8.

Maguire, P., C. Swain, R. Masotti, and M. Khan (1994). A crustal and uppermost mantle cross-sectional model of the Kenya Rift derived from seismic and gravity data. *Tectonophysics 236*, 217-249, doi: 10.1016/0040-1951(94)90178-3.

Morrison, F.A (2014). Obtaining uncertainty measure on slope and intercept of a least squares fit with Excel's LINEST. www.chem.mtu.edu/~fmorrison/cm3215/Uncertainty Slope Intercept of Least Squares Fit.pdf

Maus, S., D. Gordon, and D. Fairhead (1997).Curie-temperature depth estimation using a self-similar magnetization model. *Geophysical Journal International 129*, 163-168, doi: 10.1111/j.1365-246X.1997.tb00945.x.

Modisi, M. P., E.A. Atekwana, A.B. Kampunzu, and T.H. Ngwisanyi (2000). Rift kinematics during the incipient stages of continental extension: evidence from the nascent Okavango rift basin, northwest Botswana, *Geology 102*, 363-376.

Mullins, C.E (1977). Magnetic susceptibility of the soil and its significance in soil science; A review. *Journal of Soil Science 28*, 223-246.

Muravyeva, N., Belyatsky, B., 2009. Petrology and geochemistry Toro Ankole Kamafugite magmas: isotopic constraints, EGU General Assembly Conference Abstracts, p. 12651, doi: 10.1134/S0016702909090031.

Nyakecho, C, and S.Hagemann (2014). An overview of gold systems in Uganda. Australian Journal of Earth Sciences 61, 59-88, doi:10.1080/08120099.2013.831773.

Okubo, Y., R.J. Graf, R.O. Hansen, K. Ogowa, and H. Tsu (1985). Curie point depth of the island of Kyushu and surrounding areas, Japan, *Geophysics 50,* 481-494.

Okubo, Y., H. Tsu, K.Ogawa (1989). Estimation of Curie point and geothermal structure of island arcs of Japan. *Tectonophysics 159*, 279-290.

Pavlis, N.K., S.A. Holmes, S.C. Kenyon and J.K. Factor, (2012). The development and evaluation of the Earth Gravitational Model 2008 (EGM2008). *Journal of Geophysical Research*: Solid Earth (1978–2012) 117, doi: 10.1029/2011JB008916.

Ravat, D., A. Pignatelli, I. Nicolosi and M.Chiappini (2007). A study of spectral methods of estimating the depth to the bottom of magnetic sources from near-surface magnetic anomaly data. *Geophysical Journal International 169*, 421-434, doi: 10.1111/j.1365-246X.2007.03305.x.

Ring, U (2008). Extreme uplift of the Rwenzori Mountains in the East African Rift, Uganda: Structural framework and possible role of glaciations. *Tectonics 27*, TC4018, doi: 10.1029/2007TC002176.

Roberts, E.M., N.J. Stevens, P.M. O'Conner, P.H.G.M. Dirks, M.D. Gottfried, W.C. Clyde, R.A. Armstrong, A.I.S. Kemp, and S. Hemming (2012). Initiation of the western branch of the East African Rift coeval with the eastern branch, *Nature Geoscience 5*, 289-294.

Rooney, T.O, C. Herzberg, and I.D. Bastow (2012). Elevated mantle temperature beneath East Africa. *Geology 40*, 27-30, doi:10.1130/G32382.1.

Rosenthal, A., S.F. Foley, D.G. Pearson, G.M. Nowell, and S. Tappe (2009). Petrogenesis of strongly alkaline primitive volcanic rocks at the propagating tip of the Western Branch of the East African Rift. *Earth and Planetary Science Letters 284*, 236-248, doi:10.1016/j.epsl.2009.04.036.

Rosendaht, B.R., E.Kilembe, and K. Kaczmarick (1992). Comparison of Tanganyika, Malawi, Rukwa and Turkana rift zones from analyses of seismic reflection data. *Tectonophysics 213*, 235-256.

Russo, R, and R. Speed (1994). Spectral analysis of gravity anomalies and the architecture of tectonic wedging, NE Venezuela and Trinidad. *Tectonics 13*, 613-622, doi: 10.1029/94TC00052.

Sanchez-Rojas, J., and M. Palma (2014). Crustal density structure in northwestern South America derived from analysis and 3-D modeling of gravity and seismicity data. *Tectonophysics 634*, 97-115, doi:10.1016/j.tecto.2014.07.026.

Saria, E., E. Calais, D. Stamps, D. Delvaux, and C. Hartnady (2014). Present-day kinematics of the East African Rift. *Journal of Geophysical Research, Solid Earth 119*, 3584-3600, doi: 10.1002/2013JB010901.

Schott, B, and H. Schmeling (1998). Delamination and detachment of a lithospheric root. Tectonophysics 296, 225-247, doi: 10.1016/S0040-1951(98)00154-1.

Sigmundsson, F (2006). Plate tectonics: Magma does the splits. *Nature 442*, 251-252, doi: 10.1038/442251a.

Simiyu, S.M, and G.R. Keller (2001). An integrated geophysical analysis of the upper crust of the southern Kenya rift. *Geophysical Journal International 147*, 543-561, doi: 10.1016/S0040-1951(97)00109-1.

Spector, A, and F. Grant (1970). Statistical models for interpreting aeromagnetic data. *Geophysics 35*, 293-302, doi: 10.1190/1.1440092.

Stamps, D.S., E. Calais, E. Saria, C. Hartnady, J.M. Nocquet, C. Ebinger, and R.M. Fernandes (2008). A kinematic model for the East African Rift. *Geophysical Research Letters 35*, L05304, doi: 10.1029/2007GL032781.

Tack, L., M.T.D. Wingate, B. De Waele, J. Meert, E. Belousova, B. Griffin, A and Tahon, M. Fernandez-Alonso (2010). The 1375Ma "Kibaran event" in Central Africa: Prominent emplacement of bimodal magmatism under extensional regime. *Precambrian Research 180*, 63-84, doi:10.1016/j.precamres.2010.02.022.

Tanaka, A., Y. Okubo, and O. Matsubayashi (1999). Curie point depth based on spectrum analysis of the magnetic anomaly data in East and Southeast Asia. *Tectonophysics 306*, 461-470, doi: 10.1016/S0040-1951(99)00072-4.

Tesha, A.L., A.A Nyblade, G.R. Keller, and D.I Doser (1997). Rift localization in suture-thickened crust: evidence from Bouguer gravity anomalies in northeastern Tanzania, East Africa. *Tectonophysics 278*, 315-328, doi: 10.1016/S0040-1951(97)00110-8.

Tselentis, G.-A., J. Drakopoulos, and K. Dimitriadis (1988). A spectral approach to Moho depths estimation from gravity measurements in Epirus (NW Greece). *Journal of Physics of the Earth 36*, 255-266, doi.org/10.4294/jpe1952.36.255.

Upcott, N., R. Mukasa, C. Ebinger, and G.Karner (1996). Along-axis segmentation and isostasy in the Western rift, East Africa. *Journal of Geophysical Research 101*, 3247-3268.

Valentine, G.A, and K.E. Krogh (2006). Emplacement of shallow dikes and sills beneath a small basaltic volcanic center–The role of pre-existing structure (Paiute Ridge, southern Nevada, USA). *Earth and Planetary Science Letters 246*, 217-230, doi:10.1016/j.epsl.2006.04.031.

Westerhof, P A.B., H. Paavo, E. Isabirye, E. Katto, T. Koistinen, E. Kuosmanen, T. Lehto, I. Matti, Lehtonen, H. Mäkitie, T. Manninen, I. Mänttäri, Y. Pekkala, J. Pokki, K. Saalmann, and P. Virransalo (2014). Geology and Geodynamic Development of Uganda with Explanation of the 1:1,000,000 -Scale *Geological Map. Geological Survey of Finland, Technical report number 55*, 2014.

Wilson, D., R. Aster, M. West, J. Ni, S. Grand, W. Gao, W.S. Baldridge, S. Semken, and P. Patel (2005). Lithospheric structure of the Rio Grande rift. *Nature 433*, 851-855, doi: 10.1038/nature03297.

Wright, T.J., C. Ebinger, J. Biggs, A. Ayele, G. Yirgu, D. Keir, and A. Stork (2006). Magma-maintained rift segmentation at continental rupture in the 2005. Afar diking episode. *Nature 442*, 291-294, doi: 10.1038/nature04978.

Van Wijk, J (2005). Role of weak zone orientation in continental lithosphere extension. *Geophysical Research Letters 32*, doi: 10.1029/2004GL022192.

Vauchez, A., G. Barruol, and A. Tommasi, (1997). Why do continents break-up parallel to ancient orogenic belts? *Terra Nova 9*, 62-66, doi: 10.1111/j.1365-3121.1997.tb00003.x.

Wallner, H, and H. Schmeling (2010). Rift induced delamination of mantle lithosphere and crustal uplift: a new mechanism for explaining Rwenzori Mountains' extreme elevation? *International Journal of Earth Sciences 99*, 1511-1524.

Wheildon, J., P. Morgan, K.H. Williamson, T.R. Evans, and C.A. Swanberg (1994). Heat flow in the Kenya rift zone. *Tectonophysics 236,* 131-149.

Wölbern, I., G. Rümpker, A. Schumann, and A. Muwanga, (2010). Crustal thinning beneath the Rwenzori region, Albertine rift, Uganda, from receiver-function analysis. *International Journal of Earth Sciences 99*, 1545-1557, doi: 10.1007/s00531-009-0509-2.

Wölbern, I., G. Rümpker, K. Link, F. Sodoudi (2012). Melt infiltration of the lower lithosphere beneath the Tanzania craton and the Albertine rift inferred from S receiver functions. *Geochemistry, Geophysics, Geosystems 13*, doi: 10.1029/2012GC004167.

TABLE 1

Rift	Borehole location	Lon. (°)	Lat. (°)	Temp. grad °/km	Total Depth (km)	K $Wm^{-1}K^{-1}$	Heat flow mWm^{-2} Borehole	Error ±	Heat flow mWm^{-2} CPD	Error ±	Difference
Albertine	Ngari1	0.42	29.78	37	1733	2.17	81	2	86	2	5
Albertine	Mputa 1	1.44	30.96	19	1121	2.17	42	1	45	1	3
Albertine	Mputa 2	1.46	30.95	23	770	2.17	50	2	53	2	3
Albertine	Mputa 3	1.43	30.97	42	920	2.17	92	1	97	0	5
Albertine	Mputa 4	1.44	30.98	30	1033	2.17	64	1	68	0	4
Albertine	Waraga 2	1.56	31.10	53	1591	2.17	116	1	123	1	7
Albertine	Nzinzi 2	1.41	30.91	55	950	2.17	120	1	127	2	7
Albertine	Turaco 1	1.03	30.30	30	2129	2.17	64	2	68	2	4
Albertine	Turaco 2	1.03	30.30	27	2311	2.17	59	1	62	1	4
Albertine	Turaco 3	1.03	30.30	23	2753	2.17	49	0	52	2	3
Albertine	Turaco 4	1.03	30.30	28	2872	2.17	60	2	64	1	4
Albertine	Nzinzi 3	1.41	30.92	34	882	2.17	73	1	77	2	4
Rhino	Odyek 1	2.25	31.31	41	983	2.17	89	2	94	2	5
Rhino	Riwu 1	2.41	31.41	29	342	2.17	63	1	67	1	4

Table 1: Comparison between heat flow values calculated from the Curie Point Depth (CPD) obtained using two-dimensional (2D) radially-average power spectral analysis of aeromagnetic data and those calculated from geothermal gradient measurement from boreholes in the Albertine-Rhino Graben.

TABLE 2

Station	Lat (°)	Lon (°)	Region	Moho Depth (km) Seismic Wolbern et al., 2010	Moho Depth (km) Gravity Katumwehe et al., 2016	Difference
BURO	0.86	30.1	Rwenzori NW	32±2	32±1	0
ITOJ	0.84	30.2	Rwenzori NE	21±2	29±3	-8
KABA	0.78	30.1	Rwenzori NW	36±2	37±2	-1
KABE	0.87	30.5	Rift shoulder NW	34±2	37±2	-3
KABG	0.63	30.7	Rift shoulder NW	30±2	37±2	-7
KAGO	0.68	30.5	Rift shoulder NW	36±2	37±2	-1
KARA	0.09	29.9	Rwenzori S	28±2	27±2	-1
KARU	0.79	30.2	Rwenzori NE	21±2	29±2	-8
KASE	-0.03	30.2	Rift Valley	30±2	30±2	0
KASS	0.57	30.3	Rift shoulder NW	24±2	33±1	-9
KILE	0.21	30.0	Rwenzori SE	22±2	29±2	-7
KINY	0.51	30.1	Rwenzori E	18±2	27±1	-9
KISA	0.60	30.7	Rift shoulder	30±2	37±1	-7
KMTW	0.74	30.4	Rift shoulder	30±2	37±1	-7
MBAR	-0.60	30.7	Rift shoulder	30±2	34±2	-4
MIRA	0.66	30.6	Rift shoulder	29±2	37.±1	-8
MWEY	-0.19	29.9	Rift valley	25±2	28±2	-3
NGIT	0.64	30.0	Rwenzori NW	32±2	30±2	2
NYAN	0.21	30.5	Rift Shoulder	32±2	29±2	3
RUBO	0.34	30.0	Rwenzori SE	21±2	28±2	-7
RUGA	-0.26	30.1	Rift shoulder	38±2	32±1	6
RWEB	0.32	30.5	Rift shoulder	32±2	30±2	2
SEML	0.91	30.4	Rift valley	34±2	33±4	1
SEMP	0.835	30.168	Rwenzori NW	36±2	33±1	3
BURO	0.862	30.173	Rwenzori NW	32±2	32±1	0
ITOJ	0.844	30.229	Rwenzori NE	21±2	29±3	-8

Table 2: Comparison of results of crustal thickness beneath the Albertine-Rhino Graben from two-dimensional (2D) radially-averaged power spectral analysis of World Gravity Model 2012 (WGM 2012) satellite gravity data with results from passive seismic data by *Wolbern et al.* [2010].

APPENDICES

TABLE 3

Depth Z_o (km)	D_t (Z_t) km	2ZO_Zt CPD km	Temp. Grad $^{(o)}$C/km)	Heat (1.9) mWm^{-2}	Heat (2.1) mWm^{-2}	Heat (2.3) mWm^{-2}	Heat (2.5) mWm^{-2}	Heat (2.77) mWm^{-2}	Error
12.8	3.9	21.7	26.7	50.8	27.2	61.5	66.8	157.5	1
11.8	2.3	21.3	27.2	51.7	25.1	62.6	68.1	160.4	1
14.1	2.8	25.4	22.8	43.4	30.0	52.5	57.1	134.5	1
11.7	2.3	21.1	27.5	52.2	24.9	63.2	68.7	162.0	1
12.3	2.3	22.3	26.0	49.4	26.2	59.8	65.0	153.2	1
12.4	2.6	22.2	26.1	49.6	26.4	60.1	65.3	153.9	1
11.8	2.3	21.3	27.2	51.7	25.1	62.6	68.1	160.4	1
12.9	2.7	23.1	25.1	47.7	27.4	57.7	62.8	147.9	1
13.4	3.1	23.7	24.5	46.5	28.5	56.3	61.2	144.2	1
12.5	1.8	23.2	25.0	47.5	26.6	57.5	62.5	147.3	1
12.6	3.1	22.1	26.2	49.9	26.8	60.4	65.6	154.6	1
12.6	1.8	23.4	24.8	47.1	26.8	57.0	62.0	146.0	1
12.3	2.1	22.5	25.8	49.0	26.2	59.3	64.4	151.9	1
13.1	2.4	23.8	24.4	46.3	27.9	56.1	60.9	143.6	1
12.3	2.6	22.0	26.4	50.1	26.2	60.6	65.9	155.3	1
13.0	2.4	23.6	24.5	46.6	27.7	56.4	61.3	144.6	1
11.3	2.6	20.0	29.0	55.1	24.0	66.7	72.5	170.9	1
14.0	1.9	26.1	22.2	42.2	29.8	51.1	55.6	130.9	1
10.5	2.1	18.9	30.7	58.4	22.4	70.7	76.8	181.0	1
12.7	1.7	23.7	24.5	46.6	27.0	56.4	61.3	144.4	1

11.9	2.1	21.7	26.7	50.8	25.3	61.5	66.8	157.5	1
12.6	2.1	23.1	25.1	47.7	26.8	57.7	62.8	147.9	1
13.8	3.8	23.8	24.4	46.3	29.4	56.1	60.9	143.6	1
11.9	2.2	21.6	26.9	51.0	25.3	61.8	67.1	158.2	1
11.3	2.2	20.4	28.4	54.0	24.0	65.4	71.1	167.5	1
11.5	2.3	20.7	28.0	53.2	24.5	64.4	70.0	165.1	1
11.6	2.5	20.7	28.0	53.2	24.7	64.4	70.0	165.1	1
11.5	2.2	20.8	27.9	53.0	24.5	64.1	69.7	164.3	1
11.2	2.1	20.3	28.6	54.3	23.8	65.7	71.4	168.3	1
11.7	2.3	21.1	27.5	52.2	24.9	63.2	68.7	162.0	1
9.3	2.2	16.4	35.4	67.2	19.8	81.3	88.4	208.4	1
12.4	2.2	22.6	25.7	48.8	26.4	59.0	64.2	151.2	0
12.8	2.4	23.2	25.0	47.5	27.2	57.5	62.5	147.3	0
12.2	2.2	22.2	26.1	49.6	25.9	60.1	65.3	153.9	1
12.4	1.9	22.9	25.3	48.1	26.4	58.3	63.3	149.2	1
12.5	2.0	23.0	25.2	47.9	26.6	58.0	63.0	148.6	1
13.8	2.4	25.2	23.0	43.7	29.4	52.9	57.5	135.6	1
11.9	3.1	20.7	28.0	53.2	25.3	64.4	70.0	165.1	1
12.8	2.7	22.9	25.3	48.1	27.2	58.3	63.3	149.2	1
13.1	2.4	23.8	24.4	46.3	27.9	56.1	60.9	143.6	1
13.1	2.4	23.8	24.4	46.3	27.9	56.1	60.9	143.6	1
12.6	1.9	23.3	24.9	47.3	26.8	57.3	62.2	146.7	1
12.3	2.4	22.2	26.1	49.6	26.2	60.1	65.3	153.9	1
12.6	2.9	22.3	26.0	49.4	26.8	59.8	65.0	153.2	1
12.2	2.3	22.1	26.2	49.9	25.9	60.4	65.6	154.6	1
12.0	2.3	21.7	26.7	50.8	25.5	61.5	66.8	157.5	1
12.0	2.6	21.4	27.1	51.5	25.5	62.3	67.8	159.7	1
12.0	2.9	21.1	27.5	52.2	25.5	63.2	68.7	162.0	1

12.3	2.5	22.1	26.2	49.9	26.2	60.4	65.6	154.6	1
12.6	2.5	22.7	25.6	48.5	26.8	58.8	63.9	150.5	1
12.0	2.4	21.6	26.9	51.0	25.5	61.8	67.1	158.2	1
14.0	2.8	25.2	23.0	43.7	29.8	52.9	57.5	135.6	1
12.7	3.3	22.1	26.2	49.9	27.0	60.4	65.6	154.6	1
12.6	2.8	22.4	25.9	49.2	26.8	59.6	64.7	152.6	1
13.5	1.8	25.2	23.0	43.7	28.7	52.9	57.5	135.6	1
12.7	2.5	22.9	25.3	48.1	27.0	58.3	63.3	149.2	1
10.0	3.6	16.4	35.4	67.2	21.3	81.3	88.4	208.4	1
13.0	2.2	23.8	24.4	46.3	27.7	56.1	60.9	143.6	1
12.5	2.2	22.8	25.4	48.3	26.6	58.5	63.6	149.9	1
13.3	2.3	24.3	23.9	45.3	28.3	54.9	59.7	140.6	1
12.6	3.4	21.8	26.6	50.6	26.8	61.2	66.5	156.8	1
13.3	2.2	24.4	23.8	45.2	28.3	54.7	59.4	140.1	1
13.5	2.0	25.0	23.2	44.1	28.7	53.4	58.0	136.7	1
12.2	1.9	22.5	25.8	49.0	25.9	59.4	64.5	152.1	1
12.0	2.3	21.7	26.7	50.8	25.5	61.5	66.8	157.5	
13.3	2.2	24.4	23.8	45.2	28.3	54.7	59.4	140.1	1
12.0	2.1	21.9	26.5	50.3	25.5	60.9	66.2	156.0	1
12.8	2.7	22.9	25.3	48.1	27.2	58.3	63.3	149.2	1
12.1	2.1	22.1	26.2	49.9	25.7	60.4	65.6	154.6	1
12.2	2.1	22.3	26.0	49.4	25.9	59.8	65.0	153.2	1
12.9	2.4	23.4	24.8	47.1	27.4	57.0	62.0	146.0	1
13.0	2.1	23.9	24.3	46.1	27.7	55.8	60.7	143.0	1
12.4	1.9	22.9	25.3	48.1	26.4	58.3	63.3	149.2	1
11.2	1.7	20.7	28.0	53.2	23.8	64.4	70.0	165.1	1
10.7	1.5	19.9	29.1	55.4	22.8	67.0	72.9	171.7	0
13.0	2.0	24.0	24.2	45.9	27.7	55.6	60.4	142.4	0

12.2	2.2	22.2	26.1	49.6	25.9	60.1	65.3	153.9	1
12.5	1.9	23.1	25.1	47.7	26.6	57.7	62.8	147.9	1
13.8	1.9	25.7	22.6	42.9	29.4	51.9	56.4	133.0	0
14.2	2.3	26.1	22.2	42.2	30.2	51.1	55.6	130.9	1
12.0	1.4	22.6	25.7	48.8	25.5	59.0	64.2	151.2	1

Table 3: Curie point depth (CPD) estimates from 2dimensional (2D) spectral analysis method of airborne magnetic data

TABLE 3

Block	**lat (o)**	**lon (o)**	**Moho (km)**	**Error (±km)**
S1	3.75	30.75	27	0
S2	3.75	31	28	0
S3	3.75	31.25	36	7
S4	3.75	31.5	41	8
S5	3.75	31.75	41	2
S6	3.75	32	29	5
S7	3.75	32.25	33	2
S8	3.75	32.5	38	3
S9	3.75	32.75	32	4
S13	3.25	32.75	30	3
S14	3.25	32.5	32	0
S15	3.25	32.25	34	0
S16	3.25	32	34	0
S17	3.25	31.75	34	1
S18	3.25	31.5	38	0
S19	3.25	31.25	35	2
S20	3.25	31	36	2
S21	3.25	30.75	36	1
S30	3	31.5	32	3
S22	2.75	30.75	30	7
S23	2.75	31	37	1
S24	2.75	31.25	28	4
S25	2.75	31.5	34	3
S26	2.75	31.75	27	4

S27	2.75	32	32	9
S28	2.75	32.25	32	2
S29	2.75	32.5	35	1
S35	2.25	32.75	38	4
S36	2.25	32.5	27	2
S37	2.25	32.25	37	5
S38	2.25	32	34	0
S39	2.25	31.75	35	9
S40	2.25	31.5	35	5
S41	2.25	31.25	30	3
S42	2.25	31	29	1
S43	2.25	30.75	33	3
S44	2.25	30.5	35	0
S45	2.25	30.25	32	4
S46	1.75	30.25	34	1
S47	1.75	30.5	24	1
S48	1.75	30.75	32	4
S49	1.75	31	38	1
S50	1.75	31.25	33	1
S51	1.75	31.5	34	1
S52	1.75	31.75	38	2
S53	1.75	32	34	1
S54	1.75	32.25	33	0
S55	1.75	32.5	40	3
S56	1.75	32.75	32	1
S63	1.25	32.75	38	3
S64	1.25	32.5	35	2
S65	1.25	32.25	39	2
S66	1.25	32	37	4
S67	1.25	31.75	31	3
S68	1.25	31.5	29	2
S69	1.25	31.25	37	3
S70	1.25	31	38	0
S71	1.25	30.75	34	3
S72	1.25	30.5	20	0
S73	1.25	30.25	32	3
S74	1.25	30	32	0
S75	1.25	29.75	31	0
S76	1.25	29.5	36	3
S77	0.75	29.5	37	2
S78	0.75	29.75	34	1

S79	0.75	30	29	0
S80	0.75	30.25	30	2
S81	0.75	30.5	37	0
S82	0.75	30.75	43	2
S83	0.75	31	34	2
S84	0.75	31.25	30	1
S85	0.75	31.5	30	1
S86	0.75	31.75	34	3
S87	0.75	32	36	1
S88	0.75	32.25	32	0
S89	0.75	32.5	33	2
S90	0.75	32.75	26	5
S104	0.25	32.75	25	2
S105	0.25	32.5	34	4
S106	0.25	32.25	32	0
S107	0.25	32	36	1
S108	0.25	31.75	29	0
S109	0.25	31.5	42	3
S110	0.25	31.25	29	2
S111	0.25	31	31	1
S112	0.25	30.75	30	0
S113	0.25	30.5	29	2
S114	0.25	30.25	30	1
S115	0.25	30	30	0
S116	0.25	29.75	27	1
S117	0.25	29.5	30	2
S118	-0.25	29.5	31	3
S119	-0.25	29.75	35	0
S120	-0.25	30	25	1
S121	-0.25	30.25	32	0
S122	-0.25	30.5	30	0
S123	-0.25	30.75	35	0
S124	-0.25	31	36	3
S125	-0.25	31.25	30	2
S126	-0.25	31.5	32	3
S127	-0.25	31.75	29	2
S128	-0.25	32	43	2
S129	-0.25	32.25	39	1
S130	-0.25	32.5	35	1
S131	-0.25	32.75	36	1
S150	-0.75	32.75	32	2

S151	-0.75	32.5	33	3
S152	-0.75	32.25	35	0
S153	-0.75	32	38	3
S154	-0.75	31.75	29	3
S155	-0.75	31.5	30	2
S156	-0.75	31.25	33	2
S157	-0.75	31	36	1
S158	-0.75	30.75	35	1
S159	-0.75	30.5	31	1
S160	-0.75	30.25	34	0
S161	-0.75	30	28	0
S162	-1.25	29.5	31	0
S163	-1.25	29.75	33	0
S164	-1.25	30	40	1
S165	-1.25	30.25	31	1
S166	-1.25	30.5	37	0
S167	-1.25	30.75	33	3
S168	-1.25	31	33	2
S169	-1.25	31.25	31	3
S170	-1.25	31.5	29	3
S171	-1.25	31.75	27	0
S172	-1.25	32	36	0
S173	-1.25	32.25	38	0
S174	-1.25	32.5	35	2
S175	-1.25	32.75	31	1
S219	1.75	29.75	35	1
S220	1.75	29.5	37	1
S221	2.25	30	33	2
S222	2.25	29.75	41	3
S223	2.25	29.5	31	2
S224	2.75	30.25	38	3
S225	2.75	30	38	3
S226	2.75	29.75	34	0
S227	2.75	29.5	33	0
S228	3.25	30.75	34	0
S229	3.25	30.5	32	0
S230	3.25	30.25	34	1
S231	3.25	30	29	3
S232	3.25	29.75	29	1
S233	3.25	29.5	32	3
S234	3.75	30.5	36	2

S235	3.75	30.13	30	0
S236	3.75	29.88	36	0
S237	3.75	29.63	38	2
S238	3.75	29.38	32	1
S161	-0.75	29.75	39	3
S162	-0.75	29.5	28	3

Table 3: Crustal thickness (Moho) estimates from Satellite gravity based on the 2dimensiponal Spectral analysis.

VITA

Andrew B Katumwehe

Candidate for the Degree of
DOCTOR OF PHILOSOPHY

Thesis: THE ROLE OF PRE-EXISTING PRECAMBRIAN STRUCTURES AND THERMAL ANOMALY IN RIFT INITIATION AND EVOLUTION-THE ALBERTINE AND RHINO GRABENS IN UGANDA

Major Field: GEOLOGY

Biographical

Education:

Completed the requirements for the Doctor of Philosophy in Geology at Oklahoma State University, Stillwater, Oklahoma in May, 2016.

Completed the requirements for the Master of Science in Applied Geophysics from International Institute of Aerospace Surveys and Earth Observations (ITC), Delft, Netherlands, 2000.

Completed the requirements for the Bachelor of Science (Honors) in Geology and Chemistry at Makerere University, Kampala, Uganda 1995.

Experience: Teaching, Research Assistant, Boone Pickens School of Geology August 2011-May 2016. Principal Geophysicist at the Directorate of Geological Surveys and Mines, Uganda 1997-2011.

Professional Memberships:
Society of Exploration Geophysicists (SEG)
American Geophysical Union (AGU)
American Association of Petroleum Geologists (AAPG) and Tulsa Geological Society (TGS)
SEG Global Association Member (GAC) Country representative for Uganda, Faculty Advisor Makerere University SEG student Chapter
Member for SEG Committee on University and Student Programs (CUSP)
Member of the geophysics in the Onsite inspection (OSI) regime for the Comprehensive Nuclear Test Ban Treaty Organization (CTBTO) under the Continuation phase techniques.
Geodynamic Processes at Rifting and Subduction Margins (GeoPRISMS)
Global member of the Prospectors and Developers Association of Canada (PDAC)
Member of Geological Society of Uganda
Member of the Netherlands Fellowship Alumni (Uganda Chapter).